Starting point	: 9° 21.66'S·156° 15.57'E
Terminal point	: 9° 21.68'S·156° 18.65'E
Towed azimuth	: 90°
Distance observed	: 3.0 miles
Water depths observed	: between 2,238 m and 2,635 m
Duration of observation	: 2 hours and 54 minutes
Number of photographs taken	: 102 points

The observation was carried out in the azimuth of W ~ E on the top of the seamount which is on the south side of the track line 93SFDC08, lying on the south side of the seafloor spreading center. The location of the track line is shown in Annexed Figure 3(9) and the route map is shown in Annexed Figure 4(9).

Outcropped rock is relatively prominent on this track line. The range within which sandy ~ muddy sediments are observed is relatively narrow. Talus breccias are distributed on the westward marginal part of the top, pillow lava is prominent on the top, and slaggy lava and pillow lava is prominent on the eastward marginal part of the top. The pillow lava presents a pillow shape with average diameters between 1 m and 2 m. The sediments assume light brown and ripple marks are commonly observed on their surface.

No apparent sign of mineralization is identified on this track line.

Living things observed on this track line include echinoderms such as crinoids, hydrozoas and holothurians, and fishes, sponges and red shrimps.

2) Characteristics of Samples Collected

Samples are mainly collected by chain buckets and a finder mounted power grab. The chain buckets are iron nets on which a pipe for collecting muddy substances is mounted. Samples are collected by dredging these chain buckets on the seafloor. On the other hand, the finder mounted power grab can observe the seafloor and collect samples simultaneously. There are some cases in which rock samples are caught in the FDC frame and collected during the FDC survey.

The collected samples are listed and weighed roughly. Then, a part of them are collected for laboratory experiments. (i.e. chemical analysis and powder X-ray diffraction test) and a part of the remainder is preserved.

The locations of sampling, water depths and amount collected are shown in Appendix Table 2.

The collected samples are mainly comprised of rocks and their altered substances, and crust adhered to the rocks. A small amout of muddy sediments composed of clay, calcareous shells of foraminifera and clastic minerals are also collected. As the property of the muddy sediments in this area is described in the paragraph "Characteristics of Samples" of the "Regional Geochemical Survey". We will not discuss it here. Furthermore, white argillized rock and siliceous rock collected from the sampling points 93SDPG04 and 93SDCB11, will be described in the paragraph "Mineralized Zone".

The collected rocks are mainly composed of basalt～ andesite and pumiceous dacite.

The basalt ～ andesite rocks occur as pillow lava assuming black and as vesicular scoria subrounded gravel with browned surface.

The pillow lava always has a vitreous film on its surface and presents the zonal structure of gradually becoming crystalline from the rim toward the inner part of the rock (see photographs ① to ③ of Fig. 5-2-2-1(1)). The thickness of the surface vitreous film is usually between several mm and 1 cm. The vitreous film presents a smooth ～ botryoidal surface, and adhered submarine organisms and thin layers of black iron-manganese oxides (described later) are identified. In case there are plenty of traces of adhesion of submarine organisms or in case the rock is crusted with black iron-manganese oxides, then the alteration in the inner side of lava is usually advanced and becomes the morphology of close to subrounded pebbles (e.g. 93SDCB07 and 93SDCB09). The amount of megaphenocryst in crystalline part varies from 0% to 10%, and the phenocrystis also identified in the vitreous film of the samples with large quantity of phenocryst (e.g. 93SDCB01). The phenocryst is plagioclase in most cases but olivine and pyroxene are also identified macroscopically and commonly. The groundmass (matrix) presents a hyaline ～ pilotaxitic texture and mostly is vesicular groundmass. Most of such pillow lava samples are collected from the circumference of the seafloor spreading center at the southeastern part of the survey area and relatively fewer at its northeastern part. With the objective of examining the origin of these lava samples, the observation of thin sections (preparates) and chemical analysis were conducted. According to the description of thin sections, all the rock samples collected from the southwestern part of the survey area (93SDCB01, 93SDCB05 and 93SDCB07) are olivine basalt ～ non-porphyritic basalt of the tholeiite series, on the other hand, the basic rocks collected from the area a little to the northwest

① Pillow lava (Sectional plane)

0 5cm

93SDCB01

② Pillow lava (Sectional plane)

0 5cm

93SDCB01

③ Pillow lava (Sectional plane)

0 5cm

93SDCB05

④ Siliceous Rock

0 5cm

93SDCB11

⑤ Argillized rock

0 5cm

93SDCB11

⑥ Argillized rock (Sectional plane)

0 5cm

93SDCB11

⑦ "Chimney" (Whole view)

0 5cm

93SDCB11

⑧ "Chimney" (Sectional plane)

0 5cm

93SDCB11

Figure 5-2-2-1 Photos of Sample collected during detailed survey(rock) (1)

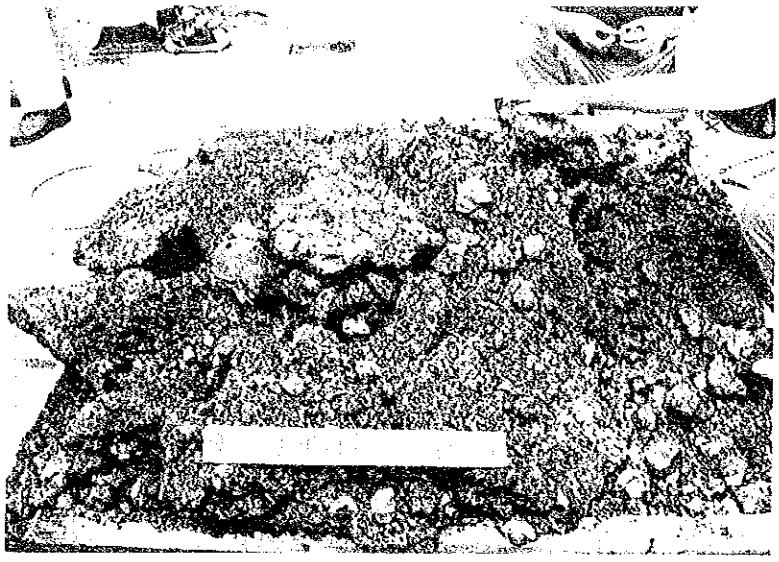

① Green clay mineral (montmorillonite, 93SDPG02)

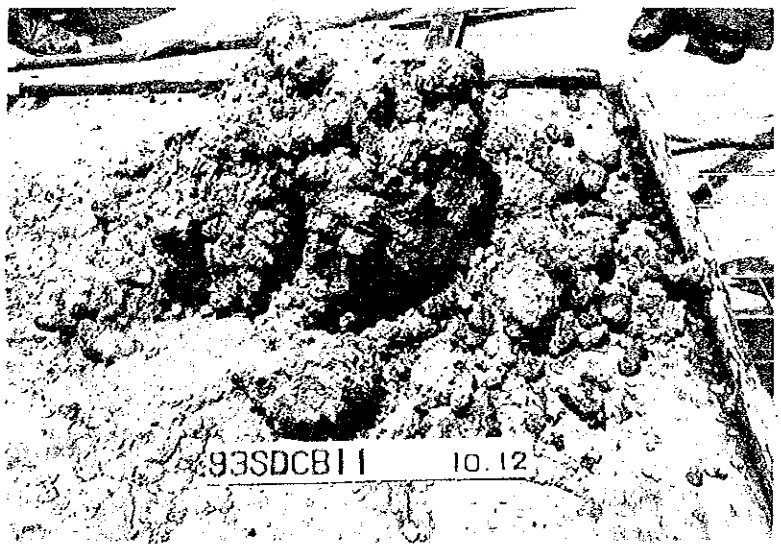

② Light gray clay (sericite, 93SDCB11)

Figure 5-2-2-1 Photos of Samples Collected during detailed survey (altered mineral · caly) (2)

of the survey area are olivine basalt of the tholeiite series containing augite phenocryst (93SDCB09), augite hypersthene basaltic andesite and non-porphyritic basaltic andesite (93SDPG01 and 93SDPG03) of the calc-alkaline series. There is a clear difference between the two zones. Furthermore,according to the results of the chemical analysis, of the four samples regarded as the tholeiite series, the basalt collected from the southwestern part of the survey area (93SDCB01, 93SDCB05 and 93SDCB07) was identified as corresponding to the "olivine tholeiite" of Yoder & Tilley (1962), the olivine basalt containing augite-hypersthene collected from the seamount lying in the area a little to the northeast of the survey area (93SDCB09) was identified as corresponding to the "tholeiite oversaturated with silica." As a result, the fact that the character of island arc becomes stronger in order of 93SDCB01 → 93SDCB05 → 93SDCB07 → 93SDCB09 was identified. The chemical component of the two samples from 93SDCB01 and 93SDCB05 are virtually the "MORB (Mid-Oceanic Ridge Basalt)" and the degree of the partial melting of the sample of 93SDCB05 is a little bit stronger than that of the other, and at the same time, the former has an undifferentiated character. The details of these results will be discussed later.

As the sampling operation on the Coleman Seamount was conducted only once at 93SDPG01, we could not make a definite remark about the difference of the volcanism between the Coleman Seamount and the Kana Keoki Seamount. We, however, can point out the following. First, both resemble each other in the volcanism mainly composed of basaltic andesite of the calc-alkaline series. Secondly, the chemical data of both seamounts are plotted in the same province as the Kavachi Seamount, which lies in an area to the east of them, in a diagram of SiO_2-K_2O/TiO_2 (described later). This indicates that these three seamounts are active under nearly the same geological environment. On the other hand, the data of the chemical analysis show that the differentiation of the Kana Keoki Seamount advances slightly than that of the Coleman Seamount.

The results of the ore grade analysis, conducted on board the ship, on the black iron - manganese oxides covering basalt lava surface are as shown below. It is poor in manganese component but rich in Fe component when compared with manganese nodules, and poor in Co component when comparing with cobalt-rich crusts.

Sampling point	Co (%)	Cu (%)	Ni (%)	Mn (%)	Fe (%)
93SDCB07	0.25	0.05	0.20	14.50	19.09
93SDCB09	0.14	0.62	0.15	18.44	17.59

Chemical analysis on whole rock components and trace level elements was conducted for the black oxides, including the above-mentioned samples, which are covering rocks (as for the method of analysis, see the paragraph of "Mineralized Zones"). The results of the chemical analysis are shown in Table 5-2-3-1. The results plotted on a triangular diagram of Mn/Fe/(Cu+Ni+Zn)×10 is shown in Figure 5-2-2-2. They are plotted in the province where the components of Mn is poorer and Fe is richer than manganese nodules.

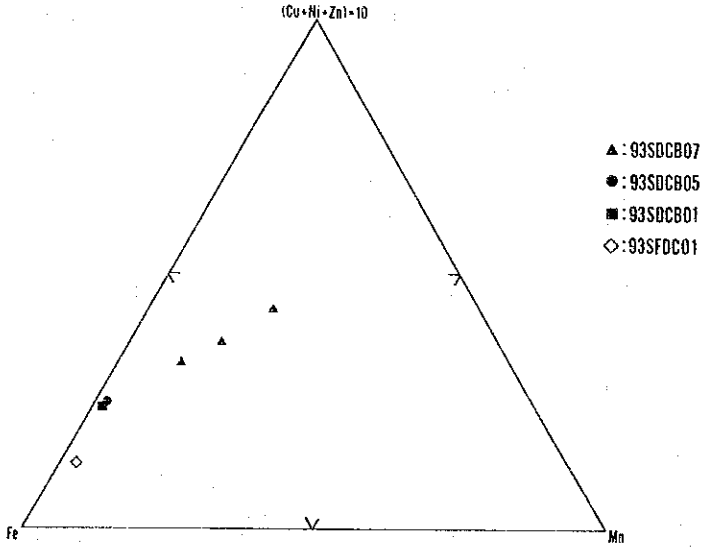

Figure 5-2-2-2 Mn-Fe-10(Cu+Ni+Zn) Diagram for Black Oxides

Most of the scoria are subrounded with brown surfaces which indicates that they have been distributed on the seafloor. Their sorting index is not good and they have various diameters of smaller than the cobble size.

Pumiceous dacite is a leucocratic and vesicular rock with black phenocryst whose maximum diameters are between 2 mm and 3 mm and vitreous groundmass. It has considerably strong magnetic susceptibility. The description of the thin section indicate that it is an "augite hypersthene dacite". The details of the results will be described later. The results of the whole rock analysis are as shown in Table 5-2-3-1 (93SDPG02-02), it belongs to the "non-alkali andesite" of Miyashiro and Kushiro (1975), to the "hypersthene series" under Kuno's (1950) AFM diagram and to the "calc-

Table 5-2-3-1 Result of Whole Rock Analysis and Trace Level Analysis for ores

	93SFDC01 -01	93SDCB01 -01	93SDCB05 -01	93SDCB07 -01	93SDCB07 -02	93SDCB07 -05	93SDPG02 -02	93SDPG02 -03	93SDPC04 -02	93SDCB11 -01	93SDCB11 -02	93SDCB11 -03	93SDCB11 -04	93SDCB11 -05	93SDCB11 -06	93SDCB11 -07	93SDCB11 -08
SiO_2 (%)	54.19	49.05	49.27	41.46	18.58	37.94	58.50										
TiO_2 (%)	0.73	1.21	0.87	0.98	0.91	1.05	0.57										
Al_2O_3 (%)	17.15	16.28	16.55	13.20	5.93	11.87	14.91										
Fe_2O_3 (%)	2.59	2.00	2.46	12.96	29.40	15.01	4.74										
FeO (%)	4.93	6.64	5.77	1.13	0.27	0.94	2.42										
MnO (%)	0.21	0.16	0.16	2.45	14.77	4.72	0.24										
MgO (%)	5.20	8.60	9.00	3.96	2.03	3.70	3.27										
CaO (%)	10.15	11.62	12.42	7.56	5.48	6.87	6.84										
BaO (%)	0.01	< 0.01	< 0.01	0.02	0.09	0.03	0.02										
Na_2O (%)	2.30	2.67	2.27	2.78	2.35	2.51	3.21										
K_2O (%)	0.69	0.10	0.04	1.05	0.55	0.97	1.42										
P_2O_5 (%)	0.14	0.08	0.05	0.31	0.99	0.43	0.20										
LOI (%)	0.95	< 0.01	0.29	10.12	17.24	11.51	3.91										
Total (%)	99.24	98.41	99.15	97.98	98.59	97.55	100.25										
Au (ppb)	25	< 5	< 5	< 5	< 5	< 5	< 5	< 5	240	< 5	180	> 10000	190	275	200	200	230
Au (oz/t)												0.370					
Ag (ppm)	0.02	< 0.02	< 0.02	< 0.02	0.06	< 0.02	< 0.02	< 0.02	0.26	0.08	2.16	7.24	5.92	6.04	3.68	4.20	5.92
Cu (ppm)	9.2	30.0	30.0	134.0	375.0	134.0	23.6	22.0	84.6	43.4	676.0	2810.0	380.0	180.0	160.0	109.0	258.0
Pb (ppm)	3.5	< 0.5	0.5	102.0	573.0	171.5	6.0	2.0	27.0	1325.0	3900.0	263.0	670.0	74.0	75.0	56.0	140.5
Zn (ppm)	12	32	31	179	587	230	29	20	157	379	3400	283	216	64	48	94	341
Mn (ppm)	1375	1085	1065	> 10000	> 10000	> 10000	1700	> 10000	130	1370	580	475	545	50	140	45	60
Total-Fe(%)	5.15	6.08	5.63	9.94	19.48	10.82	4.76	21.31	4.92	3.26	6.29	3.55	3.39	6.84	2.84	5.05	6.32
Total-S (%)	0.022	0.087	0.093	0.042	0.144	0.048	0.037	0.023	7.090	0.352	2.430	2.170	2.890	8.220	2.570	6.310	7.660
Cd (ppm)	< 0.1	< 0.1	< 0.1	0.4	2.2	0.7	< 0.1	< 0.1	1.0	0.1	1.0	0.2	0.1	0.1	< 0.1	0.2	1.0
Bi (ppm)	0.1	< 0.1	< 0.1	0.7	4.0	1.0	0.1	< 0.1	0.1	< 0.1	0.1	1.2	0.2	0.1	< 0.1	0.2	0.1
Ni (ppm)	57	132	128	253	1360	470	24	12	31	29	21	12	28	18	25	16	20
Co (ppm)	32	41	41	237	1515	502	30	6	24	22	22	16	19	15	19	14	16
As (ppm)	27.8	4.2	2.6	34.2	139.5	59.8	3.2	18.8	30.2	114.0	650.0	388.0	88.2	16.0	81.2	15.6	31.0
Sb (ppm)	< 0.2	< 0.2	< 0.2	2.4	11.6	4.0	< 0.2	< 0.2	0.6	< 0.2	< 0.2	26.6	0.2	< 0.2	< 0.2	< 0.2	< 0.2
Hg (ppb)	40	30	40	20	10	10	30	30	1700	40	300	10	20	20	30	20	40
Ba (ppm)	105	5	5	215	970	300	170	105	15	4190	860	55	100	60	115	45	200
Sr (ppm)	235	114	62	457	1330	555	389	529	447	516	771	29	87	10	14	10	18
Mo (ppm)	1.0	< 0.2	< 0.2	23.0	137.5	52.2	1.6	13.2	59.2	1.4	11.2	3.6	16.8	3.6	9.6	5.8	7.2
Sn (ppm)	< 1	< 1	< 1	< 1	< 1	< 1	< 1	< 1	< 1	< 1	< 1	< 1	< 1	< 1	< 1	< 1	< 1
W (ppm)	< 1	< 1	7	10	15	< 1	< 1	7	< 1	2	< 1	< 1	2	< 1	< 1	3	2

alkali series" under the FeO^*/MgO-SiO_2. Generally, it presents a subrounded shape of smaller than the cobble size. And, usually, a change of color into yellow advances from its surface to the inner part. Calcite, halite and phillipsite is identified as an altered mineral in such part under the powder X-ray diffraction test. At 93SDPG02, pumiceous dacite under the altered vesicular basaltic layers having the thickness between 10 cm and 20 cm, altered to a green clay mineral (see photograph ① of Fig. 5-2-2-1 (2)). Although montmorillonite is identified as an altered mineral in addition to calcite and halite from this part by the powder X-ray diffraction test, it is not clear whether this is iron saponite or nontronite. Furthermore, pumiceous dacite captured in the vitreous part of the upper surface of the vesicular basaltic layers is also identified from the samples collected from this point. Pumiceous dacite is identified characteristically in the circumference of the Kana Keoki Seamount lying on the northeastern part of the survey area.

In the above-mentioned case, the basaltic volcanism is estimated to have occurred after the volcanism of pumiceous dacite but there is a case found at 93SDPG03 in which slightly altered basaltic pebbles are captured by pumiceous dacite. We can estimate a bimodal volcanism, in which both activities overlap each other, at the Kana Keoki Seamount.

In addition to the above-mentioned "essential" rocks, some "accidental" pebbles appearing to be terrigenous rocks are collected at 93SDPG01 (in the vicinty of the summit of the Coleman Seamount). Samples collected here were mainly fragments of vesicular (～ scoriaceous) black ～ green altered basalt, but in addition to them, some well-rubbed subrounded pebbles, with a maximum diameter of 10 cm, of the rock species as mentioned below were also collected. They are green schist (high susceptibility), granitic rock (high susceptibility), altered tuff captured by basaltic rock, altered basalt (high susceptibility), altered basaltic lapilli tuff and fine-grained diorite. The observation of thin sections was conducted on the typical rocks among them. As a result of which, augite hornblende dioritic porphyry (93SDPG01-03), dioritic porphyry (93SDPG01-04), andesite meta-lapilli tuff (93SDPG01-05) and meta-hypersthene augite andesite (93SDPG01-06) were identified. The details of the results will be described later.

<Observation of Thin Sections (Preparates)>

The results of the observation for the individual samples are described hereunder.

The transmitted microphotographs are shown in Fig. 5-2-2-3.

- 93SDCB01-02 .... "Tholeiitic Olivine Basalt"

  It was collected from the vicinities of the regional geochemical sampling point 93SRGC01 (at the water depth of 3800 m) near the southwestern corner of the survey area (rocks were collected from this sampling point: see Regional Geochemical Survey"). This point is estimated to be inside of the expected seafloor spreading center. It is, macroscopically, a black basalt rich in phenocryst.

  Its phenocryst is a small amount of plagioclase (euhedral, diameters between 1 mm and 5 mm) and olivine (euhedral, diameters between 1 mm and 5 mm). Its groundmass is composed of abundant glass and a small quantity of euhedral plagioclase and olivine. It presents a porphyritic, spherulitic and variolitic texture and is an underwater quenched basalt with low degree of vesicularity. Unaltered.

- 93SDCB05-02 .... "Tholeiitic Olivine Basalt"

  It was collected from the vicinities of the regional geochemical sampling point 93SRGC11 (at the water depth of about 3,600 m) a little to the southwest from the center of the survey area (rocks were collected from this sampling point: see "Regional Geochemical Survey"). This point is estimated to be inside of the expected seafloor spreading center. Macroscopically, it is a black basalt poorer in phenocryst than the sample of 93SDCB01-02.

  Its phenocryst is a small amount of plagioclase (euhedral, diameters between 1 mm and 5 mm) and olivine (euhedral, diameters between 0.1 mm and 1 mm). Its groundmass is composed of abundant glass, a moderate quantity of euhedral plagioclase and a small amount of euhedral olivine and anhedral augite. The amount of phenocryst only accounts for less than 10% of the whole. It presents an intersertal texture and is an unvesiculated underwater quenched basalt. Unaltered.

- 93SDCB07-03 .... "Tholeiitic Non-porphyritic Basalt"

  It was collected from the vicinity of the summit (at the water depth of about 2,400 m) of the seamount (93S01 Smt.) on the north side of the expected seafloor spreading center located in the area a little to the west from the center of the survey area. Macroscopically, it is a black vesicular and vitreous basalt with fewer and smaller phenocryst than the sample of 93SDCB05-02.

93SDCB01-02 open nicol

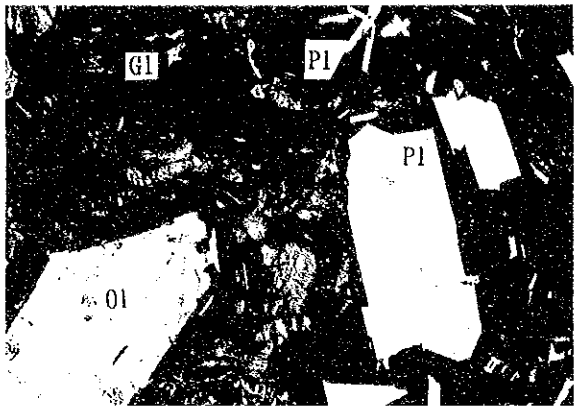

93SDCB01-02 cross nicol

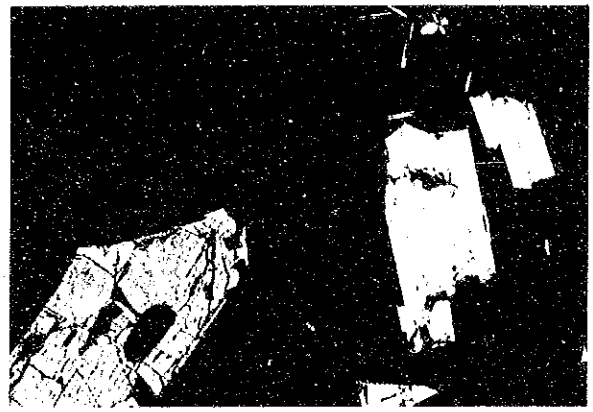

93SDCB05-02 open nicol

93SDCB05-02 cross nicol

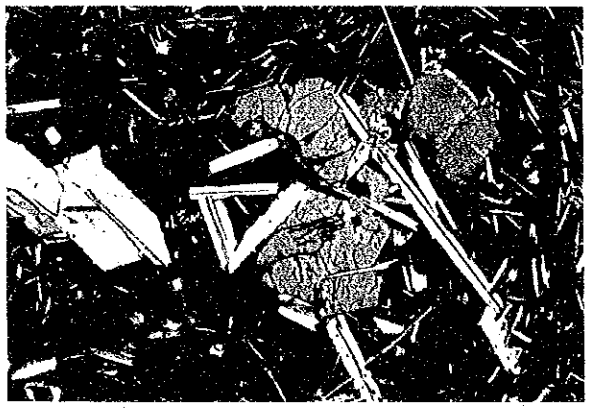

93SDCB07-03 open nicol

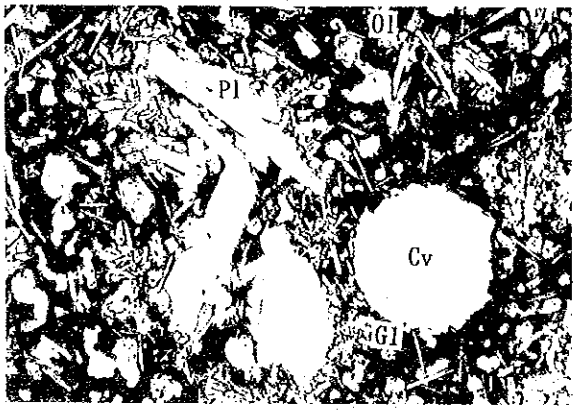

93SDCB07-03 cross nicol

93SDCB01-02 : Tholeiitic Olivine Basalt
93SDCB05-02 : Tholeiitic Olivine Basalt
93SDCB07-03 : Tholeiitic Non-porphyritic Basalt

Figure 5-2-2-3 Microscopic Photos of Rock on Detailed Survey (1)

93SDCB09-01 open nicol

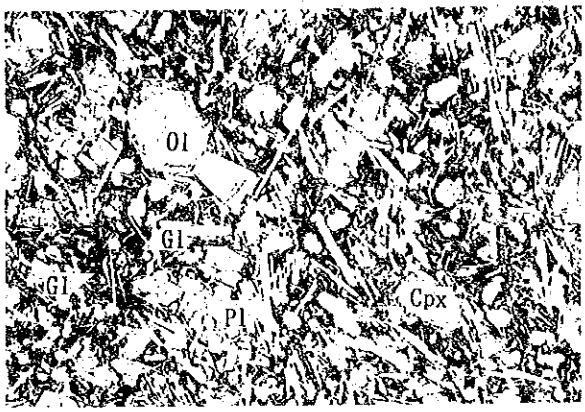

0 500μm

93SDCB09-01 cross nicol

0 500μm

93SDPG01-01 open nicol

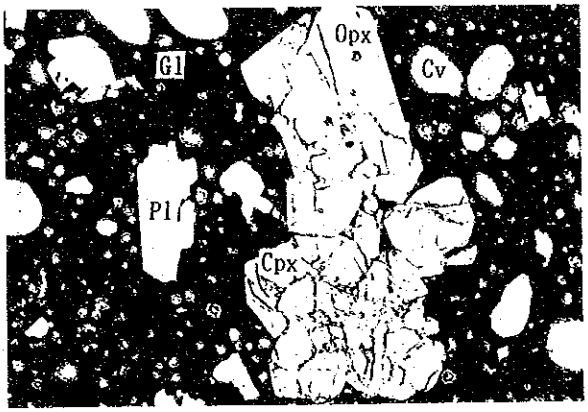

0 500μm

93SDPG01-01 cross nicol

0 500μm

93SDPG01-03 open nicol

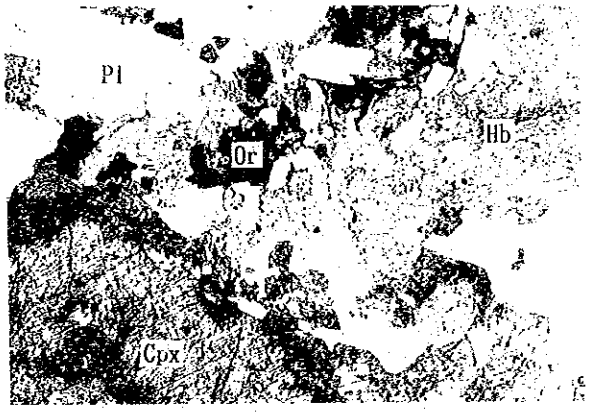

0 500μm

93SDPG01-03 cross nicol

0 500μm

93SDCB09-01 : Tholeiitic Olivine Augite Basalt
93SDPG01-01 : Calcalkalic Augite Hypersthene Andesite
93SDPG01-03 : Augite Hornblende Dioritic Porphyrite

Figure 5-2-2-3 Microscopic Photos of Rock on Detailed Survey (2)

93SDPG01-04 open nicol

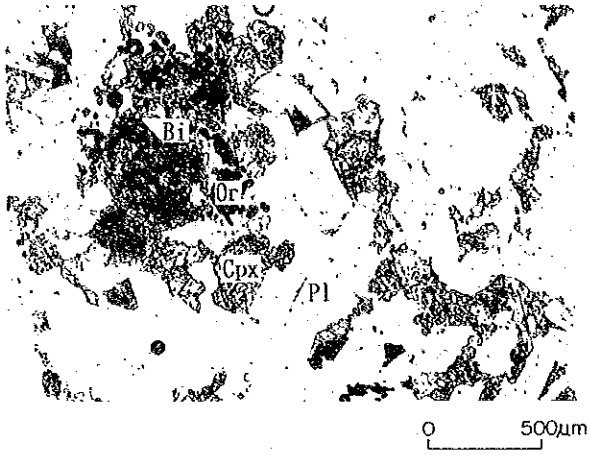

93SDPG01-04 cross nicol

93SDPG01-05 open nicol

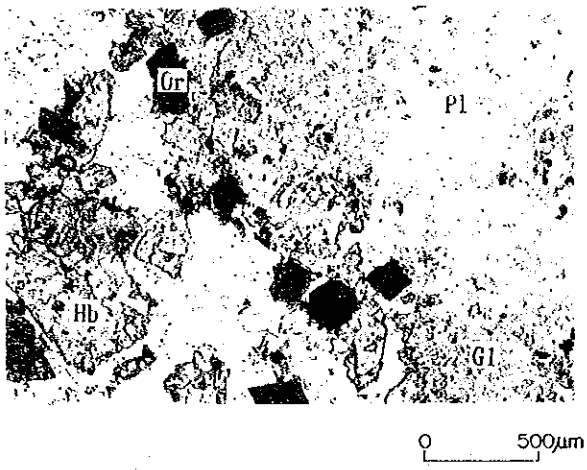

93SDPG01-05 cross nicol

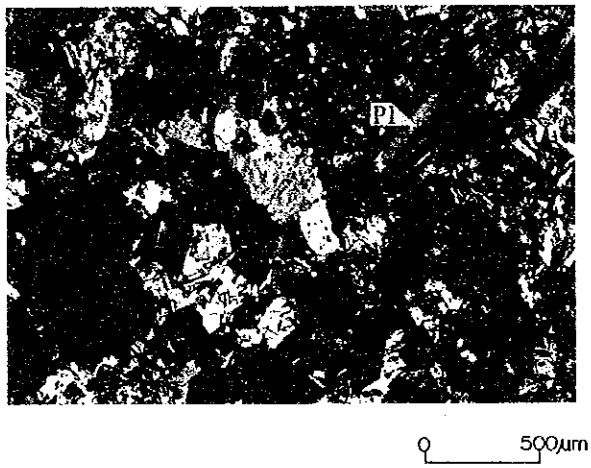

93SDPG01-06 open nicol

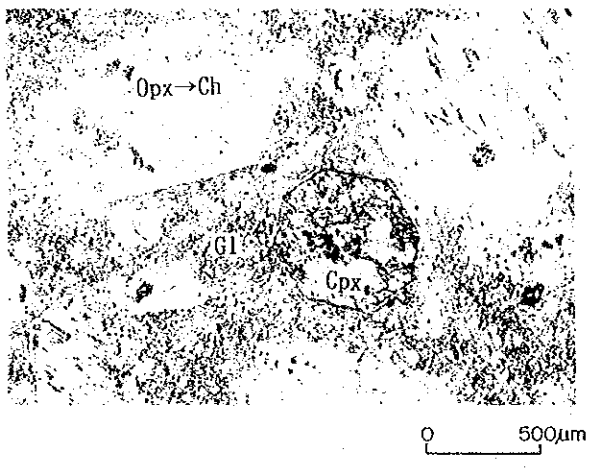

93SDPG01-06 cross nicol

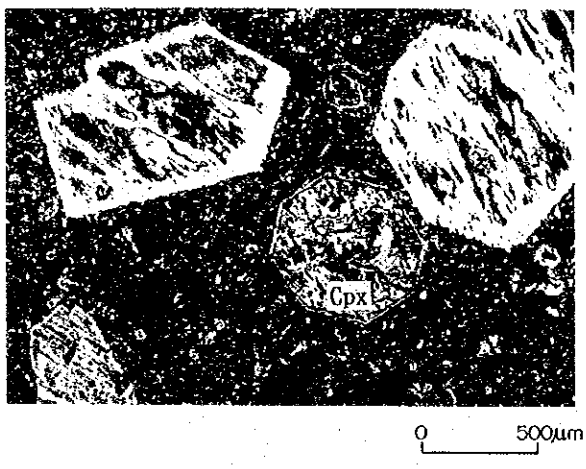

93SDPG01-04 : Dioritic Porphyrite
93SDPG01-05 : Andestic Meta Lapilli tuff
93SDPG01-06 : Meta Hypersthene Augite Andesite

Figure 5-2-2-3 Microscopic Photos of Rock on Detailed Survey (3)

93SDPG02-01 open nicol

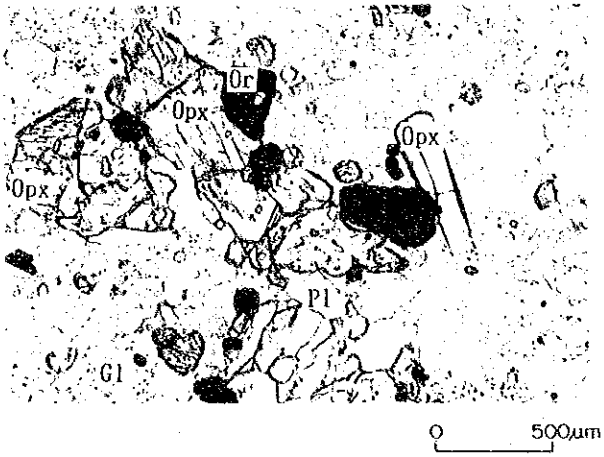

93SDPG02-01 cross nicol

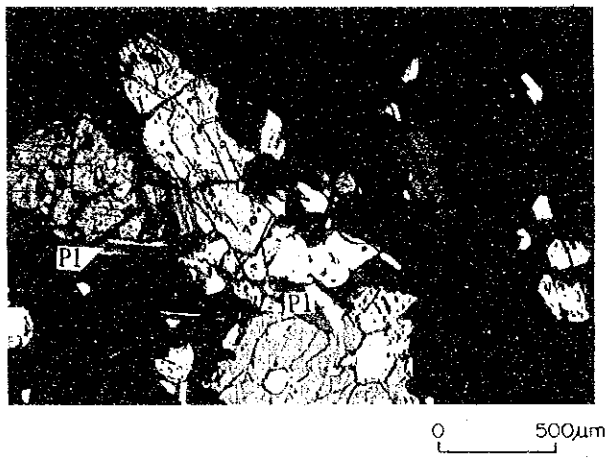

93SDPG03-02 open nicol

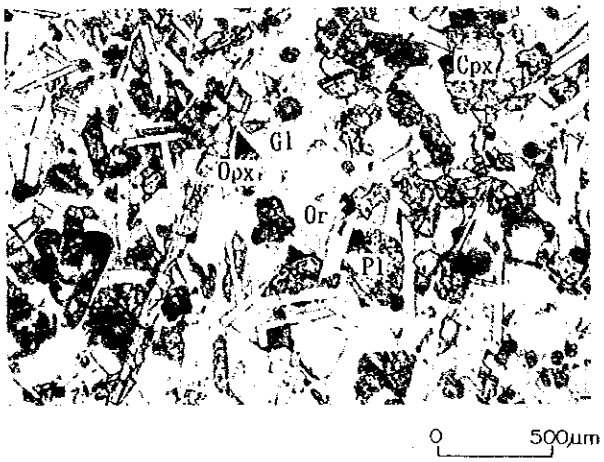

93SDPG03-02 cross nicol

93SDPG03-04 open nicol

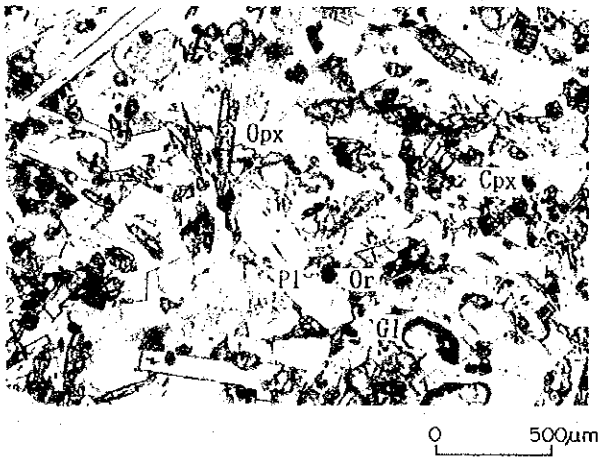

93SDPG03-04 cross nicol

93SDPG02-01 : Augite Hypersthene Dacite
93SDPG03-02 : Non-porphyritic Basaltic Andesite
93SDPG03-04 : Non-porphyritic Andesite part

Figure 5-2-2-3 Microscopic Photos of Rock on Detailed Survey (4)

93SDPG03-04 open nicol

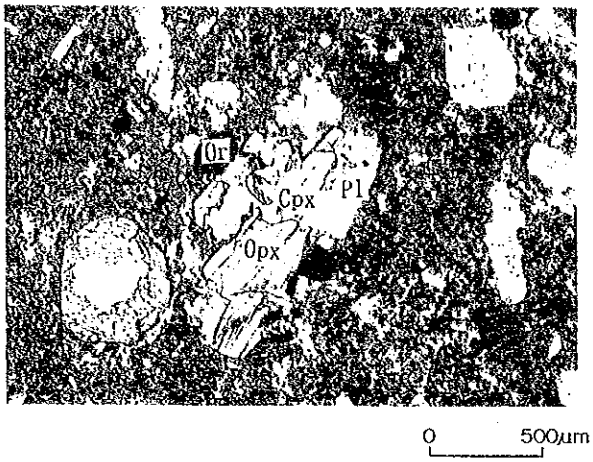

93SDPG03-04 cross nicol

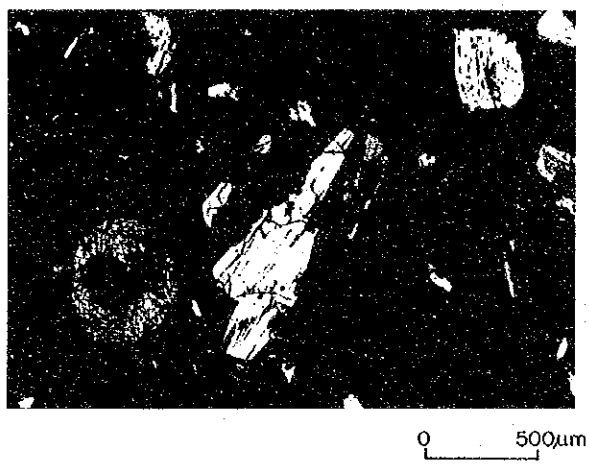

93SDPG03-04 : Augite Hypersthene Andesite part

Abbreviation Bi : Biotite Ch : Chlorite Cv : Gas cavity Gl : Glass
Hb : Hornblende Ol : Olivine Or : Opaque mineral
Pl : Plagioclase Px : Pyroxene Cpx: Clinopyroxene
Opx: Orthopyroxene Qz : Quartz Opx→Ch : Chloritized Opx

Figure 5-2-2-3 Microscopic Photos of Rock on Detailed Survey (5)

Its phenocryst is a small amount of plagioclase (euhedral, diameters between 0.1 mm and 1 mm) and olivine (euhedral, diameters between 0.1 mm and 1 mm). Its groundmass is composed of abundant glass, a moderate quantity of euhedral plagioclase and subhedral olivine, and a small amount of anhedral augite. The amount of phenocryst only account for several percent of the whole. It presents a vitreous, intersertal texture and is a well-vesiculated, vesicular underwater quenched basalt. Unaltered.

- 93SDCB09-01 .... "Tholeiitic Olivine Augite Basalt"

It was collected from the vicinity of the summit (at the water depth of about 2,000 m) of the seamount (93S05 Smt.) on the east side of the Simbo Ridge located in the area a little to the northeast from the center of the survey area. Macroscopically, it is a black compact basalt.

Its phenocryst is a small amount of augite (anhedral, diameters between 1 mm and 5 mm) and olivine (euhedral, diameters between 0.1 mm and 1 mm). Its groundmass is composed of abundant glass, euhedral plagioclase, euhedral olivine and a small amount of subhedral augite. It presents a variolitic and itersertal texture and is a moderately vesiculated underwater quenched basalt. Unaltered.

- 93SDPG01-01 .... "Calc-alkaline Augite Hypersthene Andesite"

It was collected from the vicinity of the summit (at the water depth of 618 m) of the Coleman Seamount located in the area a little to the northeast of the survey area. Macroscopically, it appears to be a basalt ~ andesite.

Its phenocryst is a moderate quantity of augite (euhedral, diameters between 0.1 mm and 1 mm), hypersthene (euhedral, diameters between 0.1 mm and 1 mm), plagioclase (euhedral, diameters between 1 mm and 5 mm). Its groundmass is abundant glass. It presents a vitreous and porphyritic texture and is a well-vesiculated underwater quenched andesite. Unaltered. It appears to be an island arc environment ~ ocean island rock.

- 93SDPG01-03 .... "Augite Horblende Dioritic Porphyry"

It was collected from the vicinity of the summit (at the water depth of 618 m) of the Coleman Seamount located in the area a little to the northeast of the survey area. Macroscopically, it appears to be a granite ~ granodiorite. It presents subrounded pebble and shows high susceptibility.

Its phenocryst is a small amount of hornblende (subhedral, diameters between 0.1 mm and 1 mm), augite (subhedral, diameters between 0.1 mm and 1 mm) and plagioclase (euhedral, diameters between 1 mm and 5 mm). Its groundmass is abundant plagioclase (euhedral, diameters between 0.1 mm and 1 mm), horblende (subhedral, diameters between 0.1 mm and 1 mm), a small amount of silica mineral (anhedral, diameters between 0.1 mm and 1 mm), potassium feldspars (anhedral, diameters between 0.1 mm and 1 mm), augite (subhedral, diameters between 0.1 mm and 1 mm), iron mineral (anhedral, diameters between 0.1 mm and 1 mm) and anhedral mesostasis. It presents an equigranular texture and is poor in phenocryst. The difference between the phenocryst and groundmass is small. It is a shoal intrusive basaltic andesite. It is slightly chloritized.

- 93SDPG01-04 .... "Dioritic Porphyry"

It was collected from the vicinity of the summit (at the water depth of 618 m) of the Coleman Seamount located in the area a little to the northeast of the survey area. Macroscopically, it appears to be a granite ~ granodiorite. It presents subrounded pebble and shows high susceptibility.

Its phenocryst is a small amount of plagioclase (euhedral, diameters between 1 mm and 5 mm). Its groundmass is abundant plagioclase (euhedral, diameters between 0.1 mm and 1 mm), augite (subhedral, diameters between 0.1 mm and 1 mm), a small amount of silica mineral (anhedral, diameters between 0.1 mm and 1 mm), potassium feldspars (anhedral, diameters between 0.1 mm and 1 mm), biotite (anhedral, diameters between 0.1 mm and 1 mm), iron mineral (anhedral, diameters between 0.1 mm and 1 mm) and anhedral mesostasis. It presents an equigranular texture and the amount of plagioclase in its phenocryst only accounts for several percent. It is a shoal intrusive basaltic andesite.

- 93SDPG01-05 .... "Andesitic Meta lapilli Tuff"

It was collected from the vicinity of the summit (at the water depth of 618 m) of the Coleman Seamount located in the area a little to the northeast of the survey area. Macroscopically, it is a dark green compact altered rock. It presents subrounded pebble and shows high susceptibility.

The rock fragment (detritus) is a large quantity of essential andesite (subrounded pebbles with diameters between 4 mm and 32 mm). Its matrix is abundant glass. Its

source rock is tuff but it has been influenced by the thermal metamorphism and transformed into an altered mineral assemblage of plagioclase - amphibole - iron mineral - quartz - epidote - potassium feldspars.

- 93SDPG01-06 .... "Meta Hypersthene Augite Andesite"

It was collected from the vicinity of the summit (at the water depth of 618 m) of the Coleman Seamount located in the area a little to the northeast of the survey area. Macroscopically, it is a dark green compact altered rock. It presents subrounded pebble.

Its phenocryst is abundant augite (enhedral, diameters between 1 mm and 5 mm), a moderate quantity of hypersthene (subhedral, diameters between 1 mm and 5 mm) and a small amount of plagioclase (subhedral, diameters between 0.1 mm and 1 mm) and iron mineral (euhedral, diameters between 1 mm and 5 mm). Its groundmass is abundant glass. It presents a porphyritic texture. It has been influenced by the thermal metamorphism and transformed into a mineral assemblage of amphibole - augite - quartz - iron mineral - epidote.

- 93SDPG02-01 .... "Augite Hypersthene Dacite"

It was collected from the vicinity of the summit (at the water depth of 764 m) of the Kana Keoki Seamount located in the area a little to the northeast of the survey area. Macroscopically, it is a pumiceous white rock with dark green phenocryst. It has magnetism.

Its phenocryst is a moderate amount of augite (euhedral, diameters between 0.1 mm and 1 mm), hypersthene (euhedral, diameters between 0.1 mm and 1 mm), plagioclase (euhedral, diameters between 0.1 mm and 1 mm) and a small amount of iron mineral (euhedral, diameters between 0.1 mm and 1 mm). Its groundmass is abundant colorless glass. It is a pumice presenting porphyritic, granular and vitreous texture.

- 93SDPG03-02 .... "Non-porphyritic Basaltic Andesite"

It was collected from the vicinity of the summit (at the water depth of 879 m) of the Kana Keoki Seamount located in the area a little to the northeast of the survey area. Macroscopically, it assumes dark green.

No phenocryst is identified. Its groundmass is abundant colorless glass, plagioclase (euhedral, diameters between 0.1 mm and 1 mm), a moderate amount of

augite (subhedral, diameters between 0.1 mm and 1 mm), hypersthene (subhedral, diameters between 0.1 mm and 1 mm) and a small amount of iron mineral (subhedral, diameters between 0.1 mm and 1 mm). It presents a spherulitic and intersertal texture. It is a vesicular, basaltic andesite cognate xenolith of clac-alkaline series. Unaltered.

· 93SDPG03-04

It was collected from the vicinity of the summit (at the water depth of 879 m) of the Kana Keoki Seamount located in the area a little to the northeast of the survey area. Macroscopically, it assumes dark green and can be clearly (intermittently) divided into the coarse-grained part and fine-grained part.

The fine-grained part .... "Non-porphyritic Andesite"

No phenocryst is identified. Its groundmass (matrix) is abundant colorless glass, plagioclase (euhedral, diameters between 0.1 mm and 1 mm), a moderate amount of augite (subhedral, diameters between 0.1 mm and 1 mm), hypersthene (subhedral, diameters between 0.1 mm and 1 mm) and a small amount of iron mineral (subhedral, diameters between 0.1 mm and 1 mm). It presents a spherulitic and intersertal texture. It is a vesicular, andesitic cognate xenolith of calc-alkaline series. It exceedingly resembles the 93SDPG03-02. Unaltered.

The coarse-grained part .... "Augite Hypersthene Andesite"

Its phenocryst is a moderate amount of plagioclase (euhedral, diameters between 0.1 mm and 1 mm), a small amount of augite (subhedral, diameters between 0.1 mm and 1 mm), hypersthene (euhedral, diameters between 0.1 mm and 1 mm) and iron mineral (anhedral, diameters between 0.1 mm and 1 mm). Its groundmass (matrix) is abundant glass and a small amount of euhedral plagioclase. It is an andesite presenting a porphyritic and hyalopilitic texture. Unaltered.

<Chemical Analysis>

In order to examine the origin of the basic rocks collected from the survey area, a chemical analysis was conducted. The number of the samples are seven. Two portions from the epidermis part (vitric part) of the lava and three portions from the inner part of each sample were analyized. Samples for the chemical analysis and samples for the observation of thin sections were taken from roughly the same part of the lava. The corresponding relation between the sample numbers of the seven samples and the

names of rocks under the thin section observation are as follows.

93SDCB01-03(93SDCB01-02: Tholeiitic olivine basalt)

93SDCB05-03(93SDCB05-02: Tholeiitic olivine basalt)

93SDCB07-04(93SDCB07-03: Tholeiitic non-porphyritic basalt)

93SDCB09-02(93SDCB09-01: Tholeiitic olivine augite basalt)

93SDPG01-02(93SDPG01-01: Calc-alkaline augite hypersthene basaltic andesite)

93SDPG03-03(93SDPG03-02: Calc-alkaline non-porphyritic basaltic andesite)

93SDPG03-05(93SDPG03-04: Calc-alkaline non-porphyritic andesite and augite hypersthene andesite)

As for the sample 93SDPG03-05, two portions at the non-porphyritic andesite part and three portions at the augite hypersthene andesite part were analyzed.

The components analyzed and limits of detection are as follows: SiO_2, TiO_2, Al_2O_3, Fe_2O_3, FeO, MnO, MgO, CaO, Na_2O, K_2O, P_2O_5, H_2O^+, H_2O^- and CO_2 (the detection limit of the above 14 components is 0.01%), Ba (1ppm), Rb (0.1ppm), Sr (1ppm), Pb (1ppm), Zr (1ppm), Nb (0.5ppm), Y (1ppm), V (1ppm), Cr (1ppm), Ni (1ppm), Cu (1ppm), Zn (1ppm), Ga (0.5ppm), S (100ppm), Sc (0.1ppm), Cs (0.1ppm), La (0.1ppm), Ce (0.1ppm), Nd (0.1ppm), Sm (0.01ppm), Eu (0.01ppm), Gd (0.1ppm), Tb (0.01ppm), Ho (0.01ppm), Tm (0.01ppm), Yb (0.01ppm), Lu (0.01ppm), Hf (0.1ppm), Ta (0.1ppm) and Th (0.1ppm). As for the elements other than the 14 components of the whole rock, the values in the ( ) are the detection limits.

The methods of analysis are as follows; The fluorescent X-ray method (XRF) for: SiO_2, TiO_2, Al_2O_3, Fe_2O_3, MnO, MgO, CaO, Na_2O, K_2O, P_2O_5, Ba, Sr and Zr. The neutralization titration method for: FeO. The instrument neutron activation analysis (INAA) for: Cr, Cs, Hf, Sc, Ta, Tb, Th, La, Ce, Nd, Sm, Eu, Gd, Ho, Yb and Lu. The ICP emission analysis after the decomposition and extraction by hydrochloric acid - potassium chlorate or hydrofluoric acid - nitric acid - perchloric acid for: Cu, Pb, Zn, Ni, V and CO_2. The fluorescent X-ray (XRF) method after processing the rock powder into pressure pellets for: Nb, Y, Rb, Ga and S. The measurement of H_2O^+ and H_2O^-: 0.200 g of test piece was weighed and its absorbed water (H_2O^-) was expelled by 105℃ nitrogen gas in a water content analyzer, the expelled H_2O^- was measured by a infrared detector. After which, the test piece was heated in a high-powered oven at 1,000℃ to expel its crystal water (H_2O^+), which was measured by the infrared detector.

The results of the analyses are shown in Table 5-2-2-1. The symbols A, B, C, D

Table 5-2-2-1 Result of Chemical Analysis for Basalts (1)

	93SDCB01 -03A	93SDCB01 -03B	93SDCB01 -03C	93SDCB01 -03D	93SDCB01 -03E	93SDCB05 -03A	93SDCB05 -03B	93SDCB05 -03C	93SDCB05 -03D	93SDCB05 -03E	93SDCB07 -04A	93SDCB07 -04B	93SDCB07 -04C	93SDCB07 -04D	93SDCB07 -04E
SiO_2 (%)	48.37	48.08	48.21	48.51	48.35	48.36	48.67	49.04	48.90	49.12	48.34	48.36	48.74	49.47	49.54
TiO_2 (%)	1.28	1.29	1.28	1.28	1.30	0.93	0.95	0.87	0.89	0.91	0.73	0.72	0.70	0.74	0.71
Al_2O_3(%)	15.72	15.53	15.81	15.85	15.92	15.88	15.54	15.55	15.73	15.67	15.59	15.49	16.11	16.02	15.95
Fe_2O_3(%)	2.21	2.09	2.56	2.44	2.68	1.95	1.59	1.27	0.77	0.78	1.37	1.17	0.63	< 0.01	0.17
FeO (%)	8.21	8.31	8.07	7.99	7.55	7.76	8.15	8.28	8.98	8.80	8.50	8.18	8.47	8.95	8.90
MgO (%)	7.97	8.04	8.05	8.02	8.00	8.91	8.90	8.84	8.86	8.77	7.65	7.61	7.87	8.03	7.70
CaO (%)	11.91	11.93	12.02	11.98	11.86	12.69	12.76	12.46	12.72	12.65	12.51	12.40	13.25	13.22	13.20
MnO (%)	0.15	0.16	0.16	0.16	0.15	0.15	0.15	0.14	0.15	0.14	0.46	0.36	0.14	0.14	0.14
Na_2O (%)	2.62	2.60	2.65	2.65	2.63	2.16	2.16	2.14	2.28	2.19	2.06	2.01	2.03	2.06	2.07
K_2O (%)	0.11	0.08	0.09	0.13	0.08	0.05	0.04	0.05	0.04	0.09	0.39	0.34	0.27	0.26	0.27
P_2O_5 (%)	0.14	0.15	0.14	0.15	0.14	0.09	0.09	0.08	0.09	0.11	0.13	0.12	0.11	0.10	0.11
H_2O^+ (%)	0.74	0.65	0.50	0.70	0.60	0.55	0.30	0.50	0.45	0.35	0.35	0.65	0.65	0.75	0.65
H_2O^- (%)	0.02	0.03	0.09	0.03	0.05	0.05	0.03	0.03	0.02	0.02	0.03	0.04	0.03	0.04	0.03
CO_2 (%)	0.03	0.03	0.03	0.06	0.06	0.06	0.03	0.06	0.03	0.03	0.03	0.06	0.06	0.06	0.06
Total(%)	99.48	98.97	99.66	99.95	99.37	99.59	99.36	99.31	99.91	99.63	98.14	97.51	99.06	99.84	99.50
Ba (ppm)	20	27	19	24	20	20	27	21	17	17	64	55	41	41	41
Rb (ppm)	0.5	0.5	0.2	1.4	0.2	1.0	0.2	0.2	1.3	0.2	5.3	4.2	3.6	2.2	3.6
Sr (ppm)	130	128	129	129	126	78	79	75	76	76	183	175	167	166	136
Pb (ppm)	9	17	8	< 5	6	< 5	6	5	5	6	22	16	< 5	8	6
Zr (ppm)	107	100	110	105	102	75	72	75	60	60	80	70	56	55	52
Nb (ppm)	4.4	3.9	2.3	2.4	4.1	6.4	2.7	1.4	3.3	5.7	3.5	3.1	4.0	3.0	2.1
Y (ppm)	28.3	27.0	27.6	27.6	32.5	20.8	21.3	21.8	22.9	24.6	19.1	15.3	9.8	12.5	13.7
V (ppm)	187	191	195	190	194	173	175	173	179	175	178	173	173	179	186
Cr (ppm)	302.0	289.0	306.0	280.0	284.0	345.0	349.0	343.0	368.0	365.0	250.0	246.0	254.0	234.0	207.0
Ni (ppm)	124	115	130	119	129	147	140	133	136	131	111	98	71	76	67
Cu (ppm)	69	70	71	69	72	83	86	82	87	84	102	96	86	83	88
Zn (ppm)	79	78	77	75	78	75	72	69	71	72	83	78	60	68	68
Ga (ppm)	17.8	14.2	15.3	16.3	17.3	15.1	19.0	16.0	16.9	15.6	14.4	12.4	13.3	12.8	13.6
S (ppm)	740	900	745	795	720	705	755	640	485	440	480	400	265	240	190
Sc (ppm)	33.2	33.5	33.1	30.6	31.3	29.8	29.7	29.4	31.2	30.7	32.3	32.6	33.5	32.8	32.5
Cs (ppm)	< 0.1	< 0.1	< 0.1	< 0.1	< 0.1	< 0.1	< 0.1	< 0.1	< 0.1	< 0.1	< 0.1	< 0.1	0.1	< 0.1	0.2
La (ppm)	2.4	2.4	2.3	2.2	2.2	0.9	0.9	0.9	1.0	1.0	6.8	5.6	2.6	2.4	2.5
Ce (ppm)	8.7	9.6	9.9	9.0	8.7	4.8	5.0	5.2	5.4	5.0	21.1	16.0	7.5	6.8	7.0
Nd (ppm)	6.7	6.8	8.1	6.7	6.9	4.7	4.1	4.0	4.2	4.1	8.6	6.6	4.8	4.8	4.0
Sm (ppm)	2.47	2.44	2.51	2.31	2.39	1.71	1.71	1.70	1.77	1.75	2.13	2.03	1.52	1.47	1.38
Eu (ppm)	1.01	0.96	1.00	0.87	0.93	0.69	0.68	0.71	0.70	0.73	0.74	0.70	0.55	0.54	0.53
Gd (ppm)	3.6	3.6	3.7	3.4	3.3	2.8	2.8	2.5	2.4	2.6	2.8	2.8	2.3	2.1	2.1
Tb (ppm)	0.69	0.70	0.68	0.63	0.63	0.54	0.54	0.53	0.48	0.53	0.60	0.60	0.52	0.43	0.39
Ho (ppm)	0.94	1.10	1.00	1.15	1.10	1.11	0.99	0.87	0.82	0.90	0.78	1.11	1.00	0.97	1.25
Tm (ppm)	0.46	0.46	0.45	0.45	0.42	0.37	0.40	0.35	0.33	0.36	0.34	0.32	0.28	0.28	0.37
Yb (ppm)	2.52	2.47	2.64	2.41	2.49	2.06	2.09	2.07	2.28	2.25	1.96	1.90	1.75	1.65	1.62
Lu (ppm)	0.38	0.38	0.39	0.35	0.37	0.31	0.31	0.30	0.31	0.31	0.31	0.28	0.26	0.25	0.24
Hf (ppm)	2.0	1.9	2.1	1.7	1.8	1.1	1.2	1.1	1.2	1.1	1.3	1.1	1.0	1.0	0.9
Ta (ppm)	< 0.1	< 0.1	< 0.1	< 0.1	< 0.1	< 0.1	< 0.1	< 0.1	< 0.1	< 0.1	< 0.1	0.2	0.4	< 0.1	0.3
Th (ppm)	0.3	0.2	0.1	< 0.1	< 0.1	< 0.1	< 0.1	< 0.1	0.3	< 0.1	0.5	0.3	0.3	0.2	0.2

Table 5-2-2-1 Result of Chemical Analysis for Basalts (2)

	93SDCB09 -02A	93SDCB09 -02B	93SDCB09 -02C	93SDCB09 -02D	93SDCB09 -02E	93SDPG01 -02A	93SDPG01 -02B	93SDPG01 -02C	93SDPG01 -02D	93SDPG01 -02E	93SDPG03 -03A	93SDPG03 -03B	93SDPG03 -03C	93SDPG03 -03D	93SDPG03 -03E
SiO_2 (%)	51.30	51.08	51.09	50.58	51.54	53.68	53.77	53.24	53.58	52.67	51.63	50.90	53.16	52.60	53.12
TiO_2 (%)	0.52	0.60	0.51	0.50	0.54	0.69	0.69	0.69	0.69	0.70	0.73	0.73	0.68	0.70	0.69
Al_2O_3(%)	15.87	15.76	15.86	15.76	16.01	16.47	16.54	16.50	16.56	16.63	16.14	15.94	15.95	15.78	15.62
Fe_2O_3(%)	0.41	1.11	1.28	0.35	0.45	2.43	1.95	1.70	2.21	2.04	2.91	2.58	2.19	2.54	2.53
FeO (%)	8.01	7.87	7.26	8.04	7.92	6.35	6.77	7.55	6.66	7.05	8.71	9.09	8.47	8.39	8.20
MgO (%)	7.69	7.62	7.64	7.60	7.65	5.86	5.74	5.74	5.90	5.85	5.20	5.10	5.11	5.94	4.76
CaO (%)	12.29	12.22	12.24	12.17	12.34	10.42	10.28	10.42	10.30	10.45	10.16	10.12	9.85	9.77	9.55
MnO (%)	0.13	0.15	0.14	0.13	0.13	0.14	0.14	0.14	0.14	0.14	0.35	0.30	0.16	0.17	0.17
Na_2O (%)	1.62	1.64	1.65	1.64	1.67	2.21	2.17	2.19	2.24	2.23	2.20	2.29	2.19	2.23	2.18
K_2O (%)	0.38	0.39	0.38	0.43	0.40	0.60	0.57	0.62	0.64	0.64	0.72	0.74	0.83	0.82	0.82
P_2O_5 (%)	0.12	0.10	0.10	0.09	0.10	0.15	0.15	0.21	0.16	0.16	0.28	0.28	0.24	0.24	0.23
H_2O^+ (%)	0.75	0.40	0.35	0.35	0.45	0.60	0.75	0.55	0.45	0.60	0.35	0.65	0.45	0.20	0.55
H_2O^- (%)	0.09	0.04	0.02	0.04	0.04	0.03	0.03	0.04	0.04	0.04	0.01	0.02	0.04	0.03	0.01
CO_2 (%)	0.03	0.03	0.09	0.03	0.03	0.06	0.06	0.06	0.06	0.09	0.09	0.12	0.03	0.06	0.03
Total(%)	99.21	99.01	98.61	97.71	99.27	99.69	99.63	99.65	99.63	99.29	99.48	98.86	99.35	98.57	98.46
Ba (ppm)	58	59	58	58	58	93	91	92	91	93	104	101	107	104	104
Rb (ppm)	5.1	5.9	5.4	5.0	5.5	10.2	10.3	9.3	9.8	9.6	14.0	14.7	17.0	15.5	16.9
Sr (ppm)	236	240	238	238	240	231	230	232	232	234	494	488	464	464	460
Pb (ppm)	6	36	6	< 5	8	5	8	7	10	10	10	13	6	7	7
Zr (ppm)	45	65	55	45	50	55	55	60	64	47	80	80	84	75	80
Nb (ppm)	2.5	2.6	1.3	1.7	4.3	3.6	3.1	2.8	3.2	5.0	3.5	3.0	3.2	2.5	2.1
Y (ppm)	9.9	11.0	10.1	10.8	10.0	14.2	16.4	15.5	16.4	15.5	13.5	14.0	16.0	14.6	13.7
V (ppm)	196	194	188	193	201	241	248	245	256	244	303	303	293	288	290
Cr (ppm)	130.0	135.0	134.0	136.0	130.0	135.0	127.0	141.0	124.0	133.0	15.0	16.6	14.1	16.3	16.0
Ni (ppm)	79	78	73	82	75	67	69	79	74	78	56	49	22	25	24
Cu (ppm)	95	96	90	90	95	59	70	65	53	48	50	52	38	99	51
Zn (ppm)	64	71	60	69	66	73	79	75	81	78	97	105	84	84	85
Ga (ppm)	12.3	13.0	13.6	15.5	12.0	16.4	17.9	17.2	15.5	16.0	17.3	16.3	17.9	18.6	17.4
S (ppm)	< 50	< 50	< 50	100	< 50	130	210	60	185	75	215	305	155	740	3055
Sc (ppm)	35.1	35.7	35.3	35.8	35.0	34.4	34.2	32.7	32.6	33.3	33.9	35.5	34.3	34.4	35.4
Cs (ppm)	0.2	< 0.1	< 0.1	< 0.1	< 0.1	0.1	0.2	0.1	0.2	0.2	0.2	0.2	0.2	0.2	0.2
La (ppm)	4.0	4.0	4.0	4.1	4.0	7.4	7.5	7.3	7.0	7.1	16.0	14.7	15.8	15.5	15.5
Ce (ppm)	9.4	10.0	9.6	10.0	9.2	17.3	17.0	16.6	15.7	16.6	34.8	31.2	32.2	32.9	31.9
Nd (ppm)	5.2	4.9	5.2	4.1	4.4	7.2	7.0	8.0	6.6	6.3	18.4	16.3	17.1	17.5	17.5
Sm (ppm)	1.34	1.34	1.35	1.41	1.37	2.06	2.07	2.02	1.94	1.97	3.69	3.45	3.57	3.51	3.52
Eu (ppm)	0.46	0.51	0.50	0.49	0.49	0.67	0.71	0.70	0.66	0.72	1.10	1.14	1.06	1.10	1.12
Gd (ppm)	1.6	1.6	1.6	1.6	1.7	2.5	2.4	2.5	2.5	2.6	3.8	3.7	3.6	3.7	3.8
Tb (ppm)	0.33	0.28	0.28	0.32	0.25	0.53	0.48	0.48	0.47	0.48	0.43	0.51	0.42	0.58	0.38
Ho (ppm)	0.77	0.85	0.75	0.75	0.77	1.21	1.21	1.13	1.21	1.14	1.22	1.23	1.14	1.10	1.17
Tm (ppm)	0.25	0.23	0.22	0.23	0.25	0.32	0.31	0.32	0.34	0.37	0.32	0.35	0.29	0.29	0.31
Yb (ppm)	1.41	1.42	1.43	1.38	1.40	2.09	2.10	2.04	1.96	2.05	1.71	1.67	1.62	1.64	1.67
Lu (ppm)	0.20	0.20	0.21	0.21	0.20	0.30	0.31	0.30	0.30	0.30	0.23	0.24	0.23	0.23	0.25
Hf (ppm)	0.7	0.8	0.8	0.8	0.7	1.2	1.2	1.1	1.1	1.2	1.4	1.3	1.4	1.4	1.3
Ta (ppm)	< 0.1	0.3	0.3	< 0.1	0.4	0.2	0.3	0.2	0.1	0.3	0.3	0.2	0.2	0.3	0.4
Th (ppm)	0.5	0.6	0.5	0.5	0.4	0.8	0.9	1.0	0.9	0.8	1.7	1.4	1.8	1.6	1.7

Table 5-2-2-1 Result of Chemical Analysis for Basalts (3)

	93SDPG03 -05A	93SDPG03 -05B	93SDPG03 -05C	93SDPG03 -05D	93SDPG03 -05E									
SiO_2 (%)	65.86	66.39	58.60	61.47	56.12									
TiO_2 (%)	0.57	0.56	0.65	0.63	0.68									
Al_2O_3(%)	14.12	14.07	15.28	14.97	15.63									
Fe_2O_3(%)	0.26	1.08	2.73	2.60	2.56									
FeO (%)	5.63	4.51	6.21	4.94	7.48									
MgO (%)	1.76	1.73	3.28	2.74	3.98									
CaO (%)	5.04	5.00	7.50	6.65	8.46									
MnO (%)	0.10	0.10	0.17	0.13	0.15									
Na_2O (%)	3.19	3.18	2.76	2.85	2.45									
K_2O (%)	1.83	1.72	1.19	1.40	1.07									
P_2O_5 (%)	0.16	0.16	0.22	0.28	0.23									
H_2O^+ (%)	0.80	0.55	0.60	0.60	0.50									
H_2O^- (%)	0.03	0.02	0.02	0.03	0.03									
CO_2 (%)	0.06	0.09	0.06	0.06	0.03									
Total(%)	99.41	99.16	99.27	99.35	99.37									
Ba (ppm)	218	211	150	172	127									
Rb (ppm)	33.6	32.1	21.6	26.6	19.4									
Sr (ppm)	349	352	439	407	452									
Pb (ppm)	9	10	14	7	8									
Zr (ppm)	108	110	95	95	80									
Nb (ppm)	3.5	4.0	4.0	3.7	2.5									
Y (ppm)	23.9	24.0	18.9	19.3	17.2									
V (ppm)	110	110	215	179	252									
Cr (ppm)	11.1	9.7	20.7	11.1	15.0									
Ni (ppm)	12	9	30	16	22									
Cu (ppm)	46	48	58	50	66									
Zn (ppm)	65	66	82	76	83									
Ga (ppm)	15.1	16.1	15.8	16.0	16.3									
S (ppm)	< 50	< 50	620	2070	1800									
Sc (ppm)	16.1	16.5	25.5	23.6	30.2									
Cs (ppm)	0.4	0.4	0.2	0.3	0.2									
La (ppm)	15.6	16.0	15.5	15.8	15.0									
Ce (ppm)	32.0	34.9	34.7	36.0	32.1									
Nd (ppm)	15.7	17.6	17.1	16.9	17.9									
Sm (ppm)	3.29	3.37	3.51	3.57	3.53									
Eu (ppm)	0.99	1.09	1.07	1.10	1.03									
Gd (ppm)	3.8	3.9	3.9	4.1	3.8									
Tb (ppm)	0.58	0.56	0.67	0.65	0.56									
Ho (ppm)	1.56	1.50	1.54	1.52	1.32									
Tm (ppm)	0.47	0.47	0.44	0.38	0.36									
Yb (ppm)	2.46	2.53	2.18	2.35	1.84									
Lu (ppm)	0.36	0.37	0.31	0.34	0.27									
Hf (ppm)	2.4	2.5	1.9	2.3	1.5									
Ta (ppm)	0.2	0.4	0.2	0.3	0.2									
Th (ppm)	1.8	2.2	1.9	1.9	1.6									

and E added to the end of the sample numbers represent the points analyzed. A and B represent the epidermic parts (vitric part) or fine-grained parts, C, D and E represent the inner parts or coarse-grained parts.

Various relational diagrams of elements, AFM diagrams and chondrite normalization diagrams were drawn, and the norm calculation was made by utilizing the results of these analyses, to examine the following matters.

A relational diagram between Na_2O and CaO is shown in Fig. 5-2-2-4 for setting up a standard to estimate the degree of alteration of various rocks. Except the fine-grained part of the sample 93SDPG03-05, all the samples are in the domain of non-spilite and, as indicated by the observation of thin sections, most of the samples are estimated to be non-altered.

Fig. 5-2-2-5 shows a diagram plotted with the results of the analyses on the simplified rock taxonomic standards by SiO_2 and MgO. All the MgO values are less than 10 wt%. SiO_2 values of those four samples classified as the tholeiitic series, i.e. 93SDCB01-03, 93SDCB05-03, 93SDCB07-04 and 93SDCB09-02, are less than 53 wt%, which means "basalt", and SiO_2 values of those two samples of augite hypersthene basaltic andesite ~ non-porphyritic basaltic andesite classified as the calc-alkaline series (93SDPG01-02 and 93SDPG03-03) are "low SiO_2 andesite" ~ "basalt" plotted in the vicinity of 53 wt%. The augite hypersthene andesite as the coarse-grained part of the sample 93SDPG03-05 is plotted as "high-SiO_2 andesite" of SiO_2 57 ~ 63 wt%. The non-porphyritic andesite as the fine-grained part of the same sample is plotted as "dacite" of SiO_2 63 ~ 70 wt%.

Furthermore, all the samples are plotted in the domains of "tholeiite" of Macdonald & Katsura (1964), "non-alkaline" of Kuno (1966) and "non-alkali basalt" ~ "non-alkali andesite" ~ "dacite" of Miyashiro and Kushiro (1975) on the SiO_2- Na_2O + K_2O diagram for simplified rock taxonomic standards (Fig. 5-2-2-6).

The results of the norm calculation are shown in Table 5-2-2-2. Norm-nepheline is not calculated up from any sample. The tholeiite series olivine basalt ~ non-porphyritic basalt determined by the observation of thin sections, i.e. three samples of 93SDCB01-03, 93SDCB05-03 and 93SDCB07-04, does not have norm-quartz and is characterized by the assemblage of norm-olivine and norm-hypersthene. But the four samples of the tholeiite series olivine basalt with augite phenocryst (93SDCB09-02) and the calc-alkaline series augite hypersthene basaltic andesite ~ non-porphyritic basaltic andesite (93SDPG01-02, 93SDPG03-03 and 93SDPG03-05) have norm-quartz.

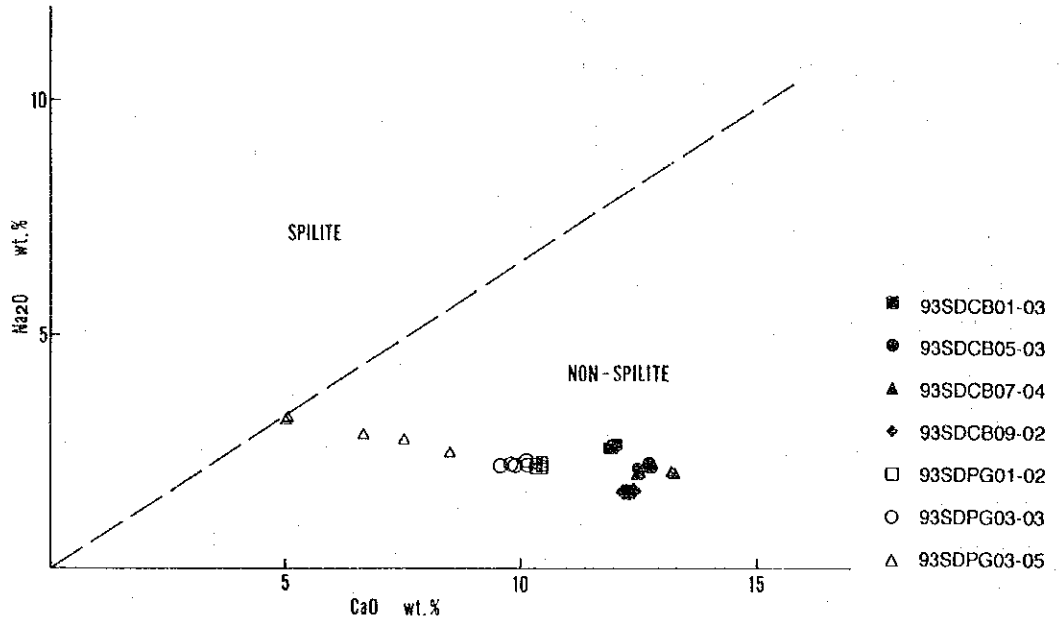

Figure 5-2-2-4 CaO versus Na_2O for basalts

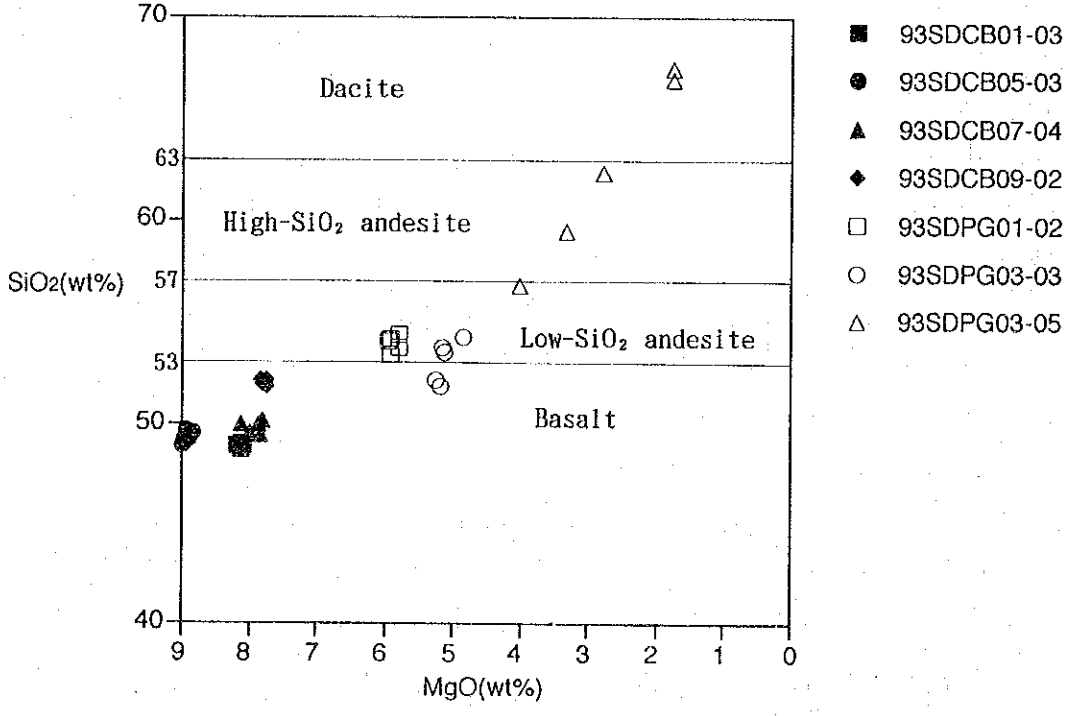

Figure 5-2-2-5 SiO_2 versus MgO for basalts

Table 5-2-2-2 Results of Norm Calculation for Basalts (1)

	93SDCB01 -03A	93SDCB01 -03B	93SDCB01 -03C	93SDCB01 -03D	93SDCB01 -03E	93SDCB05 -03A	93SDCB05 -03B	93SDCB05 -03C	93SDCB05 -03D	93SDCB05 -03E	93SDCB07 -04A	93SDCB07 -04B	93SDCB07 -04C	93SDCB07 -04D
Q														
or	0.65	0.47	0.53	0.77	0.47	0.30	0.24	0.30	0.24	0.53	2.30	2.01	1.60	1.54
ab	22.17	22.00	22.42	22.42	22.25	18.28	18.28	18.11	19.29	18.53	17.43	17.01	17.18	17.43
an	30.81	30.47	30.98	30.97	31.40	33.49	32.59	32.68	32.57	32.66	32.14	32.24	34.05	33.70
mt	3.20	3.03	3.71	3.54	3.89	2.83	2.31	1.84	1.12	1.13	1.99	1.70	0.91	
il	2.43	2.45	2.43	2.43	2.47	1.77	1.80	1.65	1.69	1.73	1.39	1.37	1.33	1.41
ap	0.32	0.35	0.32	0.35	0.32	0.21	0.21	0.19	0.21	0.25	0.30	0.28	0.25	0.23
fs-di	3.95	4.05	3.85	3.81	3.42	3.84	4.26	4.20	4.77	4.63	4.97	4.76	5.20	5.49
en-di	6.87	6.93	7.08	7.02	6.97	7.50	7.63	7.13	7.18	7.08	6.71	6.66	7.21	7.09
wo-di	11.43	11.58	11.58	11.48	11.08	12.06	12.58	11.95	12.50	12.27	12.14	11.90	12.93	13.04
en-hy	4.64	4.28	3.80	4.43	5.84	6.13	6.26	8.01	3.94	5.86	5.65	7.49	4.48	4.86
fs-hy	2.67	2.50	2.06	2.40	2.87	3.15	3.49	4.72	2.61	3.83	4.19	5.34	3.23	3.76
fa-ol	3.70	3.98	3.85	3.57	2.70	3.39	3.56	3.13	5.62	4.49	3.83	2.65	4.40	4.81
fo-ol	5.84	6.18	6.43	5.98	4.99	6.00	5.80	4.82	7.68	6.24	4.69	3.37	5.54	5.64

	93SDCB07 -04E	93SDCB09 -02A	93SDCB09 -02B	93SDCB09 -02C	93SDCB09 -02D	93SDCB09 -02E	93SDPG01 -02A	93SDPG01 -02B	93SDPG01 -02C	93SDPG01 -02D	93SDPG01 -02E	93SDPG03 -03A	93SDPG03 -03B	93SDPG03 -03C
Q		2.16	2.45	2.85	1.40	2.09	7.66	7.74	6.23	6.98	5.61	4.98	3.66	6.78
or	1.60	2.25	2.30	2.25	2.54	2.36	3.55	3.49	3.66	3.78	3.78	4.25	4.37	4.90
ab	17.52	13.71	13.88	13.96	13.88	14.13	18.70	18.36	18.53	18.95	18.87	18.62	19.38	18.53
an	33.43	34.91	34.49	34.75	34.37	35.01	33.25	33.65	33.36	33.24	33.48	32.04	31.03	31.24
mt	0.25	0.59	1.61	1.86	0.51	0.65	3.52	2.83	2.46	3.20	2.96	4.22	3.74	3.18
il	1.35	0.99	1.14	0.97	0.95	1.03	1.31	1.31	1.31	1.31	1.33	1.39	1.39	1.29
ap	0.25	0.28	0.23	0.23	0.21	0.23	0.35	0.35	0.49	0.37	0.37	0.65	0.65	0.56
fs-di	5.61	4.23	4.10	3.83	4.32	4.25	2.60	2.69	3.07	2.63	2.88	3.40	3.74	3.32
en-di	7.04	5.90	6.07	6.23	5.89	5.99	4.32	3.86	3.79	4.06	4.06	3.38	3.41	3.27
wo-di	13.08	10.55	10.64	10.57	10.61	10.67	7.29	6.84	7.08	7.02	7.23	6.90	7.24	6.71
en-hy	5.52	13.26	12.91	12.80	13.04	13.07	10.27	10.43	10.51	10.63	10.52	9.57	9.29	9.46
fs-hy	4.40	9.52	8.72	7.87	9.57	9.27	6.17	7.25	8.51	6.89	7.48	9.63	10.17	9.60
fa-ol	4.08													
fo-ol	4.64													

Table 5-2-2-2 Results of Norm Calculation for Basalts (2)

	93SDPG03 -03D	93SDPG03 -03E	93SDPG03 -05A	93SDPG03 -05B	93SDPG03 -05C	93SDPG03 -05D	93SDPG03 -05E							
Q	6.56	8.20	24.18	26.46	15.99	20.77	12.04							
or	4.85	4.85	10.81	10.16	7.03	8.27	6.32							
ab	18.87	18.45	26.99	26.91	23.35	24.12	20.73							
an	30.63	30.41	18.80	19.04	25.79	23.92	28.49							
mt	3.68	3.67	0.38	1.57	3.96	3.77	3.71							
il	1.33	1.31	1.08	1.06	1.23	1.20	1.29							
ap	0.56	0.53	0.37	0.37	0.51	0.65	0.53							
fs-di	3.32	3.21	1.51	1.21	2.08	1.39	2.57							
en-di	3.34	3.14	0.71	0.78	2.02	1.55	2.37							
wo-di	6.80	6.46	2.15	1.97	4.17	3.02	5.00							
en-hy	9.21	8.72	3.68	3.53	6.15	5.27	7.55							
fs-hy	9.14	8.93	7.85	5.44	6.31	4.73	8.20							
fa-ol														
fo-ol														

Abbreviation

Q :quartz
or :orthoclase
ab :albite
an :anorthite
mt :magnetite
il :ilmenite
ap :apatite
fs-di :ferrosilite-diopside
en-di :enstatite-diopside
wo-di :wollastonite-diopside
en-hy :enstatite-hypersthene
fs-hy :ferrosilite-hypersthene
fa-ol :fayalite
fo-ol :forsterite

Therefore, according to the taxonomy of Yoder & Tilley (1962), the former three samples will be olivine tholeiite and the latter four samples will be tholeiite oversaturated by silica. Adiagram plotted with the calculated values of norm into the Yoder & Tilley (1962) Di-Q-Hy-Ol triangular diagrams are shown in Fig. 5-2-2-7.

An AFM diagram is shown in Fig. 5-2-2-8. The samples 93SDPG03-03 and 93SDPG03-05, which have been classified as the calc-alkaline series, are plotted on the border of the Kuno's (1968) pigeonitic series and hypersthenic series, others are plotted in the domain of the hypersthenic series. Which does not confirm with the results of the observation of thin sections. But according to the classification of calc-alkaline series and tholeiite series based on Irvine & Baragar (1971), all the samples are located on the border between the two series. They also do not come under the tholeiitic trend of Perfit & Formari's (1983) Mid Pacific Ridge Basalt (N-MORB).

A relational diagram of FeO*/MgO and SiO_2 is shown in Fig. 5-2-2-9 and a relational diagram of FeO*/MgO and FeO* is shown in Fig. 5-2-2-10. Of the two samples that have been classified as the calc-alkaline series, i.e. 93SDPG03-03 and 93SDPG03-05, the sample 93SDPG03-03 is plotted in the tholeiitic domain and the sample 93SDPG03-05 is plotted on the boder between the tholeiitic domain and calc-alkaline domain. Except these two, all the remaining samples' FeO*/MgO values are below 2. Which means that they cannot be classified into any series. They seem to have the composition close to parental magma.

Although an analyzed value of Al2O3 exceeding 16.5% is resulted from the sample 93SDPG01-02, this sample is two-pyroxene andesite. So we can say that there is no high alumina basalt at least in the samples collected in this cruise.

Under the relational diagram of SiO_2 and K_2O (Fig. 5-2-2-11), all the samples are in the range of the "lower-K_2O series" of Johnson et al. (1987) and almost all the samples of "andesite" is "medium-K andesite" of Gill (1978). Under the relational diagram of SiO_2 and Na_2O (Fig. 5-2-2-12), however, the three samples classified by the thin section observation as the tholeiitic series olivine basalt ~ non-porphyritic basalt, i.e. 93SDCB01-03, 93SDCB05-03 and 93SDCB07-04, come off the range of the "lower-K_2O series" and slightly close to the higher Na_2O side. Under the relational diagram of SiO_2 and P_2O_5 (Fig. 5-2-2-13), not only the above-mentioned three samples come off the range of the "lower-K_2O series" and slightly close to the higher P_2O_5 side, but a part of the sample classified as the calc-alkaline series non-porphyritic basaltic andesite by the observation of thin sections also comes into the "higher-K_2O

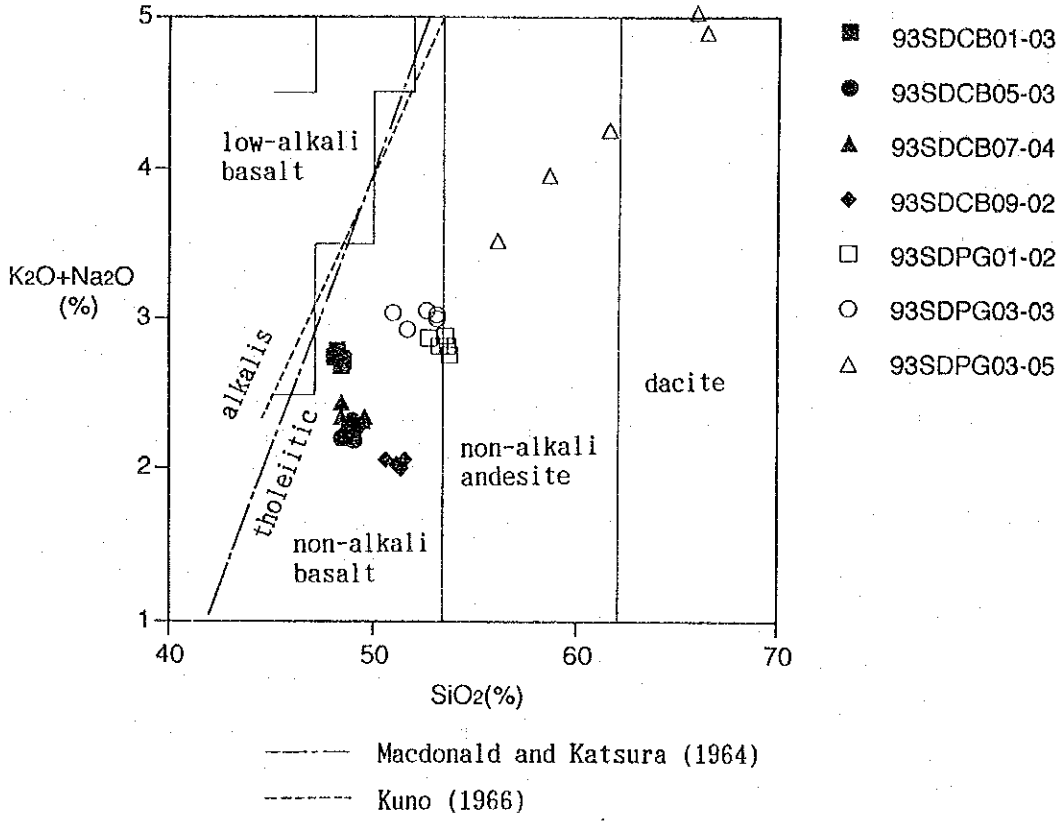

Figure 5-2-2-6 SiO_2 versus Na_2O+K_2O for basalts

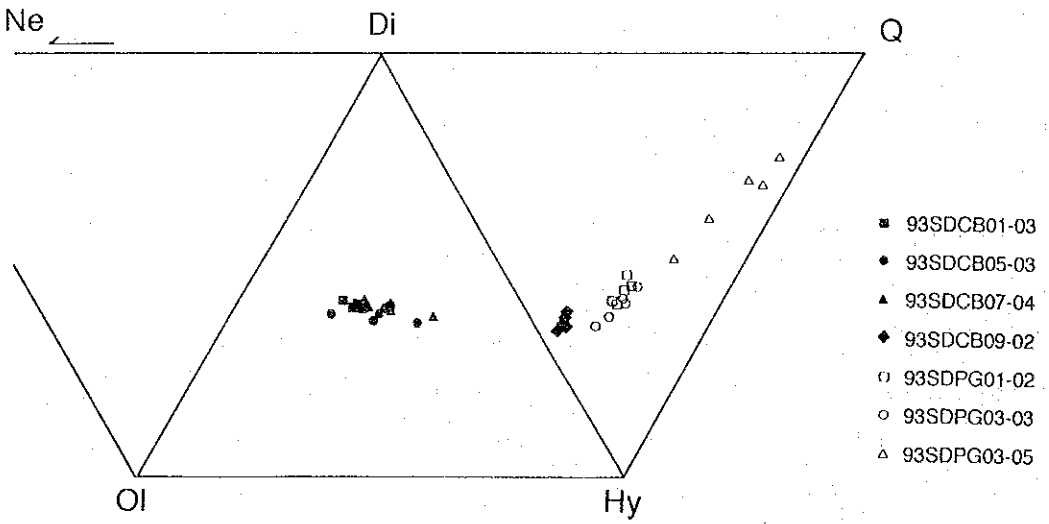

Figure 5-2-2-7 Diagram using Norm Di-Q-Hy-Ol for basalts

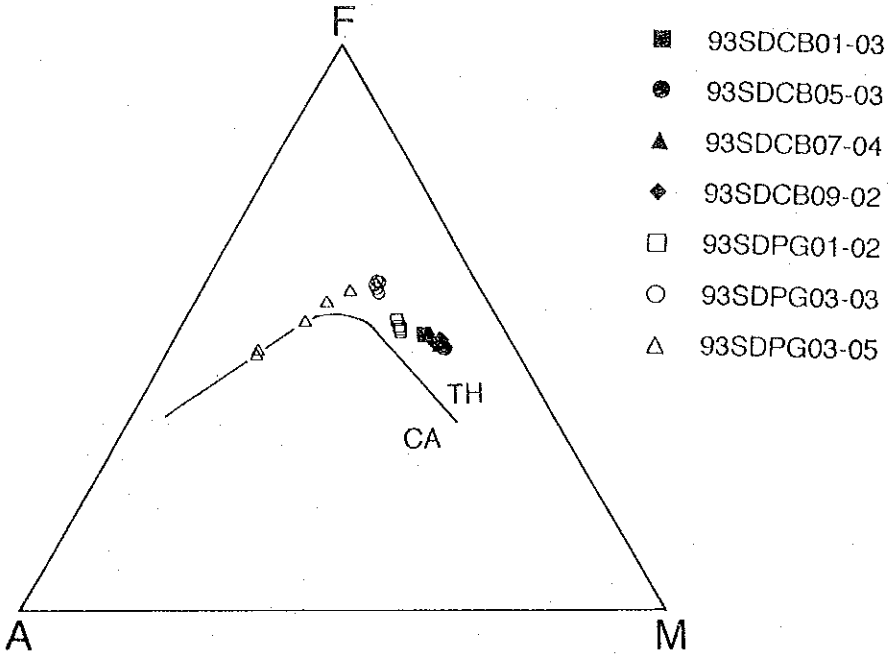

※ A: Na_2O+K_2O, F: $FeO+Fe_2O_3\times0.8998$, M: MgO
Boundary line is quoted from Irvine and Baragar (1971)

Figure 5-2-2-8 AFM diagram for basalts

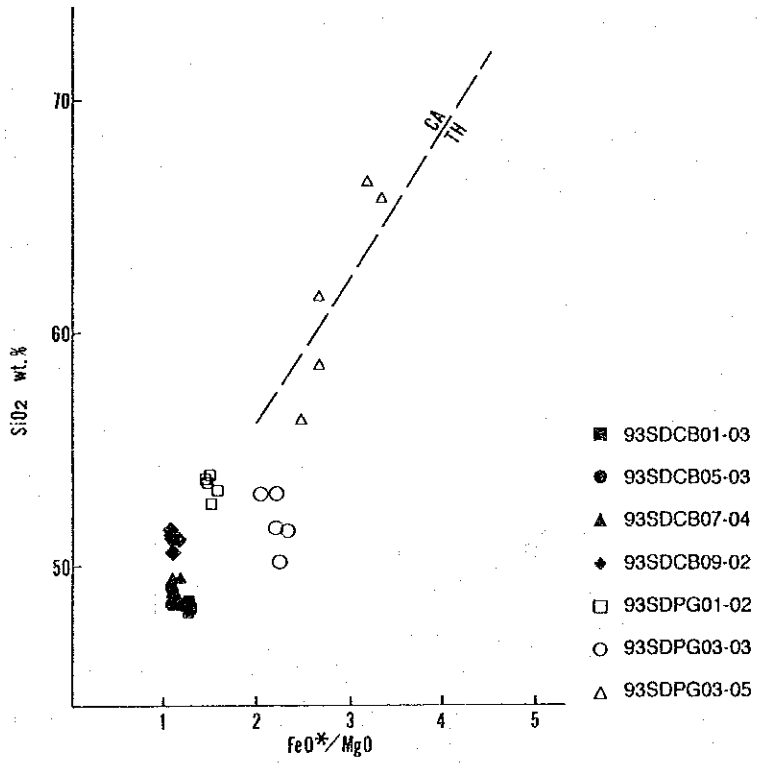

Figure 5-2-2-9 FeO*/MgO versus SiO_2 for basalts

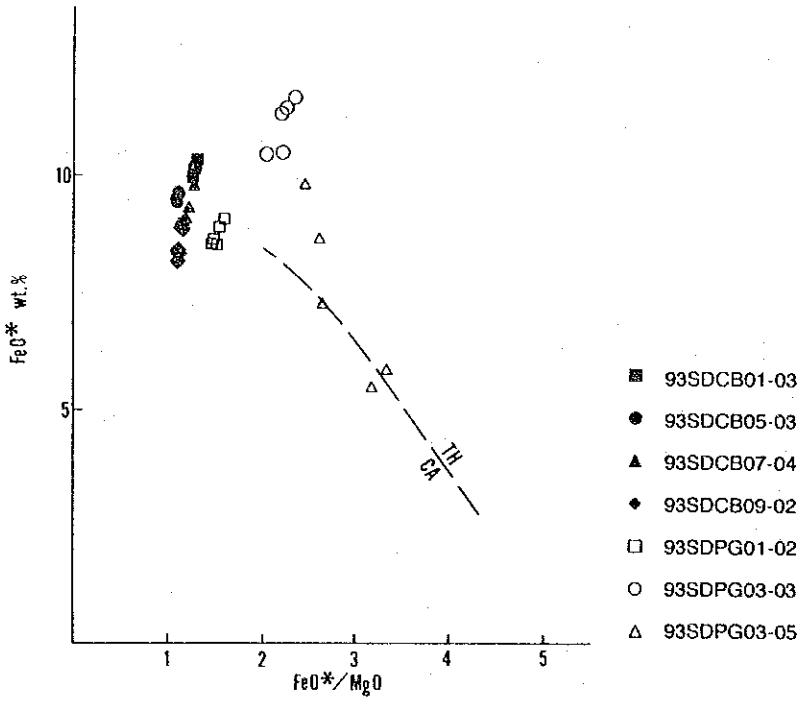

Figure 5-2-2-10 FeO*/MgO versus FeO* for basalts

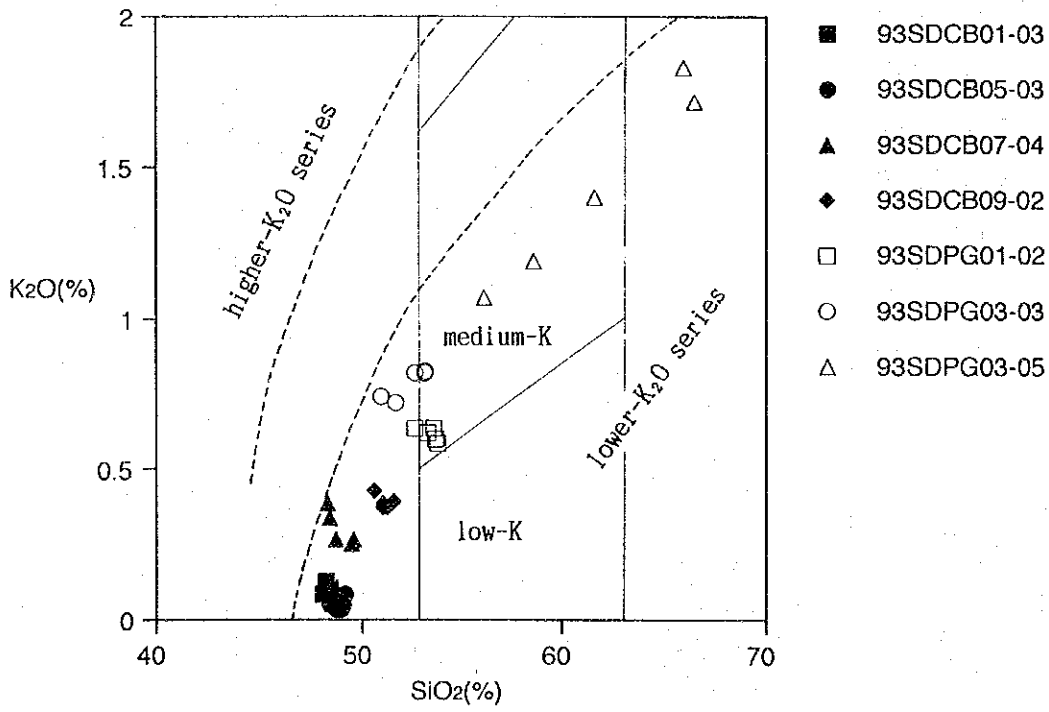

Figure 5-2-2-11 SiO_2 versus K_2O for basalts

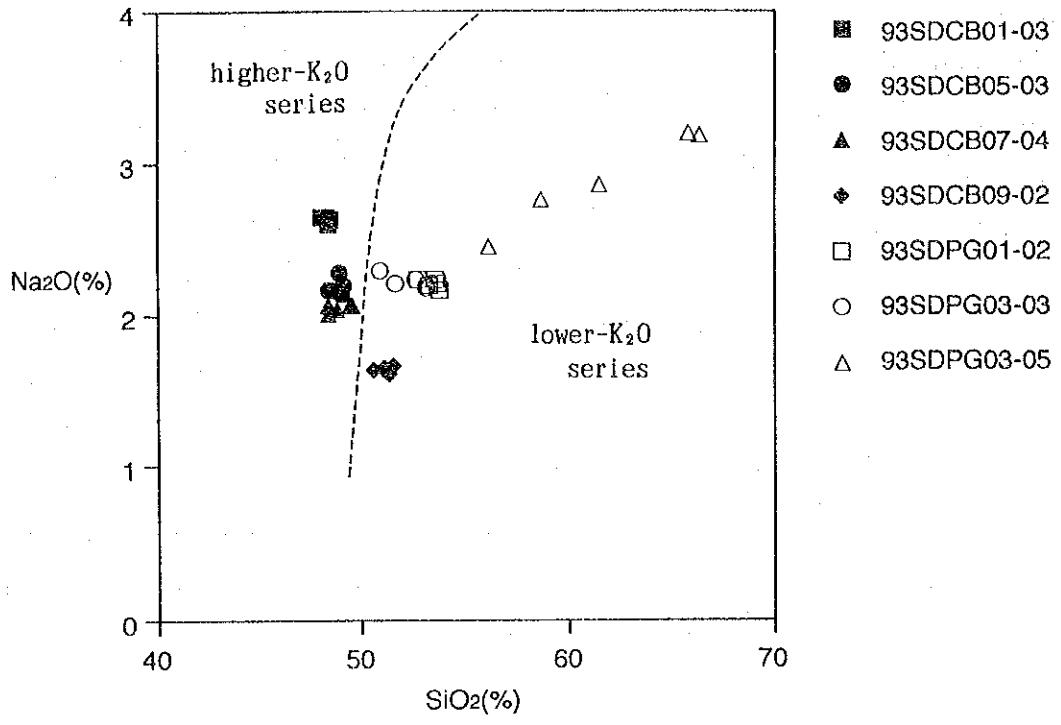

Figure 5-2-2-12 SiO_2 versus Na_2O for basalts

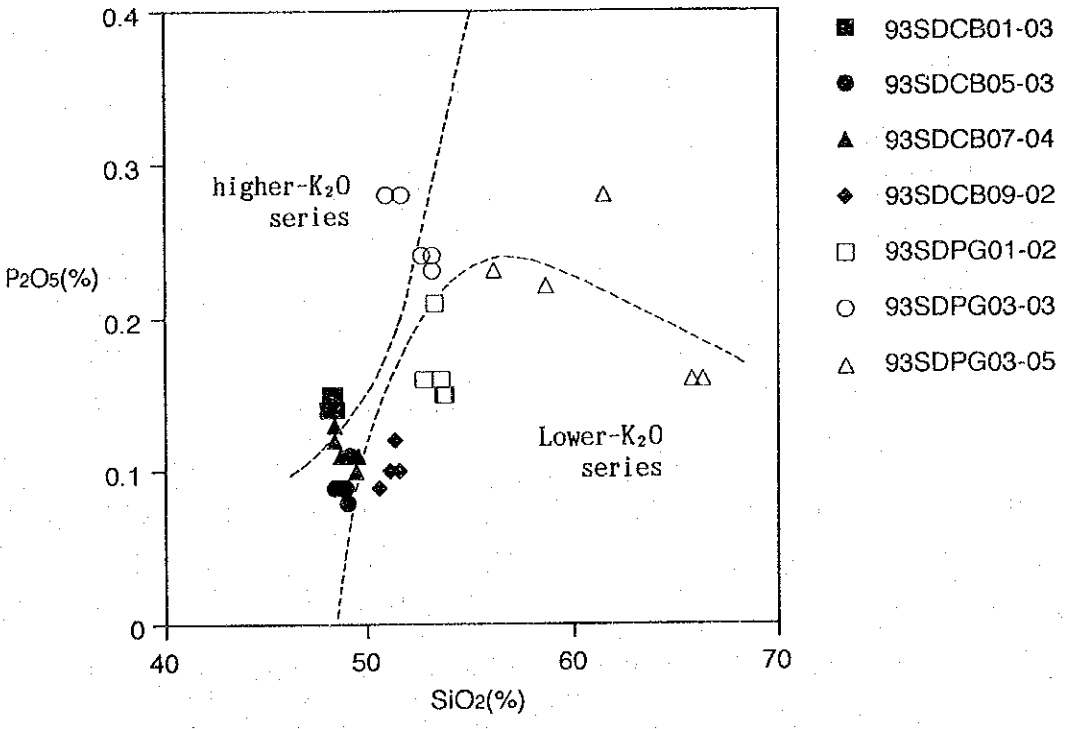

Figure 5-2-2-13 SiO_2 versus P_2O_5 for basalts

series."

A relational diagram of Zr and TiO_2 is shown in Fig. 5-2-2-14. Two samples, i.e. 93SDPG03-03 and 93SDPG03-05, are plotted in the range of Pearce & Cann's (1973) "calc-alkaline basalt", other two samples, i.e. 93SDCB05-03 and 93SDCB01-03, are plotted in the range of "seafloor basalt" and the rest of the samples in the range of "lower-K tholeiite".

A relational diagram of MgO and Ni is shown in Fig. 5-2-2-15 and a relational diagram of MgO and Cr is shown in Fig. 5-2-2-16. Both of them clearly show the trend of differentiation and from which we can see that the degree of differentiation increases in order of 93SDCB05-03 → 93SDCB01-03 → 93SDCB07-04 → 93SDCB09-02 → 93SDPG01-02 → 93SDPG03-03 → 93SDPG03-05. Especially, the three samples of 93SDCB05-03, 93SDCB01-03 and 93SDCB07-04, which show the values of NI>80ppm · Cr>200ppm, come under a primitive category even compared with the basic rock reported by Johnson et al. (1987).

A relational diagram of MgO and Al_2O_3 is shown in Fig. 5-2-2-17. All the four tholeiite series samples, i.e. 93SDCB01-03, 93SDCB05-03, 93SDCB07-04 and 93SDCB09-02, come under the range of Johnson et al. (1987) "MORB" and Bence et al.(1979) "MORB glass". Except these, all the remaining samples will roughly come under the range of "New Georgia volcanic rocks" of Johnson et al. (1987).

The highest values of Mg# (100 Mg/Mg + Fe^{2+}) are between 67.1 and 63.7, which are marked by the sample 93SDCB05-03, but such samples as exceeding Mg#70 (low TiO_2 alkaline basalt, magnesian andesite and picrite) identified by Johnson et al. (1987) are not found among the samples in this cruise. A relational diagram of Mg# and TiO_2 is shown in Fig. 5-2-2-18. Generally speaking, the samples in this cruise are poor in TiO_2, and only the sample 93SDCB01-03 come under the ranges of "MORB" of Johnson et al. (1987) and "MORB glass" of Bence et al. (1979). Among the remaining samples, 93SDCB05-03, 93SDCB07-04 and 93SDPG01-02 are plotted in the range where "MORB glass" of Bence et al. (1979) and "New Georgia volcanic rocks" of Johnson et al. (1987) overlap each other, and, 93SDCB09-02, 93SDPG03-03 and 93SDPG03-05 are plotted in the range of "New Georgia volcanic rocks" of Johnson et al.(1987).

Under the relational diagram of SiO_2 and K_2O/TiO_2 (Fig. 5-2-2-19), Johnson et al. (1987) reported that samples with values higher than 2.0 of K_2O/TiO_2 were obtained from the andesite ~ basalt collected from the trench part and samples with values lower than 2.0 of K_2O/TiO_2 were obtained from the basalt ~ andesite collected from

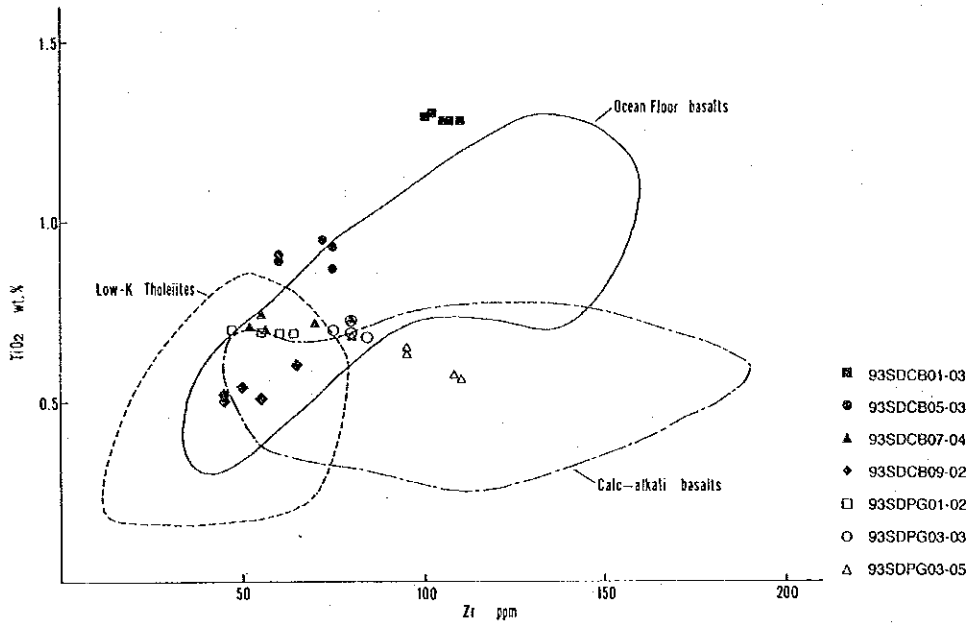

Figure 5-2-2-14 Zr versus TiO_2 for basalts

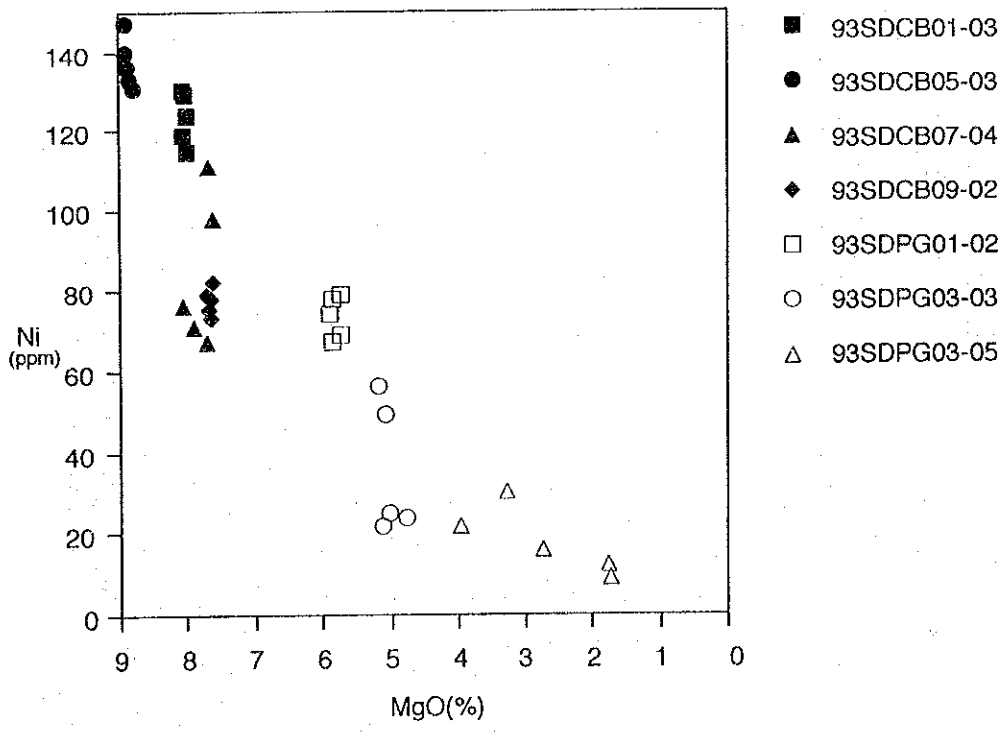

Figure 5-2-2-15 MgO versus Ni for basalts

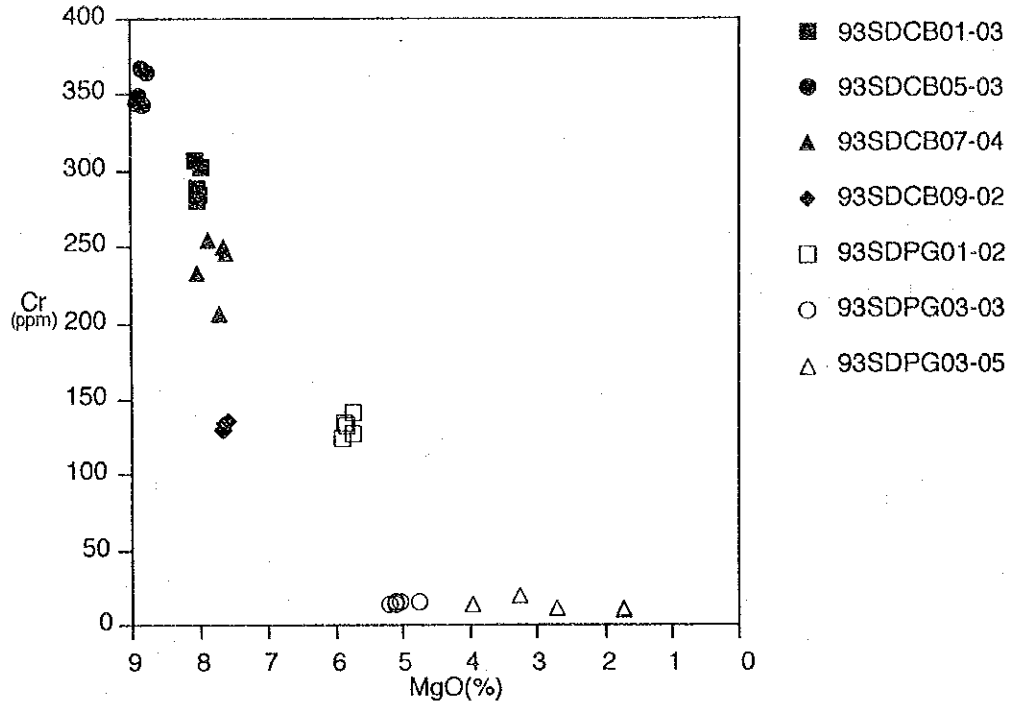

Figure 5-2-2-16 MgO versus Cr for basalts

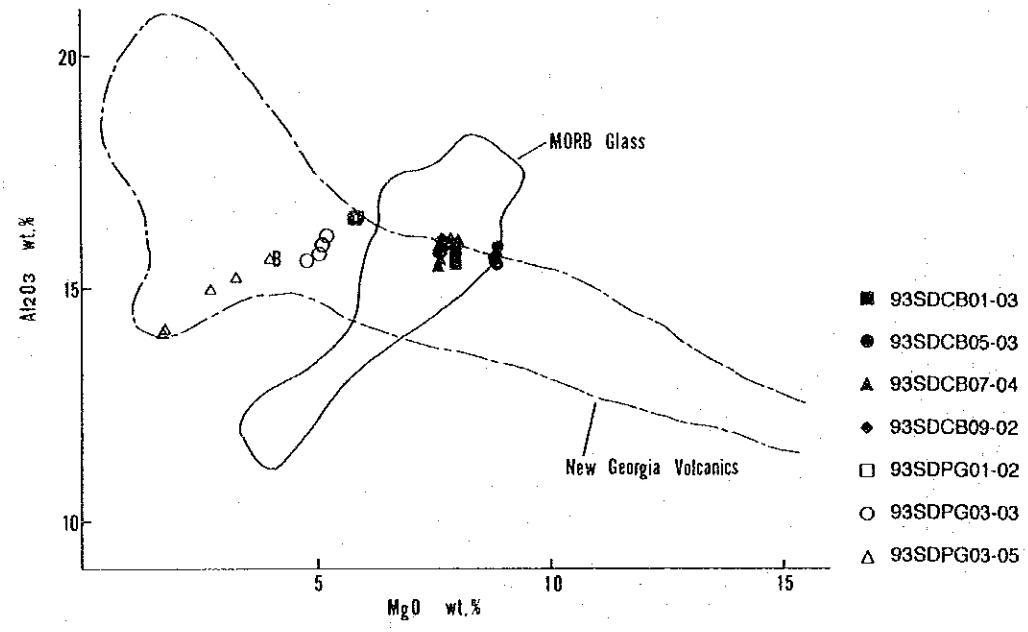

Figure 5-2-2-17 MgO versus Al_2O_3 for basalts

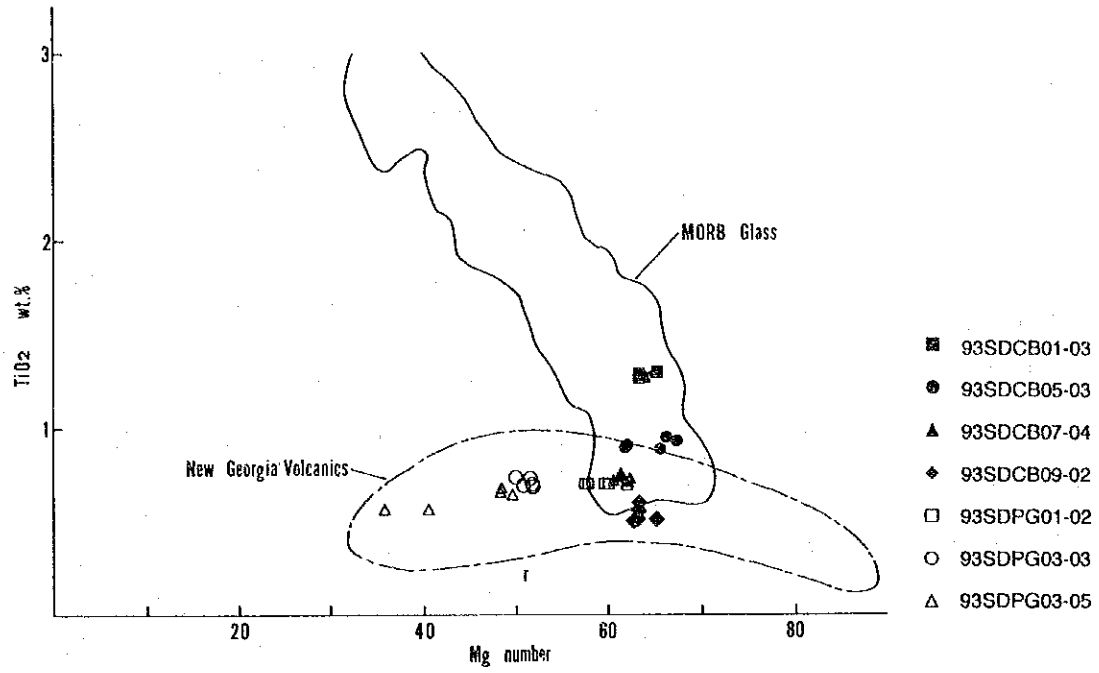

Figure 5-2-2-18 Mg# versus TiO_2 for basalts

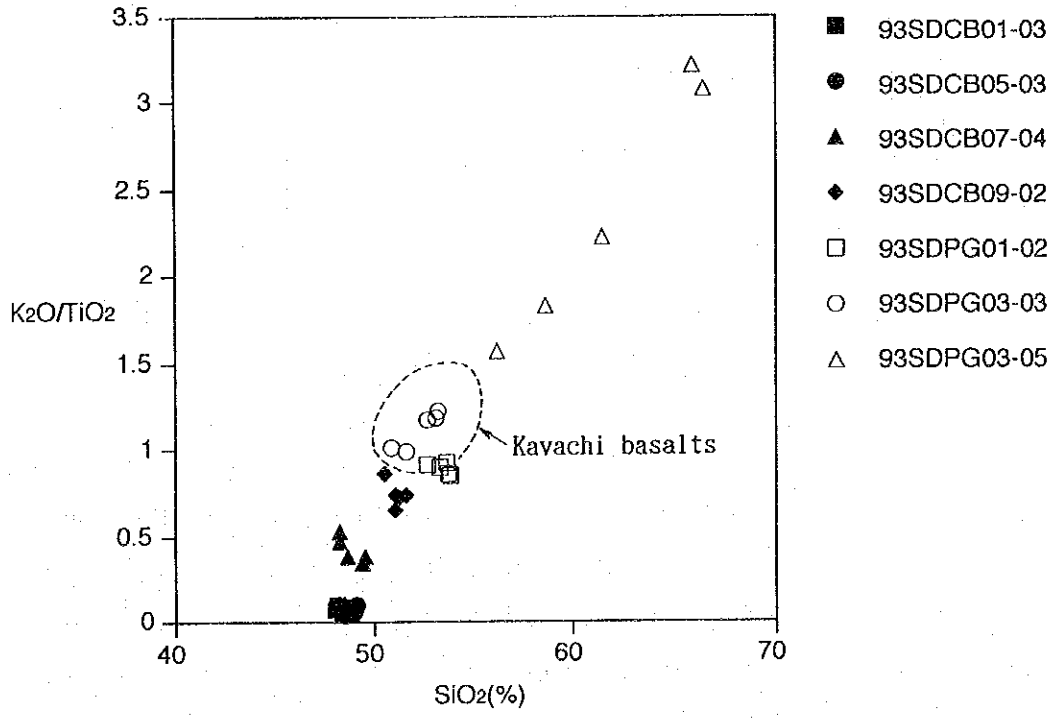

Figure 5-2-2-19 SiO_2 versus K_2O/TiO_2 for basalts

the seafloor a little bit away from the trench and from the Kavachi Seamount. They also suggested that the samples with higher values were created under a typical island arc environment. Among the samples in this cruise, however, only a part of the sample 93SDPG03-05, which is classified as the calc-alkaline series non-porphyritic andesite and two-pyroxene andesite, shows a value of K_2O/TiO_2 higher than 2.0.

A relational diagram of Na_2O and TiO_2 is shown in Fig. 5-2-2-20. Generally speaking, the samples in this cruise have a tendency to be poor in TiO_2. Except the sample 93SDPG03-05, which is plotted in the range of "New Georgia volcanic rocks" of Johnson et al. (1987), most of the samples are plotted in the range of "Mid-Atlantic Ridge MORB". Generally, basic rocks created under a back arc environment contain a higher percentage of Na_2O and a lower percentage of TiO_2.

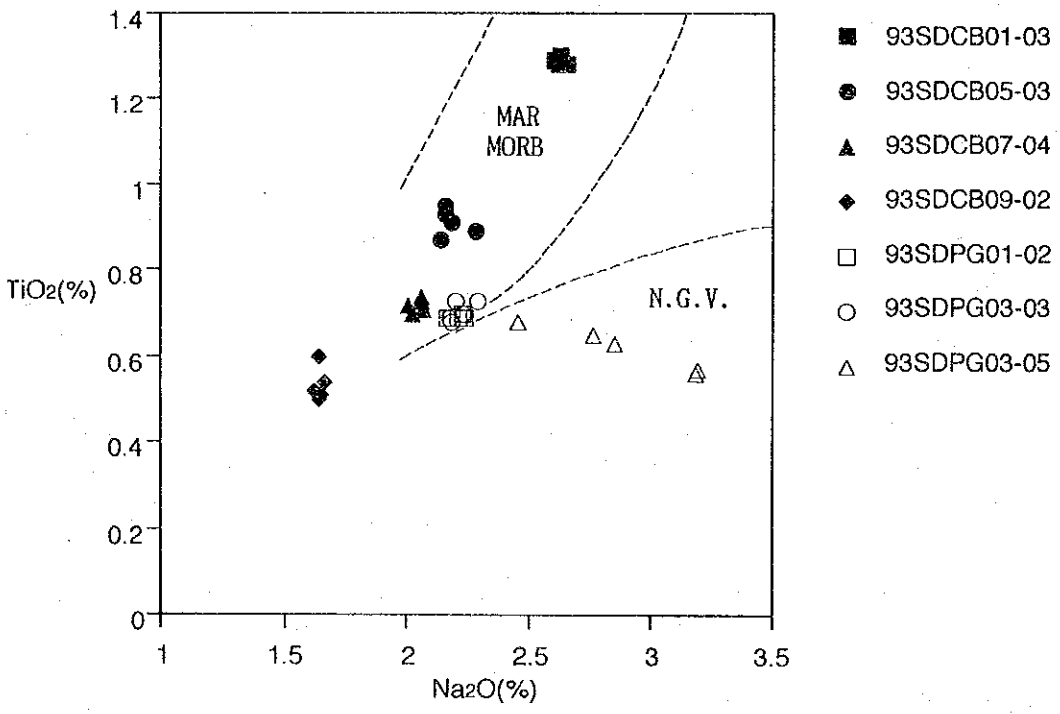

Figure 5-2-2-20 Na_2O versus TiO_2 for basalts

A relational diagram of MgO and FeO is shown in Fig. 5-2-2-21 and a relational diagram of MgO and TiO_2 is shown in Fig. 5-2-2-22. Fryer et al. (1981) used these diagrams to classify MORB and BABB (Back Arc Basin Basalt). Among the samples in this cruise, 93SDCB05-03 and 93SDCB01-03 are plotted between MORB and BABB and, 93SDCB07-04 and 93SDCB09-02 are plotted in the range of BABB.

A chondritic normalization rare earth pattern is shown in Fig. 5-2-2-23. The values used for the normalization are based on the "Recommendable chondritic values

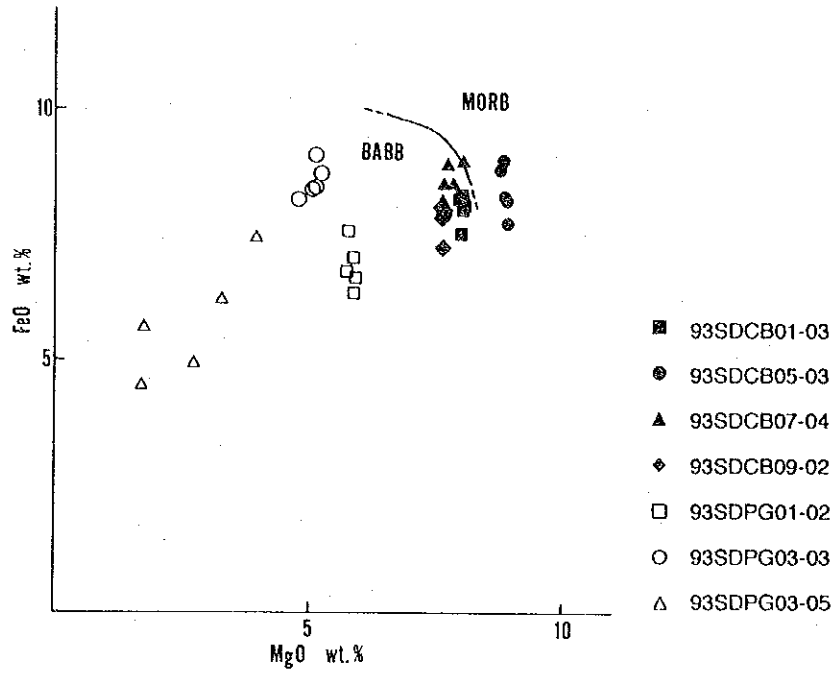

Figure 5-2-2-21 MgO versus FeO for basalts

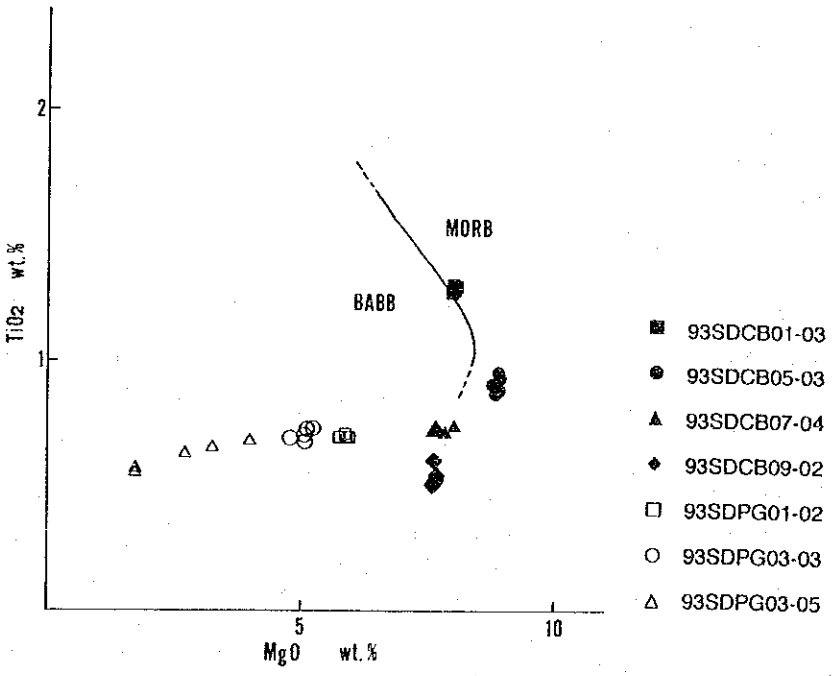

Figure 5-2-2-22 MgO versus TiO_2 for basalts

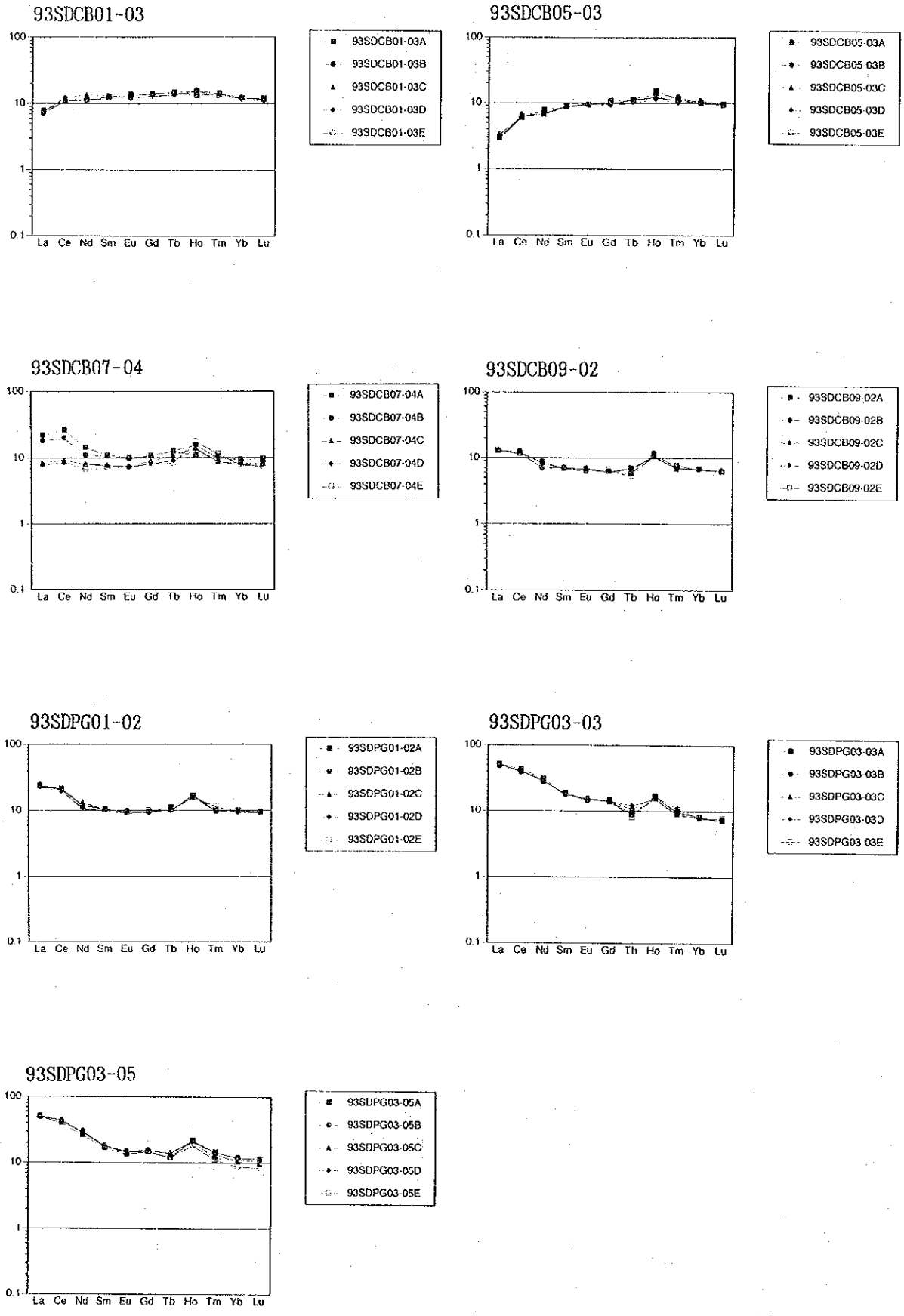

Figure 5-2-2-23 Chondrite-normalized rare earth element patterns for basalts

for normalization" by Boynton (1984). The samples 93SDCB05-03 and 93SDCB01-03 show an N-MORB similarity pattern slanting downward from the right to the left. The samples 93SDPG01-02, 93SDPG03-03 and 93SDPG03-05 show an oceanic island tholeiite ~ island arc basalt similarity pattern slanting upward from the right to the left. The rest of the samples show a middle pattern of these two.

As for the trace component, it is generally known that ridge basalt is rich in Zr, Ti, Y, La, Ce, Nd and Nb and island arc basalt is rich in Rb, Ba, Sr and Cs. We, therefore, can classify the two by combining these elements.

A relational diagram of Sr and Zr is shown in Fig. 5-2-2-24. Generally, MORB is plotted on the Sr/Zr = 1 ~ 1.5 line but island arc volcanism is rich in alkali· alkaline earth metal such as Sr and poor in HFS elements (high field strength elements) such as Zr. The samples 93SDCB05-03 and 93SDCB01-03 are plotted on this MORB line and the samples 93SDCB07-04 → 93SDCB09-02 and 93SDPG01-02 are plotted in the area from the MORB to the trend indicating the influence of island volcanism. The samples 93SDPG03-03 and 93SDPG03-05 form another group which is different from these trends. The degree of partial melting of 93SDCB05-03 differs from that of 93SDCB01-03. From which we can presume that the melting degree of 93SDCB05-03 was higher.

A relational diagram of Ce and Ba is shown in Fig. 5-2-2-25. Generally, rocks of island arc volcanism are plotted on the Ba side and rocks of back arc volcanism and MORB are plotted on the Ce side when dividing the two sides by a Ba/Ce = 5 line. The samples in this cruise are entirely plotted on the back arc ~ MORB side.

A relational diagram of Zr and Ce is shown in Fig. 5-2-2-26. Johnson et al. (1987) suggested that rocks of MORB would be plotted roughly on the Ce/Zr = 0.11 line and rocks of island arc volcanism would be plotted roughly on the Ce/Zr = 0.33 line. Among the samples in this cruise, the four samples classified as the tholeiitic series, i.e. 93SDCB05-03, 93SDCB01-03, 93SDCB07-04 and 93SDCB09-02, are regarded as corresponding to the former and the three samples classified as the calc-alkaline series, i.e. 93SDPG01-02, 93SDPG03-03 and 93SDPG03-05 are regarded as corresponding to the latter.

Fig. 5-2-2-27 shows a relational diagram of (Sr/Nd)n and MgO and Fig. 5-2-2-28 shows a relational diagram of (Ba/Ce)n and MgO. The symbol of ( )n indicates the chondritic normalization. In the case of the four samples regarded as the tholeiitic series, the island arc nature becomes stronger in order of 93SDCB01-03 → 93SDCB05-03 → 93SDCB07-04 → 93SDCB09-02.

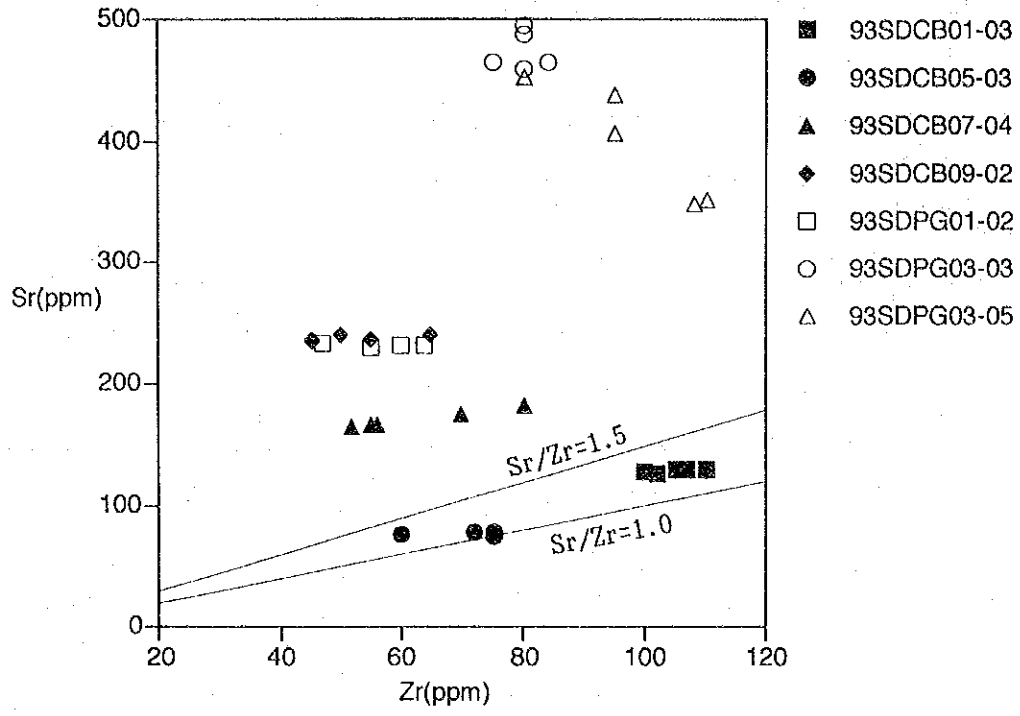

Figure 5-2-2-24 Sr versus Zr for basalts

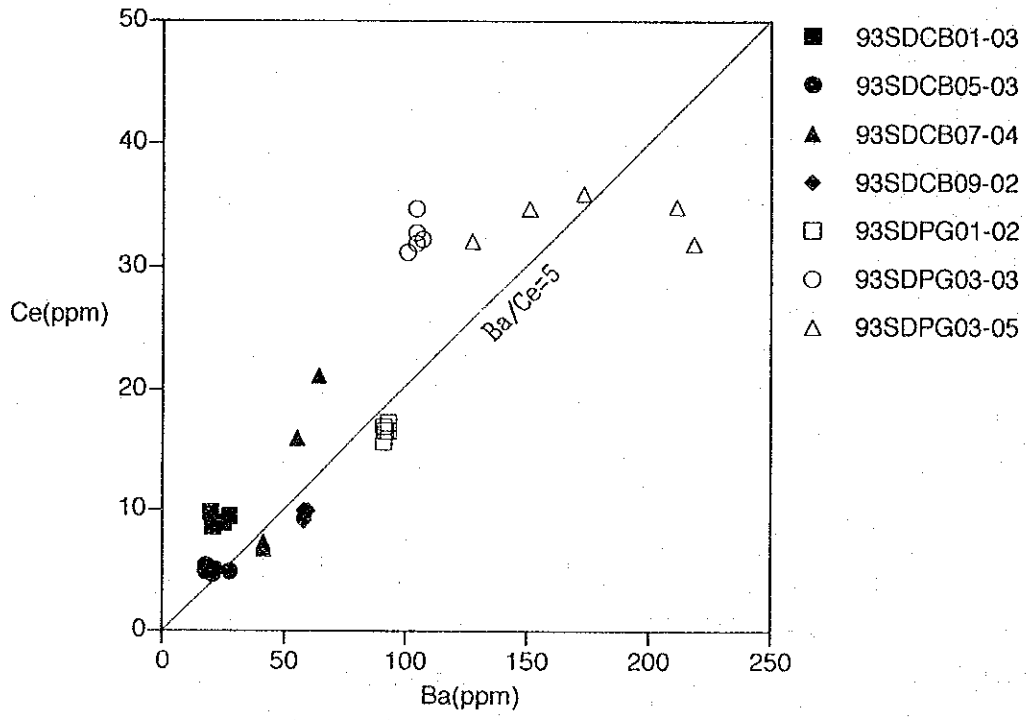

Figure 5-2-2-25 Ce versus Ba for basalts

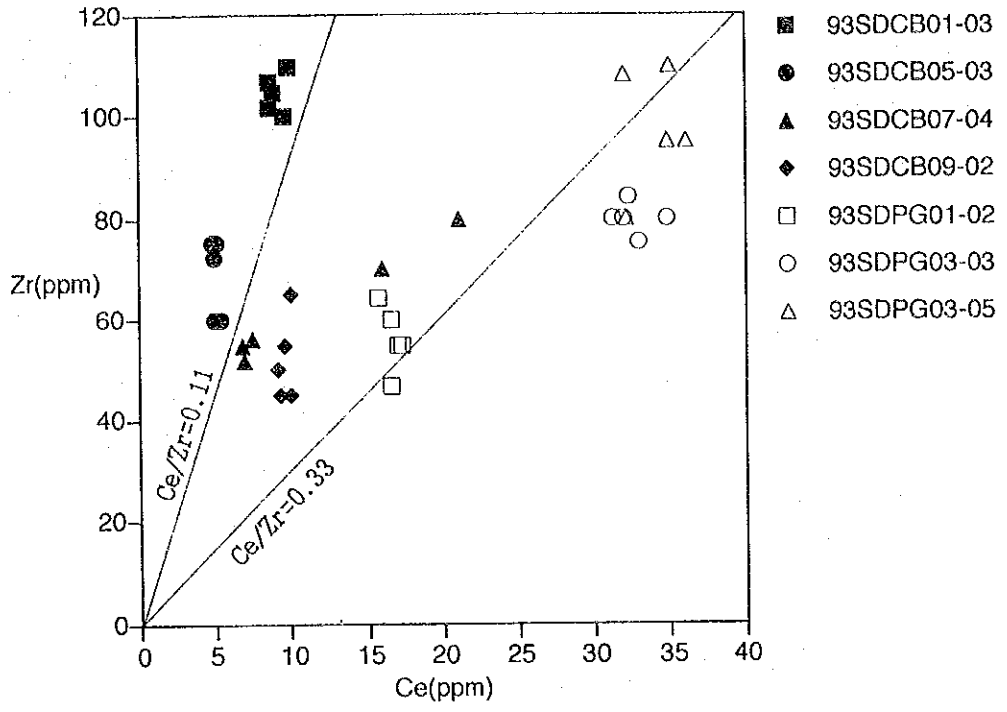

Figure 5-2-2-26 Zr versus Ce for basalts

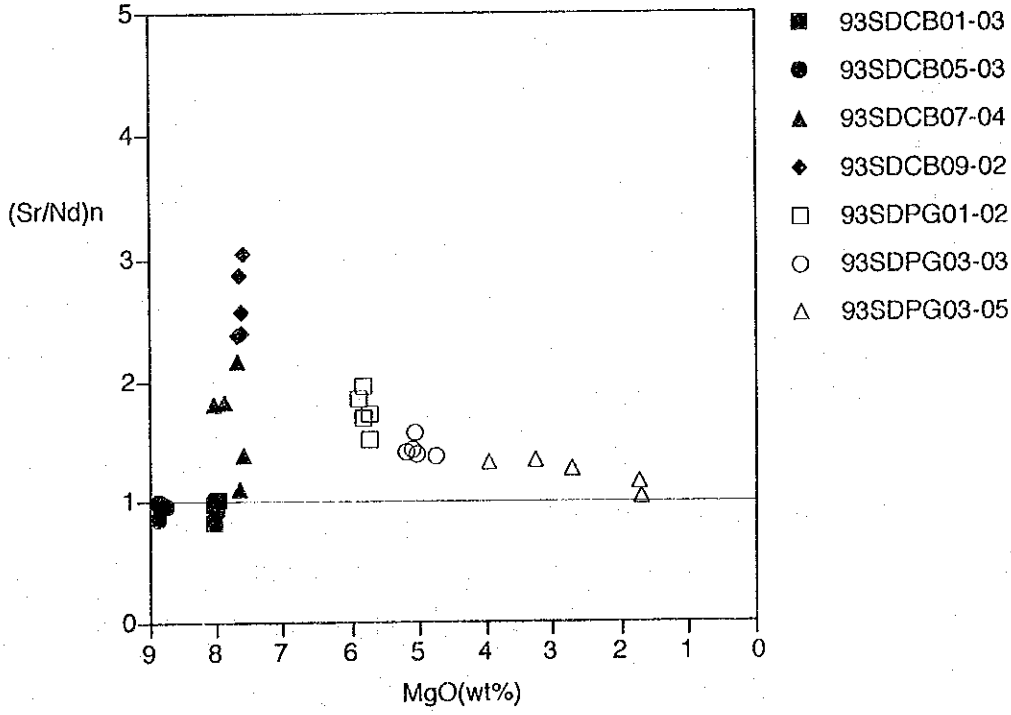

Figure 5-2-2-27 (Sr/Nd)n versus MgO for basalts

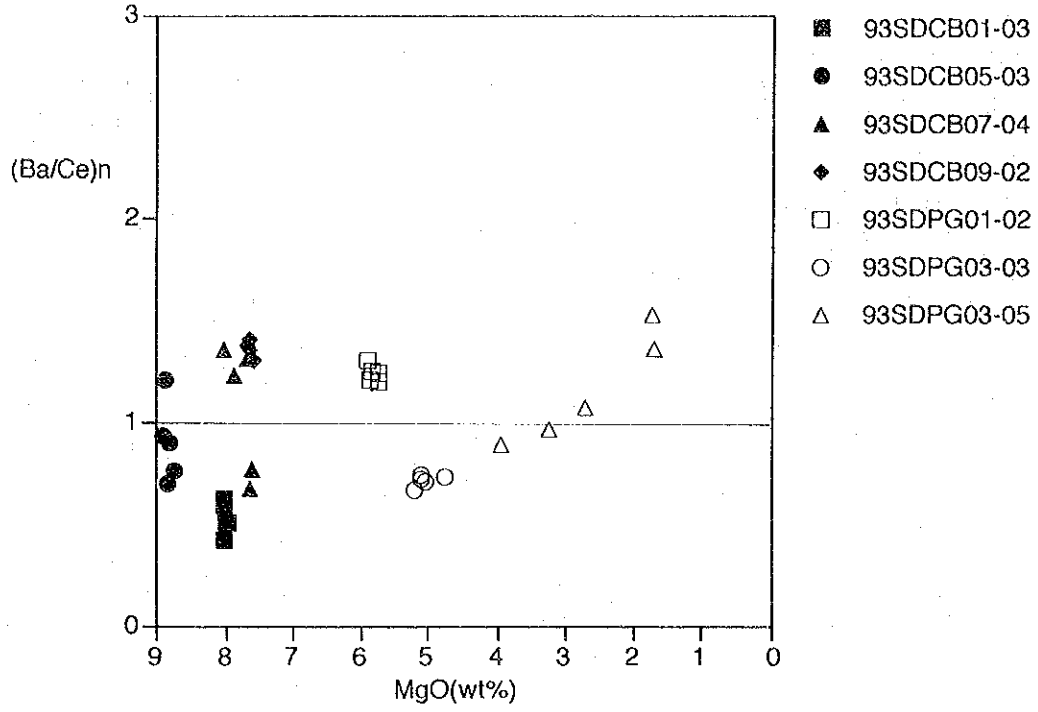

Figure 5-2-2-28 (Ba/Ce)n versus MgO for basalts

3) Mineralized Zones

After we had identified white clay, which was found sticking on the outside of the grab knife at the sampling point 93SDPG04, we conducted 93SDCB11 at roughly the same point as 93SDPG04 and seized pyrite disseminated argillized rock · siliceous rock of being affected by the mineralization of copper and zinc.

It was collected from the westward summit of the Kana Keoki Seamount which had two peaks.

Topography having the appearance of a crater with border discolored to yellow and yellow ~ reddish brown sediments extended 100 m around the topography had been identified during the FDC observation (track line 93SFDC04) conducted before the sampling at this point. For this reason, we tried the sampling by using a finder mounted power grab (93SDPG04). After we had identified the white clay sticking on the outside of the grab knife, we explored the same point with chain buckets (93SDCB11) and seized the disseminated and argillized rock · siliceous rock.

Samples obtained by 93SDCB11 include argillized rock assuming white ~ light gray, pebble-shapped siliceous rock with browned surface, altered and reddish-browned pumiceous dacite and foraminiferous sand.

The fresh part of the siliceous rock is dark gray and compact, brownish iron hydroxides are sticking or precipitating on the surface of the pebbles and in the

cavities of their inner parts. In the iron hydroxides, a small amount of bluish-green copper hydroxides are also identified (see photograph ④ of Fig. 5-2-2-1(1)). Veinlet ～ dissemination-like pyrite exists in the compact part.

In addition to pyrite, the dissemination of chalcopyrite, tetrahedrite and sphalerite is identified in the siliceous rock by the observation of polished sections. The details will be described later.

We can not clarify the source rock of the siliceous rock by the observation of thin sections. Microscopically, it changes to an assemblage of quartz-pyrite-clay minerals by devitrification and silicification.

Macroscopically, the argillized rock assumes white ～ light gray and presumed to be affected by strong mineralizing alteration (see photographs ⑤ and ⑥ of Fig. 5-2-2-1(1)). Trace dissemination of black sphalerite is identified. Spotty pyrite of fine-grained aggregates or idiomorphic pyrite is identified commonly. Most of the argillized rock occurs in light gray clay disseminated by pyrite (see photograph ② of Fig. 5-2-2-1(2)).

Under the observation of polished sections, in addition to the dissemination of pyrite, the dissemination of chalcopyrite・sphalerite in the argillized rock is also identified. The details will be described later.

According to the results of powder X-ray diffraction test, the above-mentioned white clay mineral collected at the sampling point 93SDPG04 is composed of a moderate quantity of montmorillonite and kaolinite, a small amount of halite and a trace of mixed layer mineral of sericite-montmorillonite (the greater part of it is the montmorillonite layer)・gypsum・anhydrite. On the other hand, the white clay mineral collected at the sampling point 93SDCB11 is composed of a small quantity of sericite (1M type) and a trace of halite.

Both siliceous rock and argillized rock were affected by strong mineralization. According to the results of chemical analysis (see Table 5-2-3-1, 93SDPG04-02 and 93SDCB11-03～ 08), as a whole, high content of pyrite in each sample are indicated by high values of Fe and S, and individually the following characteristics of mineralization are identified. Gold mineralization of Au 0.370 oz/t (=11.5 g/t)・Ag 7.24 g/t in addition to Cu 2810 ppm・Pb 670 ppm is identified from the dark gray siliceous rock 93SDCB11-03, from which copper hydroxides were identified macroscopically. And the redish-brown, muddy sediments 93SDCB11-02, distributed over

the siliceous rock and argillized rock, contain Pb 3900 ppm · Zn 3400 ppm. Which appears to be precipitates caused by base-metal mineralization. The pumiceous dacite 93SDCB11-01, which occurred together with the above-mentioned precipitates and altered into yellowish-brown, contains Ba 4190 ppm · Pb 1325 ppm. Dissemination of barite and galena to the pumiceous dacite is inferred just as the case of the white, pipe-shaped rock discussed in the following paragraphs.

An aggregate of a black metallic mineral and a transparent, plate-shaped mineral filled with white, pipe-shaped rock is identified from 93SDCB11 (see photographs ⑦ and ⑧ of Fig. 5-2-2-1(1)). According to the powder X-ray diffraction test and observation of polished sections, the outer, white pipe-shaped rock part is a tuff(?) changed to a mineral assemblage of barite-montmorillonite-kaolinite and the black metallic mineral and transparent plate-shaped mineral are galena and barite respectively.

Transmission and reflecting microphotographs of this sample are shown in Fig. 5-2-3-1. The country rock is chimney-shaped tuff(?) with diameters between 6 mm and 8 mm and a zonal structure of barite layers and rock layers having thicknesses of 1 mm to 3 mm. Abundant barite and galena, and a trace of pyrite are generated in the chimney. The barite is 4.5 mm to 0.2 mm long and presents idiomorphy. Besides the paragenesis of barite and galena in the chimney is observed, a small amount of barite is generated in the fissures of the tuff's zonal structure. The galena rarely presents idiomorphy but mostly presents indefinite external forms and contains plenty of dust-like impurities. A colloform texture is identified. A trace of pyrite exists in the country rock and an extremely small trace of pyrite exists in the chimney. The external forms of pyrite in the country rock presents indefinite ~ pellet shape · chrysanthemum shape with sizes between 0.05 mm and 0.001 mm. The pyrite in the chimney is pellet-shaped and the size of about 0.02 mm.

<Chemical Analysis>

A trace element analysis (20 elements) was conducted on 17 samples of rocks, altered rocks, iron-manganese oxides and clay. Among them, a whole rock analysis (13 components) was conducted on 7 samples of rocks and iron-manganese oxides. The results of the analysis are shown in Table 5-2-3-1.

The analyzed components and limits of detection are as follows: SiO_2, TiO_2, Al_2O_3, Fe_2O_3, FeO, MnO, MgO, CaO, BaO, Na_2O, K_2O, P_2O_5, and LOI (the detection limit of the

cross section 1 transmited (-)

0 500μm

cross section 2 transmited (+)

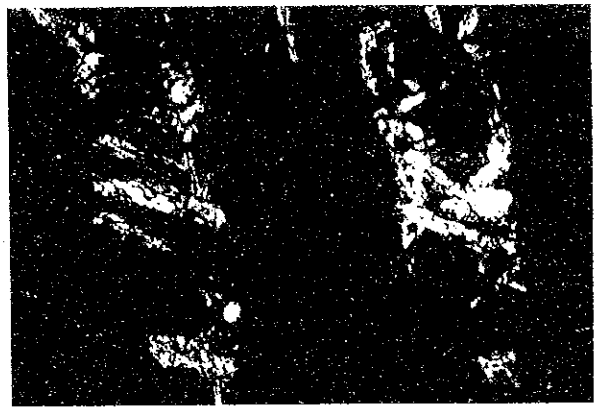

0 500μm

cross section 3 reflecting

0 500μm

vertical section 1 transmited (-)

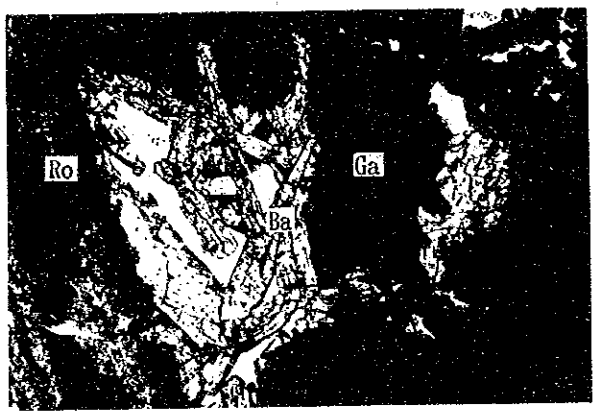

0 500μm

vertical section 2 transmited (+)

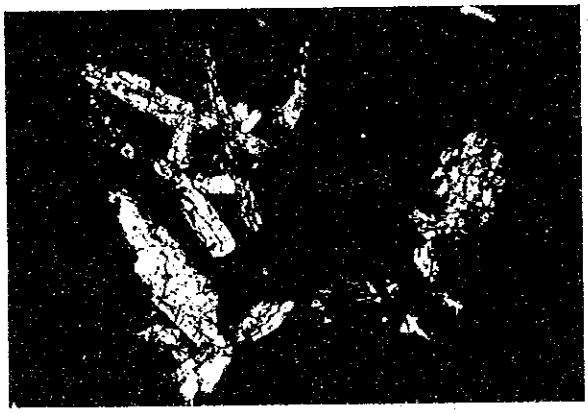

0 500μm

vertical section 3 reflecting

0 500μm

Abbreviation Ga : Galena Ba : Barite Py : Pyrite Ro : Wall rock

Figure 5-2-3-1 Microscopic Photos (Polished thin section)

above 13 components is 0.01%), Au (5ppb), Ag (0.02ppm), Cu (1ppm), Pb (1ppm), Zn (1ppm), Mn (5ppm), Total-Fe (0.01%), Total-S (0.001%), Cd (0.1ppm), Bi (0.1ppm), Ni (1ppm), Co (1ppm), As (1ppm), Sb (0.2ppm), Hg (10ppb), Ba (5ppm), Sr (1ppm), Mo (1ppm), Sn (1ppm), and W (1ppm). As for the elements other than the 13 components of the whole rock, the values in the ( ) are the detection limits.

The analytic methods are as follows: ICP emission analysis for : SiO_2, TiO_2, Al_2O_3, Fe_2O_3, MgO, CaO, MnO, BaO, K_2O, Na_2O, and P_2O_5. Neutralization titration method for: FeO. Ignition loss at 1000℃ for : LOI. ICP emission analysis after the decomposition and extraction by hydrochloric acid - potassium chlorate or hydrofluoric acid - nitric acid - perchloric acid for: Ag, Cu, Pb, Zn, Mn, Total-Fe, Cd, Ni, Co, As, Sb, Ba, Sr and Mo. After the decomposition of Hg, S, Au, Bi, Sn and W by perchloric acid - nitric acid or hydrochloric acid - hydrofluoric acid, Hg is measured by the atomic absorption method for cold vapor, S was measured by a high frequency induction heating infrared absorption photometer (LECO). Au, Bi and Sn are determined by the atomic absorption method and W is determined by the colorimetric method. In the case of Au > 10000 ppb, ore analysis was conducted by the fire assay.

<Observation of Polished Sections>

The results of individual microscopy are as follows. The white argillized rocks, in which no ore minerals are identified except pyrite, are dealt in the lump. Reflecting microphotographs are shown in Fig. 5-2-3-2.

- 93SDCB11-11 .... Disseminative, chalcopyrite ≧ pyrite > tetrahedrite > sphalerite

  The sample is a dark gray siliceous rock disseminated by pyrite.

  The external forms of the chalcopyrites are indefinite and their sizes are between 0.35 mm and 0.02 mm. No exsolution texture is identified.

  Most of the pyrites are idiomorphic and their forms are indefinite at times. Their sizes are between 0.15 mm and 0.005 mm. Some of them became iron hydoxides.

  The forms of the tetrahedrites are indefinite and their sizes are between 0.15 mm and 0.03 mm. They often coexist with chalcopyrites.

  The forms of the sphalerites are indefinite and their sizes are between 0.25 mm and 0.05 mm. No exsolution texture is identified. Also, spotty chalcopyrites is not identified.

93SDCB11-11

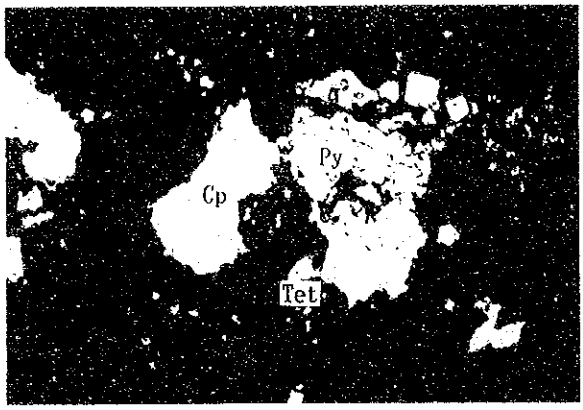

0 500μm

93SDCB11-11

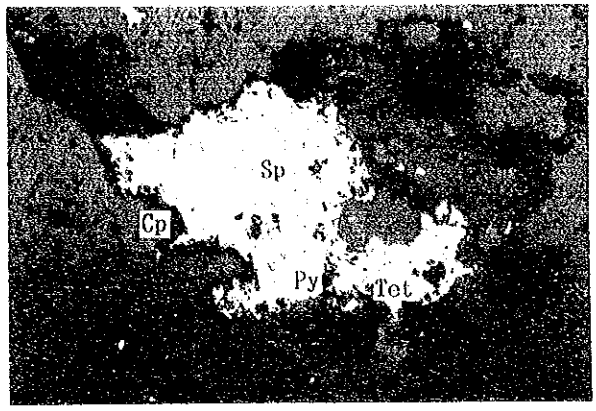

0 200μm

93SDCB11-12

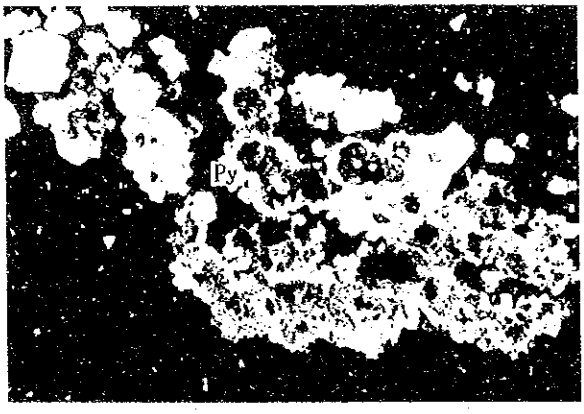

0 500μm

93SDCB11-14

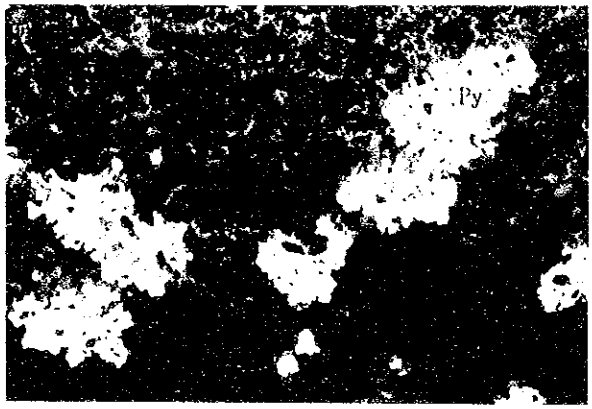

0 500μm

93SDCB11-18

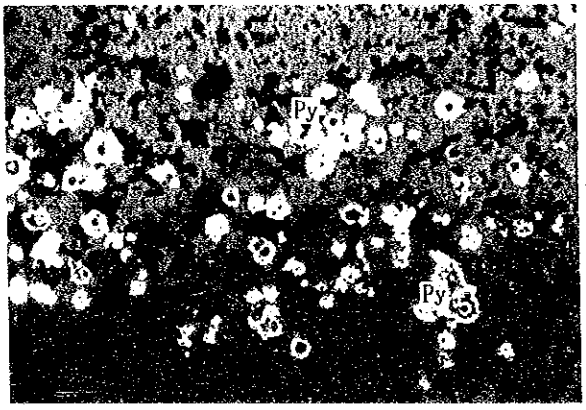

0 500μm

93SDCB11-12

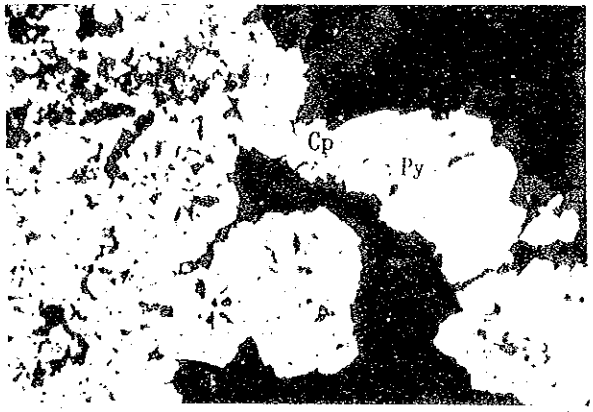

0 200μm

Abbreviation

Py : Pyrite Cp : Chalcopyrite Sp : Sphalerite Tet : Tetrahedrite

Figure 5-2-3-2 Microscopic Photos of Ore mineral on Detailed Survey

• 93SDCB11-12 .... Disseminative ~ micro veined, pyrite

The sample is a dark gray siliceous rock disseminated by vein-like pyrites.

The forms of the pyrites are aggregates of idiomorphic ~ indefinite. The sizes of the idiomorphic pyrites are between 0.2 mm and 0.005 mm. The width of micro veins are between 0.6 mm and 0.2 mm. They are composed of discontinuous aggregation of crustaceous (conchoidal) pyrites.

• 93SDCB11-14 .... Disseminative, pyrite >> sphalerite · chalcopyrite

The sample is a white argillized rock disseminated by pyrites.

Most of the pyrites are irregular external formed aggregates. Their sizes are between 2.5 mm and 0.3 mm. A small amount of crustaceous (conchoidal) pyrites and ring pyrites are also contained in them, whose sizes are between 0.25 mm and 0.02 mm. Idiomorphic pyrites with the sizes between 0.1 mm and 0.02 mm are identified rarely.

The forms of sphalerites are indefinite, but very few of them are granular. Their sizes are between 0.05 mm and 0.02 mm. No exsolution texture is identified.

The external forms of the chalcopyrites are idiomorphic ~ indefinite, but very few of them are granular. Their sizes are 0.06 mm±. No exsolution texture is identified.

• 93SDCB11-18 .... Disseminative ~ micro veined, pyrite >> chalcopyrite

The sample is a white siliceous rock disseminated by pyrites and somewhat like an opal.

Most of the pyrites are crustaceous (conchoidal) pyrites and their sizes are between 0.1 mm and 0.05 mm. Pyrites with concentric structure is identified, but rarely. Ring pyrites (of dimensions between 0.05 mm and 0.02 mm) and framboidal pyrites (of demensions between 0.05 mm and 0.03 mm) are also identified, but rarely.

The forms of the chalcopyrites are indefinite. Their sizes are 0.04 mm±. No exsolution texture is identified.

• 93SDCB11-22 .... Disseminative ~ micro veined, pyrite >> chalcopyrite

The sample is a white argillized rock disseminated by pyrites.

Ore mineral is mainly composed of idiomorphic pyrites with a small amount of crustaceous (conchoidal) pyrites. The sizes of the idiomorphic pyrites are between

0.1 mm and 0.03 mm. The sizes of the crustaceous (conchoidal) pyrites are between 0.15 mm and 0.05 mm. The sizes of the pyrite aggregates with irregular external forms are between 0.8 mm and 0.2 mm.

The forms of the chalcopyrites are between 0.06 mm and 0.03 mm. No exsolution texture is identified.

· 93SDCB11-13 · -15 · -16 · -17 · -19 · -20 · -21 · -23 .... Disseminative, pyrite

The samples are white argillized rock desseminated with pyrite.

The external forms of the pyrites are crustaceoue (conchoidal) ~ ring ~ irregular. Idiomorphic crystal and pellet-shaped crystal are rarely found. The sizes of the crustaceous (conchoidal) pyrites are between 0.5 mm and 0.05 mm and pyrites with the concentric structure and 0.05 mm in size is rarely found. The sizes of the ring pyrites are between 0.5 mm and 0.005 mm and pyrites with the cockade structure and sizes between 0.08 mm and 0.06 mm are rarely found. The sizes of the pyrite aggregates with irregular external forms (elliptical, stick-shaped and so on) are between 1.3 mm and 0.15 mm. The sizes of the idiomorphic pyrites are between 0.25 mm and 0.01 mm. The sizes of the pellet-shaped pyrites are between 0.04 mm and 0.02 mm.

4) Inhabiting Living Things

Large-sized living things observed during the FDC survey were the living things disliking the extreme change of temperature or sea water components. We could not identify the existence of living things who like a hydrothermal environment. The photographs of the major living things are shown in Figure 5-2-4-1(1) and (2).

The major large-sized living things are as follows:

- Porifera
- Coelenterata (actiniae)
- Echinodermata (asteroids, holothurians, echinoids, crinoids and so on)
- Anthropoda (Decapoda - Macrura · Anomwa · Brachyura)
- Vertebrata (fishes)

The seafloor of this area is mainly outcropped with autobrecciated lava and talus breccias on which muddy sediments are distributed.

Poriferans, holothurians, asteroids and crinoids are identified on the surfaces of muddy sediments. Holes with diameters of several centimeters, appeared to be trace

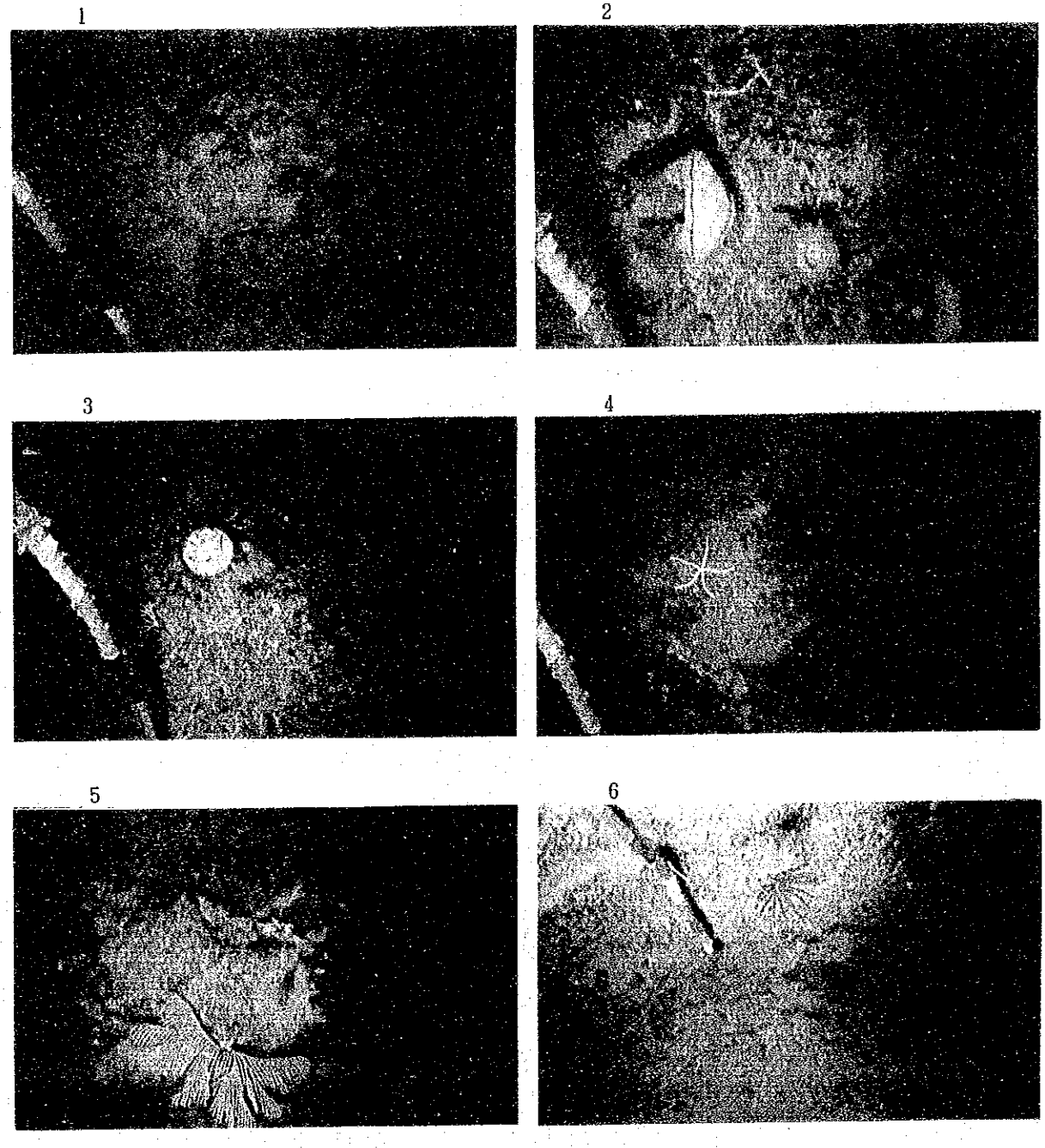

1. Anthozoa — Line93SFDC04 (8°44.14′S, 156°59.98′E, water depth 866m)
2. Porifera — Line93SFDC04 (8°45.10′S, 157°02.50′E, water depth 761m)
3. Porifera — Line93SFDC04 (8°45.31′S, 157°03.14′E, water depth 802m)
4. Asteroidea — Line93SFDC04 (8°44.29′S, 157°00.30′E, water depth 672m)
5. Hydrozoa — Line93SFDC04 (8°45.10′S, 157°02.42′E, water depth 767m)
6. Crinoidea — Line93SFDC04 (8°34.97′S, 156°29.71′E, water depth1,371m)

Figure 5-2-4-1 Living Things (1)

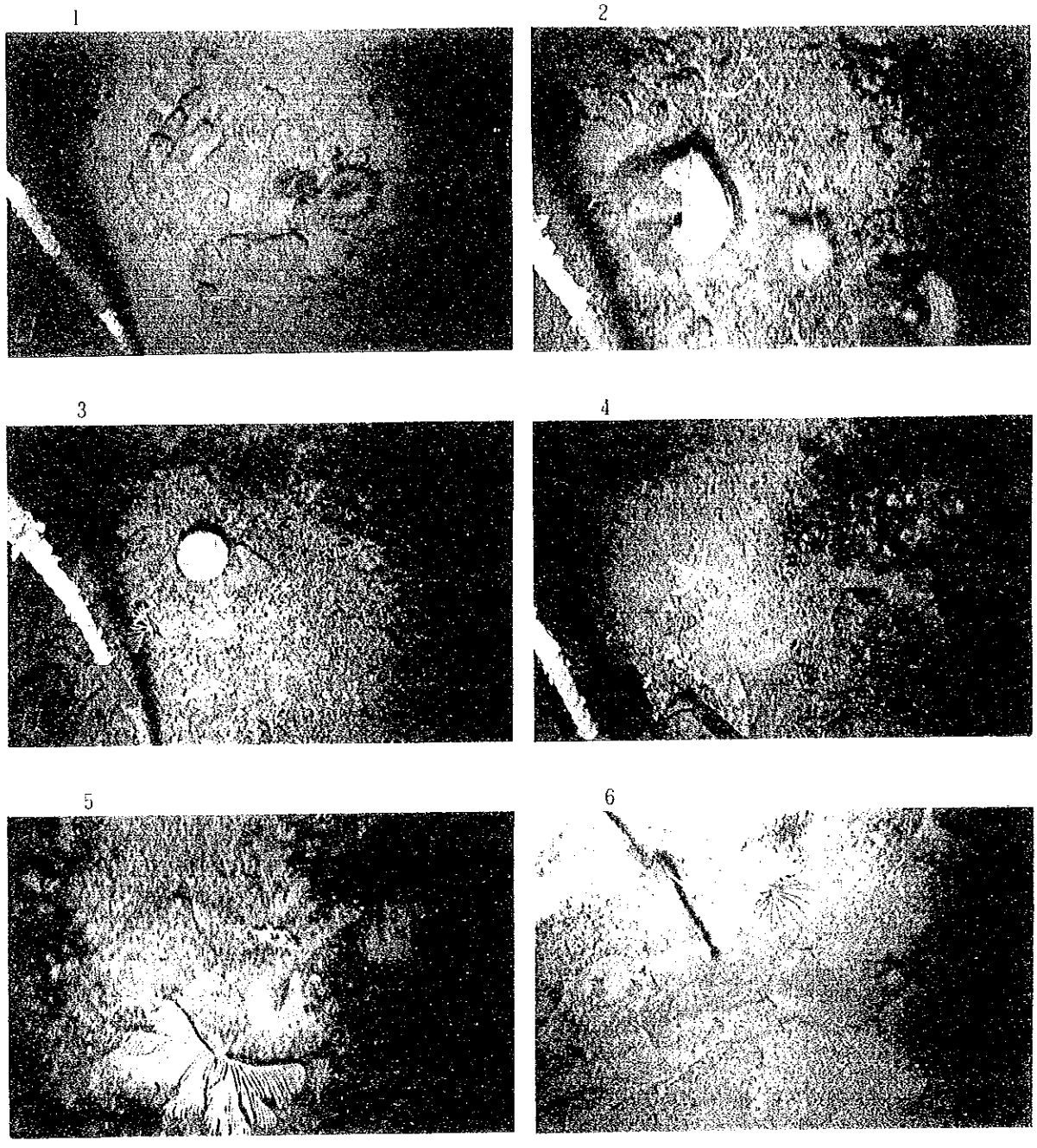

1. Anthozoa Line93SFDC04 (8°44.14′S, 156°59.98′E, water depth 866m)
2. Porifera Line93SFDC04 (8°45.10′S, 157°02.50′E, water depth 761m)
3. Porifera Line93SFDC04 (8°45.31′S, 157°03.14′E, water depth 802m)
4. Asteroidea Line93SFDC04 (8°44.29′S, 157°00.30′E, water depth 672m)
5. Hydrozoa Line93SFDC04 (8°45.10′S, 157°02.42′E, water depth 767m)
6. Crinoidea Line93SFDC04 (8°34.97′S, 156°29.71′E, water depth1,371m)

Figure 5-2-4-1 Living Things (1)

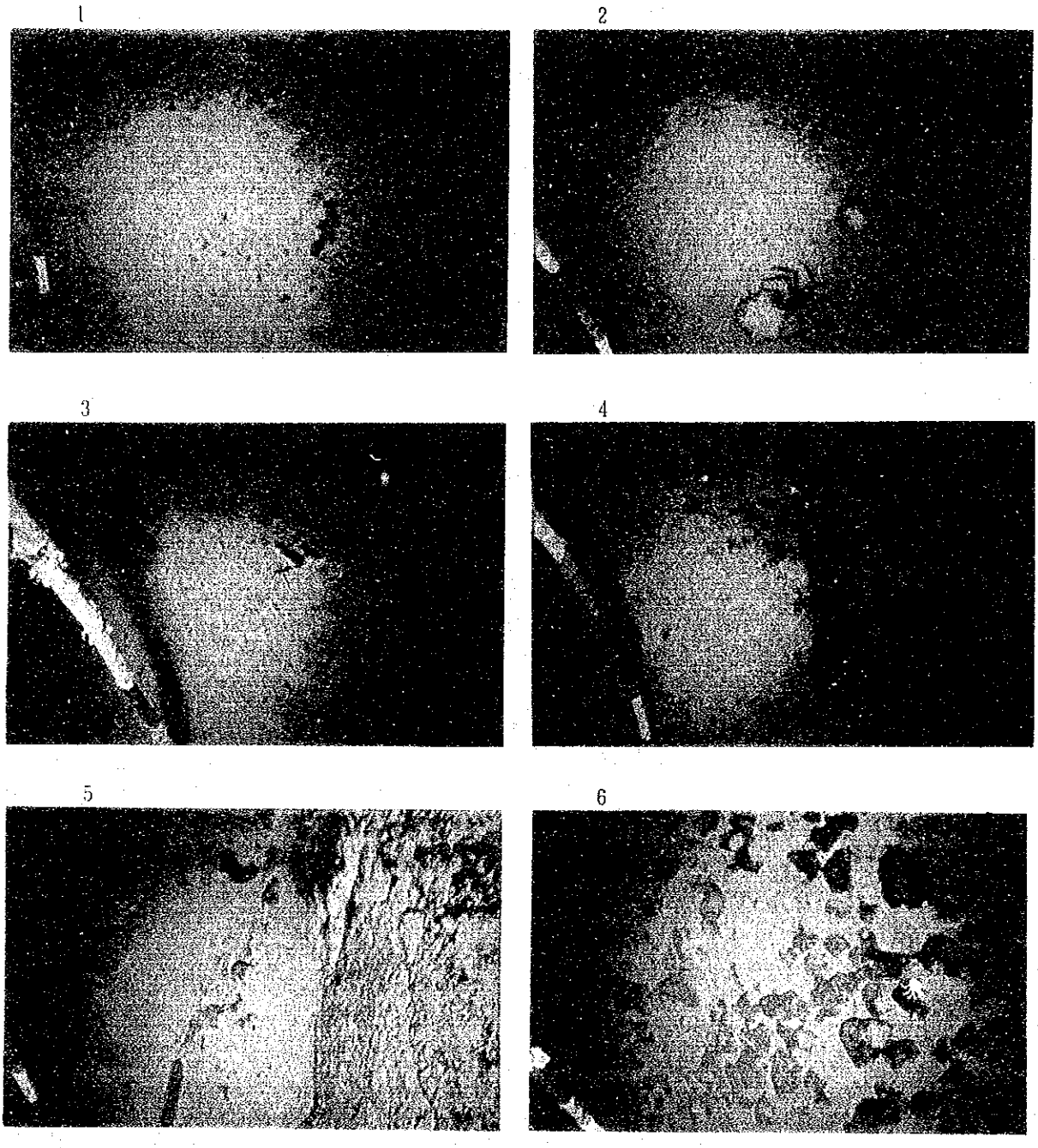

1. Macrura — Line93SFDC01 (8°38.22′S, 156°38.32′E, water depth2,529m)
2. Porifera & Macrura — Line93SFDC01 (8°39.98′S, 156°40.48′E, water depth1,646m)
3. Crab — Line93SFDC04 (8°44.94′S, 157°02.04′E, water depth 776m)
4. Macrura & Munidopsis sp — Line93SFDC04 (8°43.97′S, 156°59.61′E, water depth1,095m)
5. Holothurioidea — Line93SFDC08 (9°18.72′S, 156°15.61′E, water depth3,120m)
6. Munidopsis sp — Line93SFDC08 (9°18.70′S, 156°18.17′E, water depth2,754m)

Figure 5-2-4-1 Living Things (2)

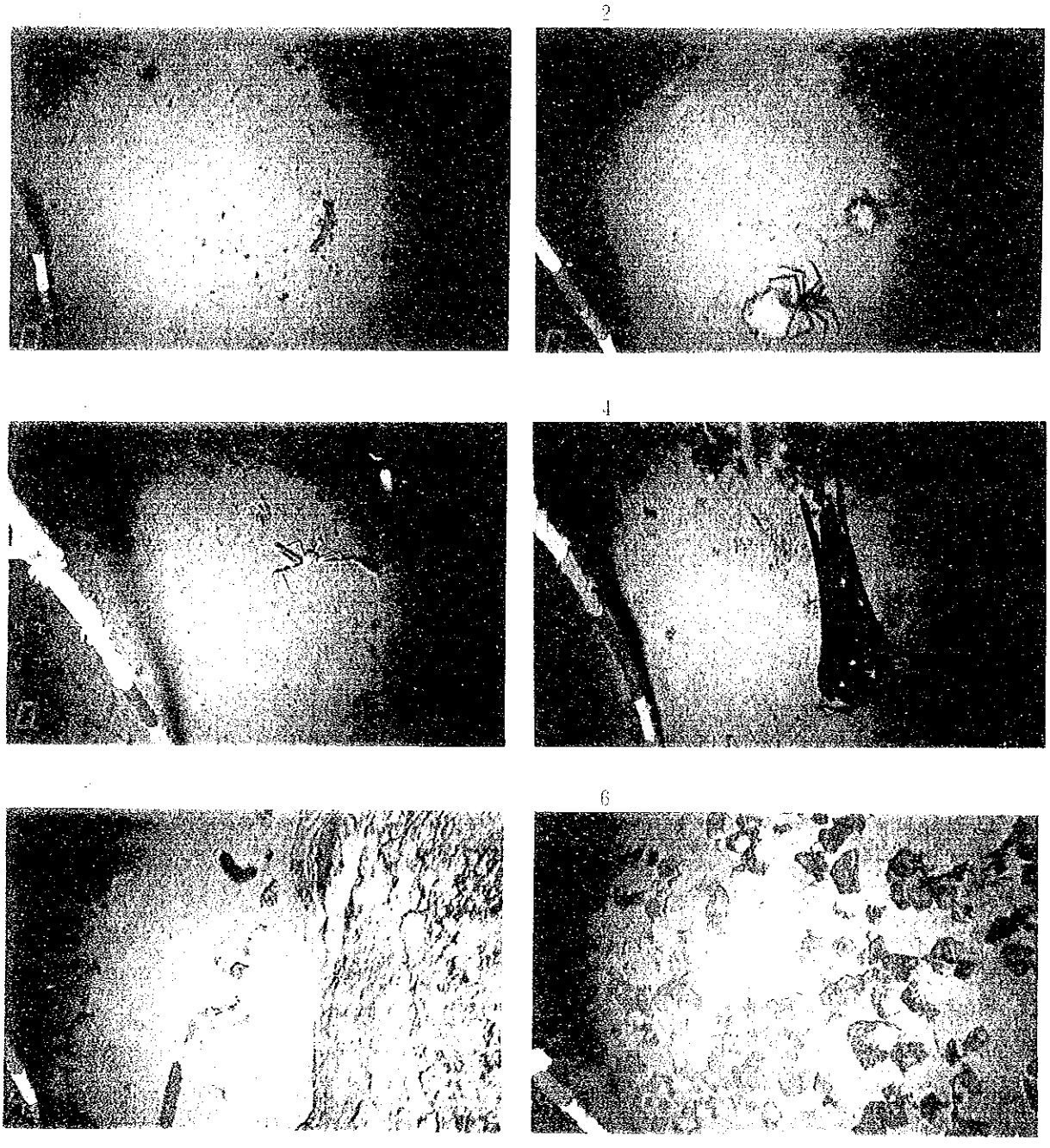

1	Macrura	Line93SFDC01 (8°38.22′S, 156°38.32′E, water depth2,529m)
2	Porifera & Macrura	Line93SFDC01 (8°39.98′S, 156°40.48′E, water depth1,646m)
3	Crab	Line93SFDC04 (8°44.94′S, 157°02.04′E, water depth 776m)
4	Macrura & Munidopsis sp	Line93SFDC04 (8°43.97′S, 156°59.61′E, water depth1,095m)
5	Holothurioidea	Line93SFDC08 (9°18.72′S, 156°15.61′E, water depth3,120m)
6	Munidopsis sp	Line93SFDC08 (9°18.70′S, 156°18.17′E, water depth2,754m)

Figure 5-2-4-1 Living Things (2)

fossils, and a number of irregular trails of holothurians are also observed.

Poriferans, actiniae and crinoids are sticking on the surfaces of rocks, and red shrimps and crabs are identified in the fissures and cracks of rocks.

There are some cases in which a number of white (Anomwa) are crowding on pieces of wood, which are rarely seen on the seafloor.

Where the water depth is shallow (especially at the water depths shallower than 1,000 m), red shrimps and crabs can be seen more frequently.

5) Temperature Anomalies

With the object of investigating hydrothermal activities, water temperature, salinity and pressure (CTD water depths) were measured at intervals of five seconds by the CTD mounted on the FDC towing vehicle.

The temperature and depth profiles are shown in Figures 5-2-5-1(1) and (2) along the FDC track lines.

The following points can be pointed out from these profiles.

Profile of track line FDC01

Temperature anomalies are nonexsistant. The temperature are between 2℃ and 3℃ and the water depths are between 1,400 m and 2,600 m. The correlation between the temperature and water depth is high.

Profile of track line FDC02

Temperature anomalies are nonexsistant. The temperature is 2℃ and is constant within the water depths between 2,200 m and 2,600 m.

Profile of track line FDC03

Temperature anomalies are nonexsistant. The temperature are between 2℃ and 4℃ and the water depths are between 1,000 m and 2,500 m. The correlation between the temperature and depth is strong.

Profile of track line FDC04

Although temperature changes is detected at the area of shallower than 2,000 m, these changes are difficult to interpret as hydrothermal event because these temperature changes are highly correlated with the water depth. The temperatures

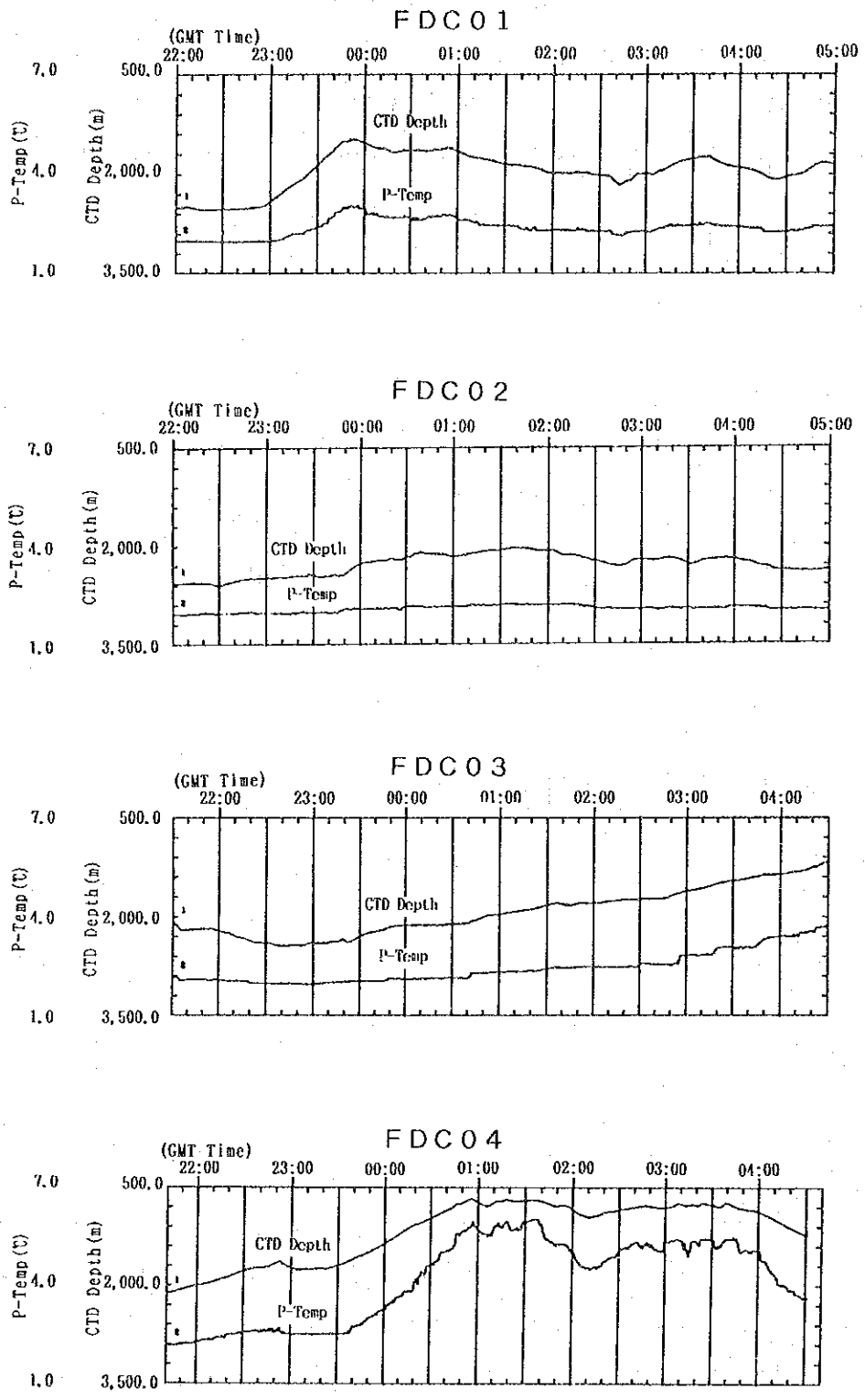

Figure 5-2-5-1 Potential Temperature · CTD Depth profiles (1)

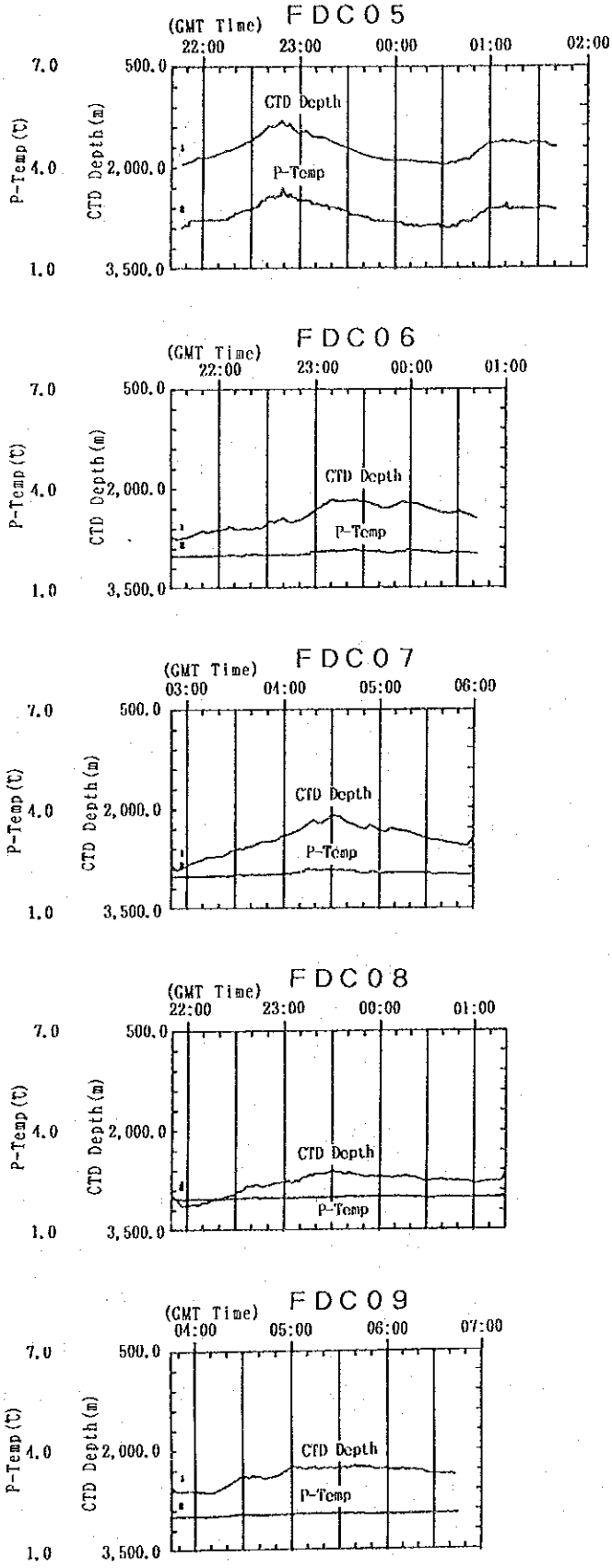

Figure 5-2-5-1 Potential Temperature · CTD Depth profiles (2)

are between 2℃ and 6℃, the water depths arebetween 500 m and 2,200 m.

Profile of track line FDC05

Although temperature changes is identified at the area of shallower than 2,000 m, these changes are difficult to interpret as hydrothermal event because these temperature changes are highly correlated with the water depth. The temperatures are between 2℃ and 4℃, the water depths arebetween 1,100 m and 2,000 m.

Profile of track line FDC06

Temperature anomalies are nonexsistant. The temperature is 2℃ and is constant within the water depths between 2,200 m and 2,800 m.

Profile of track line FDC07

Temperature anomalies are nonexsistant. The temperature is 2℃ and is constant within the water depths between 2,000 m and 2,600 m.

Profile of track line FDC08

Temperature anomalies are nonexsistant. The temperature is 2℃ and is constant within the water depths between 2,500 m and 3,200 m.

Profile of track line FDC09

Temperature anomalies are nonexsistant. The temperature is 2℃ and is constant within the water depths between 2,200 m and 2,600 m.

In conclusion, temperature anomalies caused by hydrothermal activities are not detected in the deep sea area, and in the shallow area, hydrothermal activities is uncertain because temperrature are highly correlated with the water depth.

For reference, vertical profile of conductivity, temperature, and depth measured for using MBES is shown in Figure 5-2-5-2. This profile gives evidence to show that the water temperature above 2,300 m changes in accordance with the water depths.

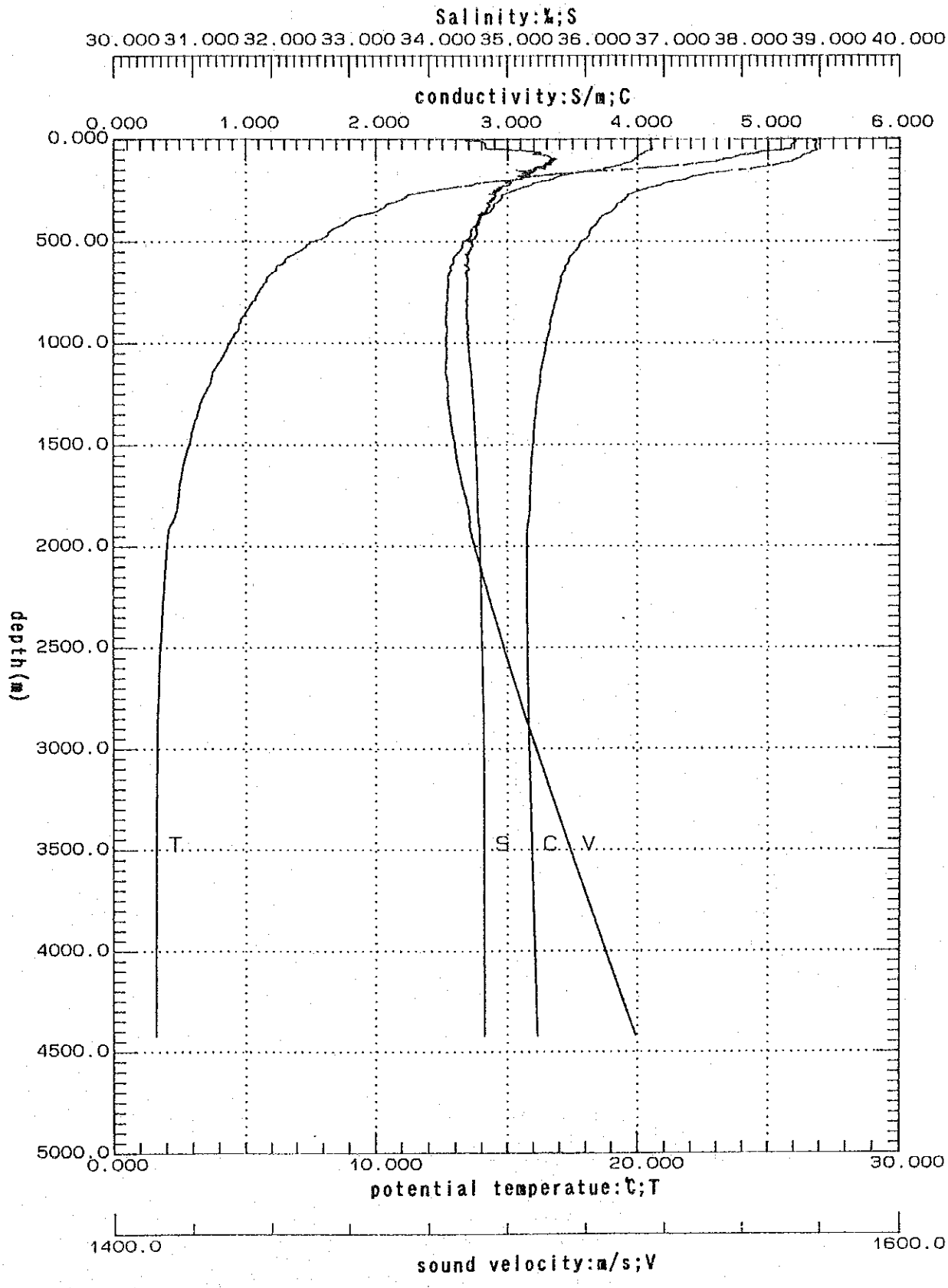

Figure 5-2-5-2 Vertical CTD profile (conductivity, salinity, potential temperature and sound velocity versus depth)

Chapter 6. Discussions

<With regard to the method of survey>

This fiscal year's survey was conducted in order of the topographical survey (and magnetic survey conducted simultoneously), regional geochemical survey and detailed survey. In general, the geochemical survey is conducted by selecting the target from seafloor sediments or sea water, seafloor sediments and sea water at the same time. Because of the effectiveness and equipment, we conducted this fiscal year's survey of regional geochemical survey only on seafloor sediments.

The detailed survey is composed of the topographical survey, seafloor observation and sampling, but, due to the limited time, we could not carry out the survey sufficiently. We, in spite of, suppose that we were afraid that we could not discover even oxidized zones nor apparent signs of mineralization before the cruise, the results of the survey are satisfactory. Of course, it is difficult to complete this survey just by one cruising. We presume it is necessary to do closer investigation of this area in the future.

<Seafloor Spreading Center and Transform Fault>

① The strike of the seafloor spreading center is bended and not straight. We envision that this bending was occurred after 0.73 Ma as the Brunhes-Matuyama boundary is nearly a straight line.

② Both the seafloor spreading center and the transform fault near the 155° 10'E line and 156° 08'E line are bathymetric depressions with roughly the same width. There is little difference of magnetism between them. From the above, we can see that the seafloor spreading center and transform fault may be analogous.

③ The distance between the Brunhes-Matuyama boundary becomes shorter toward the west (see Fig. 6-1-1-1).

④ The above ③ can be considered as evidences that the origin of the seafloor spreading center is westward propagating rifts caused by relative movement of the India-Australian and Pacific plate.

⑤ West of the Simbo Transform Fault and Fracture Zone, seamounts and ridges exist only in the vicinities of the both seafloor spreading center and transform fault, except the seamount lying at 9° 50'S·155° 47'E. These seamounts and ridges extend in the dircction of E-W and their relief are gentle. As seamounts and ridges moved

away from the seafloor spreading center, they were cooled, then contracted and disappeared.

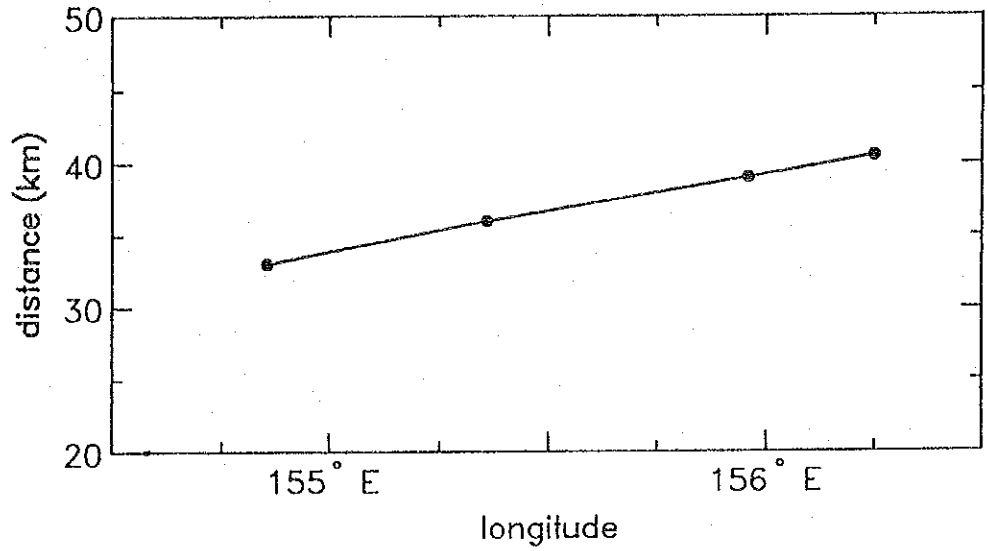

Figure 6-1-1-1 Distance between two Brunhes-Matuyama Boundaries Recorded on Both Side of the Spreading Center Plotted as Function of Longitude

<With regard to Magnetic Anomalies>

When we have produced reduction to the pole anomaly map, ① we have supplemented the places lacking data with the values of magnetic anomalies and ② have produced four kinds of reduction to the pole anomaly maps assumed inclination of 31° S, 28° S, 24° S and 20° S. After we have compared them with the magnetic anomaly map we adopted the reduction to the pole map of 28° S as the optimum one. But, east of approximately 157° 30'E, the N-S trending magnetization lineation is inconsistent with the N-S trending bathymetric depressions. So, there is a possibility that the assumed inclination is not correct. Furthermore, the effect of the values of magnetic anomalies supplemented in ① is also conceivable because this survey area is too narrow. As we take the datum 14 km under the sea level as the flat bottom because water depths varies range from 500 m to 4,600 m, and became high magnetization values at shoal area if we adopted method Carbotte et al (1992).

Taylor (1987) identified magnetic anomaly 3 (3.86 ～ 4.79 Ma) at the southeastern margin of this survey area but we could not identify magnetic anomaly 3 because there was too little data.

There is an E-W trending band with higher magnetization than that of the Ghizo Ridge on its south side. We envision that this high magnetization zone is the

reactivated seafloor spreading center.

The deviated reason of the location of the magnetization zone and the Coleman Seamount may be attributed to the intervals of the track lines being too wide. Obvious magnetic characteristics are not identified from the Simbo Transform Fault. We may explain it as it has passed a long time after a volcanism had ceased its activity. The Simbo Transform Fault shown in the geological structure is established by linking the triple junction with the eastern terminal of the spreading center. West of this Simbo Transform Fault the magnetic lineation does not cut by the Simbo Transform Fault and disappeared at a narrow bathymetric depression on the its westside. If we adopt a line disappeared magnetic lineation, we may need to draw slightly toward the west the transform fault shown in figure 3-3-1-1.

<Water Temperature Anomalies>

At the water depths shallower than 1,000 m, the correlation between the temperature and the depth is strong, in which wave-lengths are long and the temperature changes between 2℃ and 6℃. It needs a very large hydrothermal activity zone to explain it. But such a big hydrothermal activity zone was not discovered by the results of the FDC survey. It is very difficult to judge temperature anomalies related to hydrothermal activity at such a place where the water depth changes (rugged topography).

With the object of examining the relation between the temperature and depth, we plotted it by temperature versus $(\text{depth})^{-1/2}$. As a result, the relationship is found to be a straight line at the water depths between 600 m and 2,000 m as shown in Figure 6-1-1-2. Then, the water depths in which we can detect water temperature anomalies would be deeper than 2,000 m.

<With regard to Muddy Substances>

The muddy substances of this survey area are composed of clastic minerals forming basic or intermediate igneous rocks and organic fossils mainly composed of foraminiferas. They have sedimented at the rate of more than 2 ～ 3 mm/1,000 years. Only a trace of clay minerals are contained in the muddy substances and it is presumed that these clay minerals were generated from clastic mafic minerals through alteration and the possibility of being the products of hydrothermal activities or diagenesis is low.

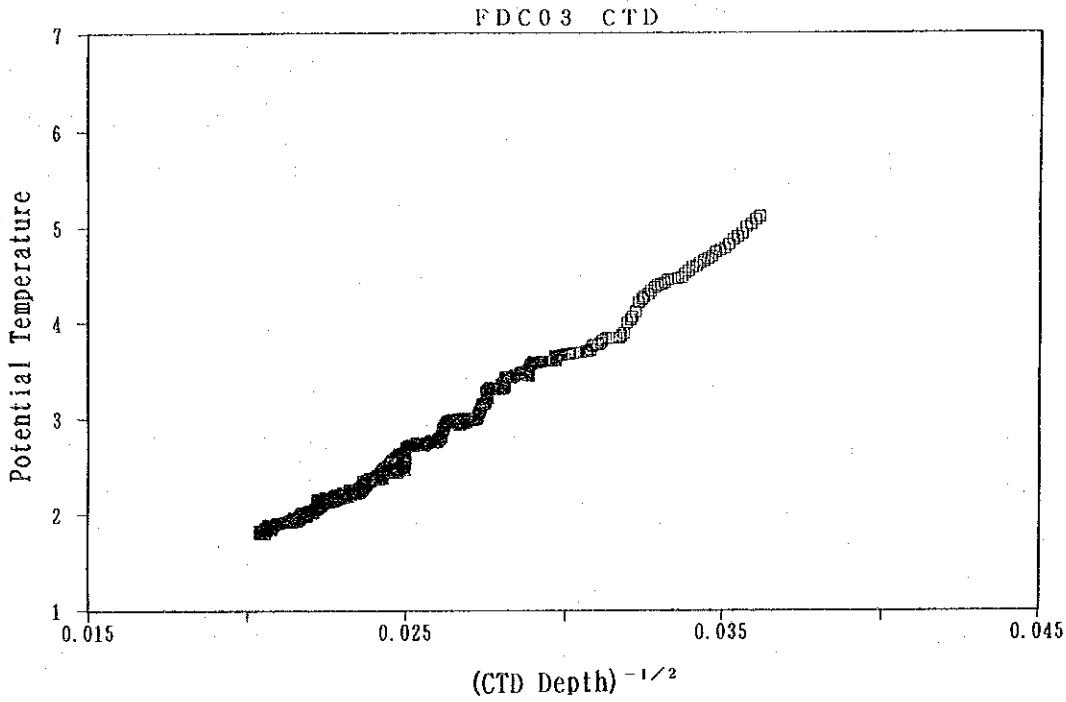

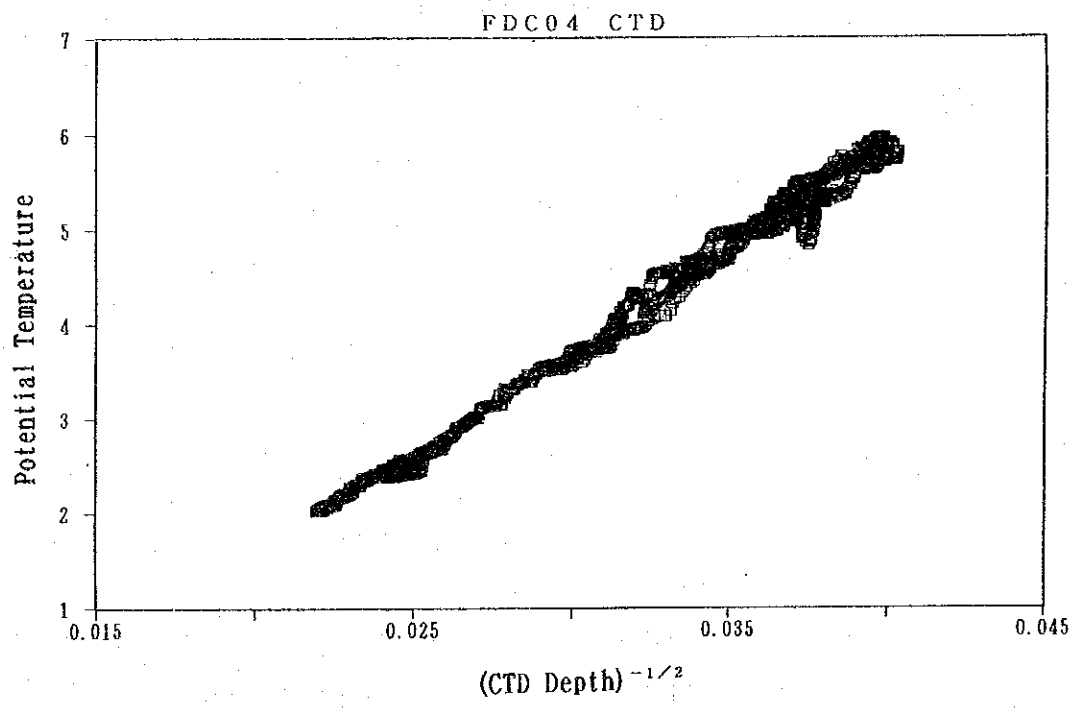

Figure 6-1-1-2 Potential Temperature Plotted as Function of (Depth by CTD) $^{-1/2}$

The color tones of the muddy substances can be classified into the brown series and olive series. Nearly always the former exists on the upper position of the latter. From the chemical composition, we can presume that the former is a sample under an oxidized environment and rich in foraminiferous fossils, and the latter is a sample in a reducing environment and rich in clastic minerals.

Samples abundantly rich in foraminiferous fossils are identified in the southwestern half of the survey area and samples abundantly rich in clastic minerals are identified in the northeastern half of the survey area.

It is considered that the parameters indicating hydrothermal ore deposits in the muddy substances are shown by the values of Al/Al+Fe+Mn and the second principal component from the principal component analysis. Anormalous values of them are always appeared in the vicinity of the southwestern tip of the survey area. However, such anormalous values are not identified in the vicinity of the seamount lying in the northeastern part of the sea area from where ore minerals were collected. As for the cause of this discrepancy, we suppose that the range which is influenced by activities of hydrothermal deposits in the vicinity of the seamount, is narrower than that accompanied by seafloor spreading center, and that the influence by activities of hydrothermal deposits are diluted by inflow and sedimentation of clastic minerals from land, and so on.

According by, in the case of more detailed survey in future, we recommend that the efficacy of the parameter above - mentioned is verified by conducting sampling at narrower interval than this cruise and expanding for southwestern side out of this survey area.

<With regard to Rocks>

Rocks are mainly collected by the GC during the regional survey and by the CB during the detailed survey. Sediments were not collected from the vicinities of prospected seafloor spreading center, from the crest of seamounts to their piedmonts and the slopes of trenches and the bit tips of the GC deformed frequently. From which we can conceive that the thickness of the sediments is extremely thin and often outcropped by rocks. Rocks distributed around the prospected seafloor spreading center is entirely olivine basalt ~ non-phenocryst basalt (mid-oceanic basalt) of tholeiite series (olivine tholeiite), but the island arc characteristics become stronger toward the vicinity of the trench lying at the northeastern part of the survey area. Rocks

distributed from the crest of the seamounts located at the northeastern part of the survey area to their piedmonts are basalt of tholeiite series (tholeiite oversaturated by silica) containing augite phenocryst or two-pyroxene andesite ~ dacite of calc-alkali series which are the products of island arc volcanism.

<Establishing FDC track lines for detailed survey of this area>

We established the FDC track lines for detailed survey along the ridges of the seamounts where assumed to be poor seafloor sediments and rich exposed rock. It is expected that the area along these valleys be surveyed in the future. There is a case in which we selected a seamount with weak reflection and a seamount with moderate reflection so as to help interpret the reflection records of Sea MARC Ⅱ. However, there is no other record of Sea MARC Ⅱ (Crook et al. 1991) except on the Simbo and Ghizo Ridges, and Kana Keoki and Coleman Seamounts. We selected the azimuths of track lines and observation carefully so as to avoid the influence of tidal currents and winds. We conducted only the FPG survey at the crest of the Coleman Seamount because of oceanographic phenomena, atmospheric phenomena and working hours. We did not carry out the FDC and FPG surveys on the seafloor spreading center because the strength of the optical fiber cables were not strong enough.

<With regard to Apparent Signs of Mineralization>

With the objective of exploring apparent signs of mineralization, we conducted the FDC survey on the seamounts lying in the vicinities of the Simbo Ridge and Ghizo Ridge. We discovered a mineralized zone with apparent signs of mineralization of Au-Cu-Pb-Zn on the crest of the Kana Keoki Seamount lying on the Ghizo Ridge. According to the FDC survey, this mineralized zone has, at least, an extent of about 100 m. Besides it, there are a number of submarine discolored areas from the crest to the piedmont of the Kana Keoki Seamount. We may expect to discover new mineralized zone in this area.

The characteristic of this mineralized zone is relatively rich in gold content and lead content. This mineralized zone differs from the 「submarine hydrothermal deposits」 concomitant with a seafloor spreading center but resembles the apparent signs of mineralization generated under a geological environment of island or back arc.

Chapter 7. Summary

In 1993, the fourth fiscal year of the second phase of the five-year SOPAC program, a survey of hydrothermal ore deposits was carried out in the eastern part of the Woodlark Basin, within the exclusive economic zone of the Solomon Islands and a part of Papua New Guinea. The survey was composed of topographical cruising for the drawing of topographic maps based on accoustic sounding, regional geochemical sampling carried out in Area 1 (located in the eastern part of the area), and a detailed survey (FDC and Sampling) carried out around the spreading center and submarine volcanoes within Area 1. Furthermore, in order to serve as an aid in estimating any geological structure, a magnetic survey was carried out in conjunction with the topographic cruising, and a CTD survey on water temperature anomalies caused by hydrothermal activities was carried out by loading a CTD on the FDC.

(The results of Acoustic Sounding)

A bathymetric map of the entire region, contoured at 200 m intervals, is shown in Figure 3-1-9. However, these scale and contour interval can be randomly selected.

Topographical cruising distance was 6,253.7 miles.

The interpretation of the geological structure, including the location of the spreading center assumed from the topographic map, is shown in Figure 3-3-1. The width of the seafloor spreading center is estimated to be between 5 km and 15 km, and the spreading rate is estimated to be between 5.7 cm/y and 7.0 cm/y. This spreading center resembles the Mid Atlantic Ridge (MAR).

(The Results of the Magnetic Survey)

The results of the total magnetic force measurements, reveal that the area is divided by the Simbo Ridge, which is a N-S trending transform fault, and that the magnetic forces of the area on the eastern side of the Simbo Ridge differ from that of the area on the western side. The western side of the Simbo Ridge is composed of an E-W trending spreading center and an orthogonal N-S trending transform fault. Magnetic anomalous areas are easily recognised exist on the western side of the ridge. On the contrary, trenches and submarine volcanoes are arrayed in a NW to SE direction on the eastern side of the ridge, with relatively irregular magnetic anomalies.

PGM towing distance was 6,120.8 miles.

(Regional Geochemical Sampling)

Sampling was carried out at 24 points as planned, including 3 points where sample was not collected, so seafloor sediments were collected actually at 21 of these points. As for the sampling method, mainly GC was employed.

Multivariate statistics was conducted simultaneously with the chemical analysis back on land, and the secondary principal components of copper, lead and zinc (which indicate hydrothermal deposits) were detected.

Microfossil discrimination was conducted on some of the samples.

(Detailed Survey)

FDC and sampling were carried out around the spreading center and the submarine volcanoes in Area 1, producing the following results;

FDC: As a result of the detailed survey conducted at the 9 track lines (Total length of the track lines: 52.0 miles. Number of photographs taken: 1,524 points), 9 oxidized zones were identified.

Sampling: 16 points (4 FPG and 12 CB) were sampled at sites where oxidized zones (apparent signs of mineralization) were expected. As a result, light gray clay and siliceous rocks including minor amounts of pyrite, were collected from the crest of a submarine volcano (Kana Keoki Seamount). The chemical analysis, X-ray diffraction and microscopic analysis were performed back on land. Assay data of one specimen was 11.5 g/t Au and 7.2 g/t Ag, with microscopic chalcopyrite, tetrahedrite and sphalerite also observed. Sericite, which is commonly present in hydrothermal deposits was also detected. Furthermore,very small chimney like structures which were composed of powdered galena and barite were collected. Rock samples from the seafloor spreading center, which is on the western side of the survey area, belong to the tholeiite rock series (MORB), and rock samples from the submarine volcanoes, which are to the east, belong to the calc-alkali rock series (Islands Arc or Back Arc).

(Survey of Water Temperature Anomalies)

Owing to the shallow depths, the water temperatures varied with depth, so enough data to adequately determine any water temperature anomalies were not collected.

(Discussion)

In spite of the fact that the detailed survey carried out in the area of the widely developed seafloor spreading center and submarine volcanoes was limited to only part of the total survey area, the oxidized zones of light gray clay, silicious rock and minor amounts of sulphide minerals are obtained. We can assume that hydrothermal activities were present in this region. We could not however, conduct a detailed survey for possible ore deposits and their extent, as the light gray clay and other samples were collected on the last day of the survey. As such, this will provide a future subject of survey and study.

[Reference]

1. Benes, V., Scott, S.D., and Binns, R.A., 1992:
   Tectonics of rift propagation into a continental margin: Western Woodlark Basin, Papua New Guinea.

2. Binns, R.A. and Wheller, G.E., 1991:
   Report on the PACLARK-V (Western Woodlark Basin) and PACMANUS-I (Eastern Manus Basin) CRUISE, RV FRANKLIN, WOODLARK and MANUS BASIN, PAPUA NEW GUINEA.

3. Bruns, T.R., Vedder, J.G., and Culotta, R.C., 1989:
   Structure and tectonics along the Kilinailau Trench, Bougainville-Buka Island Region, Papua New Guinea.
   Circum-Pacific Council for Energy and Mineral Resources, Earth Sci.Ser.12, 93-123.

4. Carbotte, S., and Macdomald, K., 1992:
   East pacific rise 8° -10° 30'N: Evolution of ridge segments and discontinuities from SeaMARC II and Three dimensional magnetic studies.
   Journal of Geophysical Research 97, B7, 6959-6982.

5. Coleman, P.J., Grover, J.C., Stanton, R.L., and Thompson, R.B., 1962:
   A first geological map of the British Solomon Islands.

6. Coleman, P.J., 1965:
   Stratigraphical and structural notes on the British Solomon Islands with reference to the first geological map.
   British Solomon Island Geological Record 2, 17-31.

7. Coleman, P.J. and Packham, G.H., 1976:
   The Melanesian borderlands and India-Pacific Plates boundary.
   Earth-Sci. Review 12, 197-233.

8. Cooper, P. and Taylor, B., 1987:
The spatial distribution of earthquakes, focal mechanisms, and subducted lithosphere in the Solomon Islands.
Circum-Pacific Council for Energy and Mineral Resources, Earth Sci.Ser.7, 67-88.

9. Crook, K.A.W. and Taylor, G.R., 1987:
Sedimentary petrology and mineral chemistry, Woodlark Basin-Solomon Islands offshore region.
Circum-Pacific Council for Energy and Mineral Resources, Earth Sci.Ser.7, 295-346.

10. Crook, K.A.W., Taylor, B., and David A.Falvey., 1991:
PACIFIC SEAFLOOR ATLAS.

11. Crook, K.A.W. and Taylor, B., 1993:
Quaternary tectonic history of the Woodlark Triple Solomon Islands. (unpublished)

12. Hobart, M.A. and Weissel, J.K., 1987:
Geothermal surveys in the Solomon Islands-Woodlark Basin region
Circum-Pacific Council for Energy and Mineral Resources, Earth Sci.Ser.7, 49-66.

13. Honza, E., 1991;
The tertiary arc chain in the western Pacific.
Tectonophysics, 187, 285-303.

14. Honza, E., Miyazaki, T., Lock, J., 1989:
Subduction erosion and accretion in the Solomon Sea region.
Tectonophysics, 160, 49-62.

15. Johnson, R.W., Jaques, A.L., Langmuir, C.H., Perfit, M.R., Staudigel, H., Dunkley, P.N., Chappell, B.W., Taylor, S.R., and Baekisapa, M., 1987:
Ridge subduction and forearc volcanism: petrology and geochemistry of rocks dredged from the Western Solomon Arc and Woodlark basin.
Circum-Pacific Council for Energy and Mineral Resources, Earth Sci.Ser.7, 155-226.

16. Johnson, R.W. and Tuni, D., 1978:
Kavachi, an active forearc volcano in the Western Solomon Islands: reported eruptions between 1950 and 1982.
Circum-Pacific Council for Energy and Mineral Resources, Earth Sci.Ser.7, 89-112.

17. Joshima, M., Okuda, Y., Murakami, F., Kishimoto, K., Honza, E., 1987:
Age of the Solomon Sea Basin from Magnetic Lineations.
Geo-Marine Letters, 6, 299-234.

18. Kroenke, L.W., 1989:
Interpretation of a multichannel seismic-reflection profile northeast of the Solomon Islands from the southern flank of the Ontong Java Plateau across the Malaita anticlinorium to the Solomon Islands Arc.
Circum-Pacific Council for Energy and Mineral Resources, Earth Sci.Ser.12, 145-148.

19. Milson, J.S., 1970:
Woodlark Basin, a minor center of sea-floor spreading in Melanesia.
Journal of Geophysical Research 75, 7335-7339.

20. Ness, G., Levi, S., and Couch, R., 1980:
Marine Magnetic Anomaly Timescales for the Cenozoic and Late Cretaceous:
A Precis, Critique, and Synthesis
Reviews of geophysics and space physics. 18, 4, 753-770.

21. Okubo, Y., Kinoshita, K., Wada, K., 1993:
Magnetic Structural Analysis by 3-D Inversion-Application to Geothermal Exploration-.

22. Perfit, M.R., Langmuir, C.H., Baekisapa, M., Chappell, B., Johnson, R.W., Staudigel, H., an Taylor, S.R., 1987:
Geochemistry and petrology of volcanic rocks from the Woodlark Basin: addressing questions of ridge subduction.
Circum-Pacific Council for Energy and Mineral Resources, Earth Sci.Ser.7, 113-154.

23. Taylor, B., 1987:
A geophysical survey of the Woodlark-Solomons region.
Circum-Pacific Council for Energy and Mineral Resources, Earth Sci.Ser.7, 25-48.

24. Taylor, B. and Exon, N.F., 1987:
An investigation of ridge subduction in the Woodlark-Solomons region: introduction and overview.
Circum-Pacific Council for Energy and Mineral Resources, Earth Sci.Ser.7, 7-24.

25. Taylor, B., Crook, K.A.W., Sinton, J.M., and Petersen, L., 1991:
Manus Basin,Papua New Guinea. SeaMARC Ⅱ Sidescan Sonar Imagery, Bathymetry, Magnetic Anomalies and Free Gravity Anomalies, 1:1,000,000. University of Hawaii.

26. Vendder, T.R., and Bruns, T.R., 1989:
Geologic setting and petroleum of basin sequences, offshore Solomon Islands and eas-tern Papua New Guinea.
Circum-Pacific Council for Energy and Mineral Resources, Earth Sci.Ser.12, 287-322.

27. Vacquier, V., 1972:
Geomagnetism in Marine Geology. Elsevier Publishing Company Amsterdam-London-New York 1972.

28. Weissel, J.K., Taylor, B., and Karner, G.D., 1982:
The opening of the Woodlark Basin, subduction of the Woodlark spreading system, and the evolution of northern Melanesia since mid-Pliocene time. Tectonophysics 87, 253-277.